

Ph. D. Thesis

**Acoustic Radiation and Scattering from Cylindrical Bodies  
and  
Analysis of Transducer Arrays**

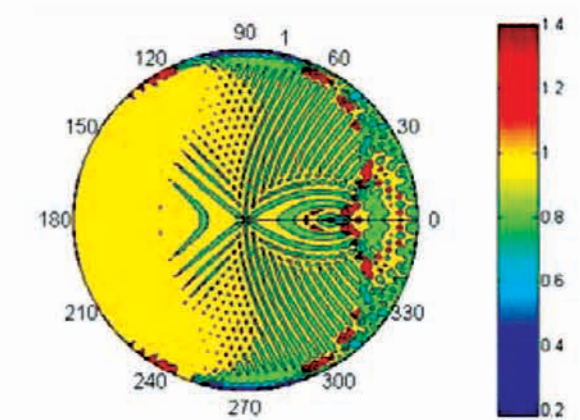
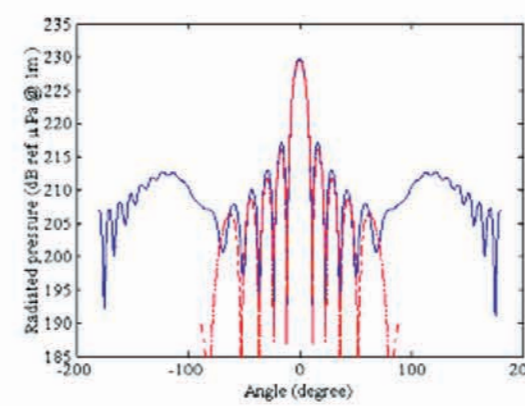
JASMINE MATHEW

*Submitted to*

**COCHIN UNIVERSITY OF SCIENCE AND TECHNOLOGY**



**NAVAL PHYSICAL AND OCEANOGRAPHIC LABORATORY**  
Defence Research and Development Organisation  
Kochi, Kerala, India, 682021



**ACOUSTIC RADIATION AND SCATTERING FROM CYLINDRICAL BODIES  
AND ANALYSIS OF TRANSDUCER ARRAYS**

Thesis submitted to the  
Cochin University of Science and Technology  
for the award of the degree of  
**DOCTOR OF PHILOSOPHY**  
under the Faculty of Science

by

**JASMINE MATHEW**

under the Guidance of  
**Dr. D. D. Ebenezer**



NAVAL PHYSICAL AND OCEANOGRAPHIC LABORATORY  
Defence Research and Development Organisation  
Kochi, Kerala, India, 682021

September 2011

## **Ph.D. Thesis in the field of Mathematical Acoustics**

### **Author**

Jasmine Mathew

Research Scholar

Registration No.3408

Naval Physical and Oceanographic Laboratory

Kochi 682021, Kerala, India

e-mail:jasminem@rajagiritech.ac.in

### **Supervising Guide**

Dr. D. D. Ebenezer

Scientist 'G' and Head, Transducer Group

Naval Physical and Oceanographic Laboratory

Kochi 682021, Kerala, India

e-mail: d.d.ebenezer@gmail.com

September 2011

Front Cover: (Left) Far-field acoustic radiation from a phased array of cylindrical transducers (blue) and a rectangular piston (red); and (Right) the magnitude of the interior pressure field in an embedded fluid cylinder ensonified by a plane acoustic wave computed using ray theory

## THESIS CERTIFICATE

This is to certify that the thesis entitled “**Acoustic radiation and scattering from cylindrical bodies and analysis of transducer arrays**” submitted by **JASMINE MATHEW** to the Cochin University of Science and Technology, Cochin for the award of degree of Doctor of Philosophy under the Faculty of Science is a bonafide record of research work carried out by her under my supervision. The contents of this thesis, in full or in parts, have not been submitted to any other institute or University for the award of any degree or diploma. The research work has been carried out at Naval Physical and Oceanographic Laboratory, DRDO, Thrikkakara, Kochi 682021.

Dr. D. D. Ebenezer  
(Supervising guide)  
Scientist ‘G’ and Head, Transducer Group  
Naval Physical and Oceanographic Laboratory  
Kochi 682021

Kochi  
Date

## DECLARATION

I hereby declare that the work presented in the thesis entitled “**Acoustic radiation and scattering from cylindrical bodies and analysis of transducer arrays**” is based on the original research work carried out by me under the supervision of Dr. D. D. Ebenezer at Naval Physical and Oceanographic Laboratory, Kochi. The results presented in the thesis or parts of it have not been presented for the award of any other degree or diploma.

Jasmine Mathew  
Research Scholar  
Registration No.3408  
Naval Physical and Oceanographic Laboratory  
Kochi 682021

Kochi  
Date

## ACKNOWLEDGEMENTS

This research was carried out at the Naval Physical and Oceanographic Laboratory (NPOL), Defence Research and Development Organization (DRDO), Ministry of Defence, Govt. of India, a recognized research institution of Cochin University of Science and Technology, during 2008-2011.

I take this opportunity to thank all those who helped me in different ways with my research work. First and foremost, I would like to express my gratitude to God Almighty for the timely completion of my thesis.

I express my most sincere gratitude to my thesis supervisor and guide Dr. D. D. Ebenezer, Scientist G, NPOL for his guidance during this research work. Without his invaluable advice, help and suggestions, this thesis work would not have been possible.

I would like to express my gratitude to the Director, NPOL Sri. S. Ananthanarayanan Scientist H, for providing the requisite facilities and encouragement to do the work. Without his support, I would not have been able to pursue my research work in NPOL and accomplish the task on time.

Let me thank my coauthor in three papers Smt. Nishamol P. A., Scientist C, NPOL for her help in this research work.

I place on record my sincere gratitude to my Doctoral Committee members Dr. A. Unnikrishnan, Scientist H, NPOL; Dr. M.P. Ajaikumar, Scientist F, NPOL; Dr. K. P. B. Moosad, Scientist F, NPOL who was my guide initially; and Dr. R. S. Chakravarti, former Head of the Department, Department of Mathematics, Cochin University of Science and Technology, for their support and guidance.

I also wish to thank the Departmental Research Committee (DRC); all the Human Resource Department (HRD) council members, NPOL; especially HRD Coordinator, Smt. Lasitha Ranjith Scientist F NPOL.

I thank Dr. R. Ramesh, Scientist F, NPOL; Dr. R. Rajesh, Scientist E, NPOL; Dr. D. Thomas, Scientist F, NPOL; and Smt. Roshen Jacob, Scientist F, NPOL for their valuable suggestions in the preparation of this thesis.

I owe a debt of gratitude to Smt. Laly Joseph, Technical Officer A; Smt. Pushpa Abraham, Technical Officer D; Smt. Nirmala Ravi, Technical Officer D; Smt. Valsa John, Technical Officer B; Sri. Satheeshkumar M. K, Senior Technical Assistant C; Sri. Satheeshkumar O. B, Senior Technical Assistant; Sri. Vinodkumar T. K., Senior Technical Assistant C; and Sri. Sreejith S. Pillai, Senior Technical Assistant C; all of

NPOL, for their encouragement, support and prayers. I also wish to thank Smt. Anila John, Scientist C; Sri. Sreekanth Raja, Scientist C; Sri. Krishnakumar, Scientist C; Sri. Manoj Prakash, Scientist C; Sri. Ajeshkumar M, Scientist C; and Sri. Rijo Mathews Abraham, Scientist B; all of NPOL, for their help and suggestions.

Last but not the least, I express my sincere gratitude to my family members for their constant encouragement and support. I gratefully acknowledge my father Mr. M. I. Mathew, my mother Smt. V. S. Rosily, my father-in-law Mr. K. J. Baby, my mother-in-law Smt. K. J. Thresia, my sister, my brother, my sisters-in-law, and my brothers-in-law for their love and support. I also place on record my heartfelt gratitude to my husband Greatin Baby, my sons Master Abhinav, and Master Athul. Their love, patience and guidance have gone a long way in making this thesis a reality.

## ABSTRACT

New mathematical methods to analytically investigate linear acoustic radiation and scattering from cylindrical bodies and transducer arrays are presented. Three problems of interest involving cylinders in an infinite fluid are studied. In all the three problems, the Helmholtz equation is used to model propagation through the fluid and the beam patterns of arrays of transducers are studied.

In the first problem, a method is presented to determine the omni-directional and directional far-field pressures radiated by a cylindrical transducer array in an infinite rigid cylindrical baffle. The solution to the Helmholtz equation and the displacement continuity condition at the interface between the array and the surrounding water are used to determine the pressure. The displacement of the surface of each transducer is in the direction of the normal to the array and is assumed to be uniform. Expressions are derived for the pressure radiated by a sector of the array vibrating in-phase, the entire array vibrating in-phase, and a sector of the array phase-shaded to simulate radiation from a rectangular piston. It is shown that the uniform displacement required for generating a source level of 220 dB ref.  $\mu\text{Pa}$  @ 1m that is omni directional in the azimuthal plane is in the order of 1 micron for typical arrays. Numerical results are presented to show that there is only a small difference between the on-axis pressures radiated by phased cylindrical arrays and planar arrays. The problem is of interest because cylindrical arrays of projectors are often used to search for underwater objects.

In the second problem, the errors, when using data-independent, classical, energy and split beam correlation methods, in finding the direction of arrival (DOA) of a plane acoustic wave, caused by the presence of a solid circular elastic cylindrical stiffener near a linear array of hydrophones, are investigated. Scattering from the effectively infinite cylinder is modeled using the exact axisymmetric equations of motion and the total pressures at the hydrophone locations are computed. The effect of the radius of the cylinder,  $a$ , the distance between the cylinder and the array,  $b$ , the number of hydrophones in the array,  $2H$ , and the angle of incidence of the wave,  $\alpha$ , on the error in finding the DOA are illustrated using numerical results. For an array that is about 30 times the wavelength and for small angles of incidence ( $\alpha < 10$ ), the error in finding the DOA using the energy method is less than that using the split beam correlation method with beam steered to  $\alpha$ ; and in some cases, the error increases when  $b$  increases; and the



errors in finding the DOA using the energy method and the split beam correlation method with beam steered to  $\alpha$  vary approximately as  $a^{7/4}$ . The problem is of interest because elastic stiffeners – in nearly acoustically transparent sonar domes that are used to protect arrays of transducers – scatter waves that are incident on it and cause an error in the estimated direction of arrival of the wave.

In the third problem, a high-frequency ray-acoustics method is presented and used to determine the interior pressure field when a plane wave is normally incident on a fluid cylinder embedded in another infinite fluid. The pressure field is determined by using geometrical and physical acoustics. The interior pressure is expressed as the sum of the pressures due to all rays that pass through a point. Numerical results are presented for  $ka = 20$  to  $100$  where  $k$  is the acoustic wavenumber of the exterior fluid and  $a$  is the radius of the cylinder. The results are in good agreement with those obtained using field theory. The directional responses, to the plane wave, of sectors of a circular array of uniformly distributed hydrophones in the embedded cylinder are then computed. The sectors are used to simulate linear arrays with uniformly distributed normals by using delays. The directional responses are compared with the output from an array in an infinite homogenous fluid. These outputs are of interest as they are used to determine the direction of arrival of the plane wave. Numerical results are presented for a circular array with 32 hydrophones and 12 hydrophones in each sector. The problem is of interest because arrays of hydrophones are housed inside sonar domes and acoustic plane waves from distant sources are scattered by the dome filled with fresh water and cause deterioration in the performance of the array.

**ACOUSTIC RADIATION AND SCATTERING FROM CYLINDRICAL BODIES  
AND ANALYSIS OF TRANSDUCER ARRAYS**

**TABLE OF CONTENTS**

Thesis Certificate .....	iii
Declaration.....	iv
Acknowledgements.....	v
Abstract.....	vii
Table of Contents.....	ix
List of Figures.....	xi
List of Tables .....	xviii
Chapter 1.....	1
Introduction.....	1
1.1 Acoustic Radiation, Scattering, and Transducer Arrays.....	1
1.2 Statements of the Problems.....	2
1.3 History of Acoustics .....	3
1.3.1 BC and Early Indian Acoustics.....	4
1.3.2 Acoustics from the 17th to 19th Centuries .....	5
1.3.3 Acoustics in the 20th and 21st Centuries.....	8
1.4 Motivation for Research .....	8
1.5 Organization of the Thesis .....	9
Chapter 2.....	10
Acoustic Radiation from Cylindrical Transducer Arrays.....	10
2.1 Introduction.....	10
2.2 Radiation from a Cylindrical Array .....	11
2.2.1 In-phase radiation from transducers.....	12
2.2.2 Phased radiation from transducers in a sector.....	17
2.3 Numerical Results and Discussions .....	20
2.4 Conclusions.....	28

Chapter 3.....	30
Error in Finding Direction of Arrival Using a Linear Array due to Scattering from an Elastic Cylinder .....	30
3.1 Introduction.....	30
3.2 Acoustic Scattering .....	32
3.3 Error in Finding Direction of Arrival (DOA) .....	37
3.3.1 Energy Method.....	38
3.3.2 Split Beam Correlation Method .....	40
3.4 Numerical Results and Discussions .....	41
3.4.1 Scattered and Total Pressure.....	42
3.4.2 Error in DOA .....	50
3.5 Conclusions.....	54
Chapter 4.....	56
Directional Response of a Circular Array in an Embedded Fluid Cylinder .....	56
4.1 Introduction.....	56
4.2 Directional Response of Hydrophone Array.....	60
4.2.1 Incident ray in the outer fluid.....	61
4.2.2 Incident ray in the inner fluid.....	62
4.2.3 Ray tracing inside the fluid cylinder .....	64
4.2.4 Divergence, Convergence, and Caustics.....	66
4.2.5 Pressure along a Ray .....	69
4.2.6 Interior Pressure Field.....	69
4.2.7 Field Theory .....	71
4.2.8 Directional Response .....	72
4.3 Numerical Results and Discussions .....	74
4.4 Conclusions.....	90
Chapter 5.....	92
Conclusions.....	92
5.1 Summary .....	92
5.2 Relevance and Applications.....	93
5.3 Future work.....	93
References.....	95
Publications Based on Work.....	102
Doctoral Committee.....	103
Curriculum Vitae .....	104

## LIST OF FIGURES

- 2-1 Schematic of a cylindrical array of transducers. Each square on the curved surface of the cylinder represents the radiating face of one transducer. The radius and length of the array are  $a$  and  $2L$ , respectively. There are  $M$  transducers in the circumferential direction.  $\psi = 2\pi/M$  is the angle subtended by each stave at the centre. Each stave has  $N$  transducers in the vertical direction. It is assumed that the array is in an infinite, rigid, cylindrical baffle that is not shown.
- 2-2 The cylindrical coordinate system  $(r, \phi, z)$  and the spherical coordinate system  $(R, \theta, \varphi)$  used in the analysis.
- 2-3 Top-view of the radiating sector of a cylindrical array. The transducers in the arc  $ACB$  radiate. Each stave is delayed by an appropriate amount to simulate radiation from the chord  $AB$ . The delay applied to the  $m^{\text{th}}$  stave with centre at  $D$  is  $ED$ . An additional delay  $OF$  is applied to all the staves. Therefore, the total delay is  $a \cos(\phi_m - \phi_c)$ .
- 2-4 Spherical coordinate system  $(R, \theta, \varphi)$  for radiation from a rectangular piston of sides  $2L_x$  and  $2L_y$ . (Junger and Feit, 1972).  $\theta = 0$  along the axis of the piston.
- 2-5 The integrand  $\Gamma_n$ , in Eq. (2-10b), that is integrated using the method of stationary phase. It is shown for array  $A$ ,  $f = 10.5$  kHz,  $n = 0$ ,  $r = 200$  m,  $z = 0$ , and  $\varphi = 0$  to illustrate the rapid oscillations except near the stationary phase point:  $k_z = 0$ .
- 2-6 Directivity patterns, in dB, due to in-phase vibration of (a) nine and (b) eleven staves out of 30 staves in array  $A$  at 10.5 kHz.
- 2-7 Pressure radiated at 10.5 kHz by phased radiation of nine staves in array  $A$  (blue solid line) and a corresponding rectangular piston (red dashed line).
- 2-8 Pressure radiated at 10.5 kHz by phased radiation of 11 staves in array  $A$  (blue solid line) and a corresponding rectangular piston (red dashed line).
- 2-9 Directivity patterns, in dB, due to in-phase vibration of 11 staves out of 32 staves in array  $B$  at a) 9 kHz, b) 7.5 kHz, and c) 6 kHz.
- 2-10 Pressure radiated at 9 kHz by phased radiation of 11 staves in array  $B$  (blue solid line) and a corresponding rectangular piston (red dashed line).
- 2-11 Pressure radiated at 7.5 kHz by phased radiation of 11 staves in array  $B$  (blue

- solid line) and a corresponding rectangular piston (red dashed line).
- 2-12 Pressure radiated at 6 kHz by phased radiation of 11 staves in array *B* (blue solid line) and a corresponding rectangular piston (red dashed line).
- 3-1 A plane wave incident at an angle  $\alpha$  on a linear array with  $2H$  hydrophones. An elastic circular cylinder is in front of the array.
- 3-2 A real linear array of hydrophones (●) is steered to an angle  $\beta$  to form a virtual array (○). A plane wave is traveling at an angle  $\alpha$  to the real array.
- 3-3 Amplitude of pressure scattered from a rigid cylinder with diameter 0.818 mm ( $ka = 1.7$ ). Solid line – computed using present method; \* from Fig. (5) in Faran (1951).
- 3-4 Amplitude of pressure scattered from a rigid cylinder with diameter 1.5875 mm ( $ka = 3.4$ ). Solid line – computed using present method; \* from Fig. (9) in Faran (1951).
- 3-5 Amplitude of pressure scattered from a rigid cylinder with diameter 2.3495 mm ( $ka = 5$ ). Solid line – computed using present method; \* from Fig. (13) in Faran (1951).
- 3-6 Amplitude of pressure scattered at 1 MHz from a steel cylinder with diameter 0.813 mm. Solid line – computed using present method; \* from Figs. (4) in Faran (1951).
- 3-7 Amplitude of pressure scattered at 1 MHz from a copper cylinder with diameter 1.588 mm. Solid line – computed using present method; \* from Fig. (7) in Faran (1951).
- 3-8 Amplitude of pressure scattered from an aluminum cylinder with diameter 2.349 cm at 1 MHz. Solid line – computed using present method; \* from Fig. (12) in Faran (1951).
- 3-9 (a) Magnitude of pressure backscattered for different frequencies.  $b = 0.5$  m (red solid line) and 1m (blue dashed line) (b) directivity pattern of pressure scattered from a titanium cylinder at 43 kHz.
- 3-10 Magnitude of scattered pressure (a) at the centre of the 1 m array (b) along a 1 m array for  $f = 37$  kHz.  $b = 0.5$  m (red solid line) and 1 m (blue dashed line).
- 3-11 (a) Magnitude and (b) Phase of total pressure along a 1 m array.  $b = 0.5$  m (red solid line) and  $b = 1$  m (blue dashed line).

- 3-12 (a) Magnitude and (b) Phase of total pressure along a 1 m array.  $b = 0.5$  m (red solid line) and  $b = 1$  m (blue dashed line).  $\alpha = 1$  deg.
- 3-13 (a) Magnitude and (b) Phase of total pressure along a 1 m array.  $b = 0.5$  m (red solid line) and  $b = 1$  m (blue dashed line).  $\alpha = 3$  deg.
- 3-14 (a) Magnitude and (b) Phase of total pressure along a 1 m array.  $b = 0.5$  m (red solid line) and  $b = 1$  m (blue dashed line).  $\alpha = 15$  deg.
- 3-15 (a) Magnitude and (b) Phase of total pressure along a 1 m array.  $b = 0.5$  m (red solid line) and  $b = 1$  m (blue dashed line).  $\alpha = 30$  deg.
- 3-16 (a) Magnitude and (b) Phase of total pressure along a 1 m array.  $b = 0.5$  m (red solid line) and  $b = 1$  m (blue dashed line).  $\alpha = 45$  deg.
- 3-17 (a) Magnitude and (b) Phase of total pressure along a 1 m array.  $b = 0.5$  m (red solid line) and  $b = 1$  m (blue dashed line).  $\alpha = 60$  deg.
- 3-18 Error in DOA computed using (a) energy method (b) split beam correlation method with beam steered to broadside ( $\beta = 0$ ) and (c) split beam correlation method with beam steering for  $\beta = \alpha$ .  $b = 0.5$  m (green dashed line), 1m (red solid line) and 1.5m (blue dash dot line).
- 3-19 Error in DOA due to cross correlation method with beam steered to neighborhood of  $\alpha$  as a function of steering angles when a plane wave is incident at (a)  $1^\circ$  and (b) at  $3^\circ$ .  $b = 0.5$  m (green dashed line), 1m (red solid line) and 1.5m (blue dash dot line).
- 3-20 Error in DOA computed using (a) energy method and (b) split beam correlation method (with beam steered to  $\alpha$ ).  $b = 0.5$  m (green dashed line), 1m (red solid line) and 1.5m (blue dash dot line). 24 mm diameter cylinder is in front of the array.
- 3-21 Error in DOA computed using (a) energy method and (b) split beam correlation method (with beam steered to  $\alpha$ ).  $b = 0.5$  m (green dashed line), 1m (red solid line) and 1.5m (blue dash dot line). 12 mm diameter cylinder is in front of the array.
- 3-22 Error in finding DOA when using the energy method. (a)  $\alpha = 1$  deg (b)  $\alpha = 3$  deg.  $b = 0.5$  m (red dots), 1 m (green diamonds) and 1.5m (blue squares).

- 4-1 A plane wave is incident on an infinite fluid cylinder embedded in another fluid of infinite extent. Transmission of a ray into the cylinder and reflection of that ray within the cylinder are shown.
- 4-2 A ray traveling in the outer fluid is incident on the interface. The tangent to the interface is  $EF$ . The radius of the cylinder is  $a$ . The angle of incidence between the ray and the normal to the interface,  $GH$ , is  $\alpha$ . The angle of transmission is  $\beta$ .
- 4-3 A ray traveling inside the fluid cylinder is incident on the interface. The tangent to the interface is  $EF$ . The angle of incidence between the ray and the normal to the interface,  $GH$ , is  $\beta$ . The angle of transmission is  $\chi$ .
- 4-4  $n=0$  rays inside the fluid cylinder: a) when  $g=h=1.1$  and b) when  $g=h=0.9$ .
- 4-5  $n=1$  rays inside the fluid cylinder: a) when  $g=h=1.1$  and b) when  $g=h=0.9$ .
- 4-6 Solid line:  $n=0$  rays. Dashed line: rays extended to meet the focal point.
- 4-7 The loci of focal points of  $n=1$  rays.
- 4-8 a) Rays passing through  $r = 0.3, \theta = 90^\circ$ .  $n = 0$  (solid line) and  $n = 1$  (dashed line). b) Three  $n = 1$  rays passing through  $r = 0.9, \theta = 0^\circ$ .
- 4-9 Schematic sector of a circular array. The hydrophones are in the arc  $ACB$ . Each hydrophone is delayed by an appropriate amount to simulate a linear array from the chord  $AB$ .
- 4-10 Magnitude of interior pressure at 20 kHz when  $g=h=1.1$  a) using Ray theory with  $n=0$  and  $n = 1$  rays b) using Field theory with 250 terms.
- 4-11 a) Real part and b) imaginary part of interior pressure field on diameter formed by  $\theta = 0^\circ$  and  $180^\circ$  radii at 20 kHz when  $g=h=1.1$ . Red solid line: Field theory with 250 terms. Blue dots: Ray theory with  $n = 0$  and 1 rays.
- 4-12 a) Real part and b) imaginary part of interior pressure field on diameter formed by  $\theta = 30^\circ$  and  $210^\circ$  radii at 20 kHz when  $g=h=1.1$ . Red solid line: Field theory with 250 terms. Blue dots: Ray theory with  $n = 0$  and 1 rays.
- 4-13 a) Real part and b) imaginary part of interior pressure field on diameter formed by  $\theta = 90^\circ$  and  $270^\circ$  radii at 20 kHz when  $g=h=1.1$ . Red solid line: Field theory with 250 terms. Blue dots: Ray theory with  $n = 0$  and 1 rays.
- 4-14 Magnitude of interior pressure at 5 kHz when  $g=h=1.1$  a) using Ray theory with  $n=0$  and  $n = 1$  rays b) using Field theory with 250 terms.
- 4-15 a) Real part and b) imaginary part of interior pressure field on diameter formed by  $\theta = 0^\circ$  and  $180^\circ$  radii at 5 kHz when  $g=h=1.1$ . Red solid line: Field theory

- with 250 terms. Blue dots: Ray theory with  $n = 0$  and 1 rays.
- 4-16 a) Real part and b) imaginary part of interior pressure field on diameter formed by  $\theta = 30^\circ$  and  $210^\circ$  radii at 5 kHz when  $g=h=1.1$ . Red solid line: Field theory with 250 terms. Blue dots: Ray theory with  $n = 0$  and 1 rays.
- 4-17 a) Real part and b) imaginary part of interior pressure field on diameter formed by  $\theta = 90^\circ$  and  $270^\circ$  radii at 5 kHz when  $g=h=1.1$ . Red solid line: Field theory with 250 terms. Blue dots: Ray theory with  $n = 0$  and 1 rays.
- 4-18 Magnitude of interior pressure at 20 kHz when  $g=h=0.9$  a) using Field theory with 250 terms b) using Ray theory with  $n=0$  and  $n = 1$  rays.
- 4-19 a) Real part and b) imaginary part of interior pressure field on diameter formed by  $\theta = 0^\circ$  and  $180^\circ$  radii at 20 kHz when  $g=h=0.9$ . Red solid line: Field theory with 250 terms. Blue dots: Ray theory with  $n = 0$  and 1 rays.
- 4-20 a) Real part and b) imaginary part of interior pressure field on diameter formed by  $\theta = 30^\circ$  and  $210^\circ$  radii at 20 kHz when  $g=h=0.9$ . Red solid line: Field theory with 250 terms. Blue dots: Ray theory with  $n = 0$  and 1 rays.
- 4-21 a) Real part and b) imaginary part of interior pressure field on diameter formed by  $\theta = 90^\circ$  and  $270^\circ$  radii at 20 kHz when  $g=h=0.9$ . Solid line: Field theory with 250 terms. Diamonds: Ray theory with  $n = 0$  and 1 rays.
- 4-22 Magnitude of interior pressure at 5 kHz when  $g=h=0.9$  a) using Field theory with 250 terms b) using Ray theory with  $n=0$  and  $n = 1$  rays.
- 4-23 a) Real part and b) imaginary part of interior pressure field on diameter formed by  $\theta = 0^\circ$  and  $180^\circ$  radii at 5 kHz when  $g=h=0.9$ . Red solid line: Field theory with 250 terms. Blue dots: Ray theory with  $n = 0$  and 1 rays.
- 4-24 a) Real part and b) imaginary part of interior pressure field on diameter formed by  $\theta = 30^\circ$  and  $210^\circ$  radii at 5 kHz when  $g=h=0.9$ . Red solid line: Field theory with 250 terms. Blue dots: Ray theory with  $n = 0$  and 1 rays.
- 4-25 a) Real part and b) imaginary part of interior pressure field on diameter formed by  $\theta = 90^\circ$  and  $270^\circ$  radii at 5 kHz when  $g=h=0.9$ . Red solid line: Field theory with 250 terms. Blue dots: Ray theory with  $n = 0$  and 1 rays.
- 4-26 a) Real part and b) imaginary part of interior pressure field on diameter formed by  $\theta = 0^\circ$  and  $180^\circ$  radii at 20 kHz when  $g=2$  and  $h=1.5$ . Red solid line: Field theory with 250 terms. Blue dots: Ray theory with  $n = 0$  and 1 rays. Green squares: Ray theory with  $n = 0, 1$  and 2 rays. Yellow diamonds: Ray theory with



$n = 0, 1, 2$  and 3 rays.

- 4-27 a) Real part and b) imaginary part of interior pressure field on diameter formed by  $\theta = 30^\circ$  and  $210^\circ$  radii at 20 kHz when  $g=2$  and  $h=1.5$ . Red solid line: Field theory with 250 terms. Blue dots: Ray theory with  $n = 0$  and 1 rays. Green squares: Ray theory with  $n = 0, 1$  and 2 rays. Yellow diamonds: Ray theory with  $n = 0, 1, 2$  and 3 rays.
- 4-28 a) Real part and b) imaginary part of interior pressure field on diameter formed by  $\theta = 90^\circ$  and  $270^\circ$  radii at 5 kHz when  $g=h=1.1$ . Red solid line: Field theory with 250 terms. Blue dots: Ray theory with  $n = 0$  and 1 rays. Green squares: Ray theory with  $n = 0, 1$  and 2 rays. Yellow diamonds: Ray theory with  $n = 0, 1, 2$  and 3 rays.
- 4-29 a) Real part and b) imaginary part of interior pressure field on diameter formed by  $\theta = 0^\circ$  and  $180^\circ$  radii at 5 kHz when  $g=2$  and  $h=1.1$ . Red solid line: Field theory with 250 terms. Blue dots: Ray theory with  $n = 0$  and 1 rays. Green squares: Ray theory with  $n = 0, 1$  and 2 rays. Yellow diamonds: Ray theory with  $n = 0, 1, 2$  and 3 rays.
- 4-30 a) Real part and b) imaginary part of interior pressure field on diameter formed by  $\theta = 30^\circ$  and  $210^\circ$  radii at 5 kHz when  $g=2$  and  $h=1.1$ . Red solid line: Field theory with 250 terms. Blue dots: Ray theory with  $n = 0$  and 1 rays. Green squares: Ray theory with  $n = 0, 1$  and 2 rays. Yellow diamonds: Ray theory with  $n = 0, 1, 2$  and 3 rays.
- 4-31 a) Real part and b) imaginary part of interior pressure field on diameter formed by  $\theta = 90^\circ$  and  $270^\circ$  radii at 5 kHz when  $g=h=1.1$ . Red solid line: Field theory with 250 terms. Blue dots: Ray theory with  $n = 0$  and 1 rays. Green squares: Ray theory with  $n = 0, 1$  and 2 rays. Yellow diamonds: Ray theory with  $n = 0, 1, 2$  and 3 rays.
- 4-32 a) Real part and b) imaginary part of internal pressure field at the point  $r=a/2$  and  $\theta = 180^\circ$  from  $ka = 20$  to 100 when  $g=h=1.1$ . Red solid line: Field theory with 250 terms. Blue dots: Ray theory with  $n = 0$  and 1 rays
- 4-33 a) Real part and b) imaginary part of internal pressure field at the point  $r=0$  and  $\theta = 0^\circ$  from  $ka = 20$  to 100 when  $g=h=1.1$ . Red solid line: Field theory with 250 terms. Blue dots: Ray theory with  $n = 0$  and 1 rays.
- 4-34 a) Real part and b) imaginary part of internal pressure field at the point  $r=3a/4$

- and  $\theta = 0^\circ$  from  $ka = 20$  to  $100$  when  $g=h=1.1$ . Red solid line: Field theory with 250 terms. Blue dots: Ray theory with  $n = 0$  and 1 rays.
- 4-35 a) Real part and b) imaginary part of internal pressure field at the point  $r=a/2$  and  $\theta = 180^\circ$  from  $ka = 20$  to  $100$  when  $g=h=0.9$ . Red solid line: Field theory with 250 terms. Blue dots: Ray theory with  $n = 0$  and 1 rays.
- 4-36 a) Real part and b) imaginary part of internal pressure field at the point  $r=0$  and  $\theta = 0^\circ$  from  $ka = 20$  to  $100$  when  $g=h=0.9$ . Red solid line: Field theory with 250 terms. Blue dots: Ray theory with  $n = 0$  and 1 rays.
- 4-37 a) Real part and b) imaginary part of internal pressure field at the point  $r=3a/4$  and  $\theta = 0^\circ$  from  $ka = 20$  to  $100$  when  $g=h=0.9$ . Red solid line: Field theory with 250 terms. Blue dots: Ray theory with  $n = 0$  and 1 rays.
- 4-38 Directional response of 12 out of 32 hydrophones in the circular array for frequency of a) 5 kHz and b) 20 kHz when  $g= h=0.9$ . Red solid line: Presence of embedded cylinder. Blue dots: Absence of embedded cylinder.
- 4-39 Directional response of 12 out of 32 hydrophones in the circular array for frequency of a) 5 kHz and b) 20 kHz when  $g= h=1.1$  Red solid line: Presence of embedded cylinder. Blue dots: Absence of embedded cylinder.

## LIST OF TABLES

- 2-I Characteristics of arrays
- 2-II Displacements and on-axis pressures for the arrays
- 4-I Magnitude of interior pressure at 20 kHz when  $g = h = 1.4$  at  $r = 0.5$  m.

## Chapter 1

### INTRODUCTION

#### 1.1 ACOUSTIC RADIATION, SCATTERING, AND TRANSDUCER ARRAYS

Acoustics is the interdisciplinary science of mechanical waves in solids, liquids, and gases, associated with fluctuations in the density of the medium (Morse and Ingard, 1968). The word acoustics is derived from the Greek word ακουστός (akoustos) which means audible or heard but the field of acoustics has grown to include infrasound, audible sound, and ultrasound, and phenomena such as generation, radiation, scattering, transmission, and attenuation of waves (Beyer, 1999). When the molecules of a fluid or solid are displaced from their normal positions and compressed or rarefied, an internal restoring force arises. This elastic restoring force coupled with the inertia of the system enables matter to participate in oscillatory vibrations or waves and thereby generate and transmit acoustic waves (Kinsler *et al.*, 1982). The science of acoustics has a wide range of defense applications such as detection, localization, classification, tracking, parameter estimation, weapon guidance, countermeasures, and communications. It also has commercial applications such as navigation aids, fish location, bottom mapping, seismic prospecting, and acoustic oceanography.

Acoustic waves are generated in solid and fluid bodies by the forced vibration of a boundary, by time varying body forces, and by thermal effects (Morse and Ingard, 1968). The waves – in the form of density fluctuations – always travel away from the source and this is known as radiation. Spherical waves are radiated when the source is small and the body is effectively unbounded because the observation time is short in comparison to the time taken for the wave to travel to a boundary. The intensity of the disturbance varies inversely with square of distance from the source. Cylindrical waves are radiated when the lateral dimensions of the body are much greater than its uniform thickness and the fluctuation is observed long after the disturbance has reached the reflecting plane boundaries. The intensity in cylindrical waves varies inversely with distance from the source. Plane waves are generated in long thin rods excited uniformly at the ends and by pistons acting on fluid cylinders. The disturbance, in the absence of dissipative forces, does not decay with distance from the source.

When an acoustic wave encounters an obstacle, new waves traveling in all

directions are generated. The difference between the actual wave and the wave in the absence of the obstacle is known as the scattered wave and the process is known as scattering (Morse and Ingard, 1968). When the source of the wave is very far away from a small obstacle, the curvature of the part of the wavefront that actually strikes the scatterer is insignificant and the wave can be considered to be plane. Some energy is scattered back in the direction it came from. The energy scattered in the forward direction – the direction in which the incident wave is traveling – is, however, often more than the backscattered energy.

Electroacoustic transducers convert electrical energy to acoustical energy and vice versa (Stansfield, 1990). In underwater applications, transducers that generate acoustic waves are known as projectors or radiators; and those that are used to sense acoustic waves are known as hydrophones. In air applications, they are known as loudspeakers and microphones, respectively. Several different types of projectors are used at their resonance frequency to radiate underwater acoustic waves and their size is inversely proportional to the frequency. In contrast, hydrophones are usually used over a wide frequency band and are usually smaller than the wavelength in water at the highest frequency.

Arrays of projectors are used in sonar systems to increase the source level and make it possible for the wave to travel a longer distance before the intensity reduces to an insignificant level. Arrays of hydrophones are used to increase the signal to noise ratio and improve the probability of detection and accuracy of localization (Waite, 1992).

In this thesis, acoustic radiation from a cylindrical array and the effect of acoustic scattering from elastic and fluid cylinders on the performance of arrays of hydrophones are investigated. The problems that are analyzed are briefly stated in the next section.

## **1.2 STATEMENTS OF THE PROBLEMS**

Three problems of interest involving cylinders in an infinite fluid are studied. New mathematical methods to analytically investigate linear acoustic radiation and scattering from cylinders and transducer arrays are presented. In all the three problems, the Helmholtz equation is used to model propagation through the fluid and the beam patterns of arrays of transducers are studied.

In the first problem, acoustic radiation from a cylindrical array of projectors is studied. The displacement on the surface of the array is specified. Analytical expressions for the radiated pressure and the far-field radiated beam pattern are of interest for three

cases: radiation from the entire array, in-phase radiation from a sector of the array, and phased radiation from a sector.

In the second problem, a plane wave is incident on a linear array of hydrophones. An infinite elastic cylinder is in the neighborhood of the array and the total pressure at the hydrophone locations is the sum of the pressures due to the incident wave and the scattered waves emanating from the cylinder. It is of interest to determine the direction of arrival of the plane wave. The error caused by the presence of the cylinder is of interest. Two data-independent signal processing methods are used in the study.

In the third problem, a fluid cylinder is embedded in another infinite fluid. A high frequency plane wave is incident on the fluid cylinder. A circular array of hydrophones is inside the embedded cylinder. The effect of the differences in the properties of the fluids on the beam pattern of a sector of the array is of interest. The interior pressure field is determined using ray theory.

A brief history of acoustics, starting from ancient acoustics but with more emphasis on recent developments is presented in the next section.

### **1.3 HISTORY OF ACOUSTICS**

The history of acoustics is presented in literature from various viewpoints. Brief accounts are presented in several books (Beyer, 1999; Graff, 1975; Pierce, 1989; Love, 1927; Soedel, 1993; Raichel, 2000). Whewell (1858) presents a view of the progress of acoustics, from ancient times, as a theoretical science and highlights discoveries of general principles that reduce many facts to one theory. The development of acoustics in ancient China (Chen, 1996) and underwater Russia (Godin and Palmer, 2008) is presented in books. There is apparently no well-researched book on the history of Indian acoustics but ancient texts and archeological evidence indicate a rich heritage. A brief note on musical acoustics in ancient India is presented by the Nobel Laureate Raman (1922) in which he laments the lack of material available for writing their history. The Bible names Jubal as the father of all who play stringed instruments such as the harp and the flute and states that four thousand Levites were appointed by King David (c. 1000 BC) to praise God with musical instruments.

Short accounts of BC and early Indian acoustics, acoustics from the 17<sup>th</sup> to 19<sup>th</sup> centuries, acoustics in the 20<sup>th</sup> and 21<sup>st</sup> centuries are presented in the following subsections.

### 1.3.1 BC and Early Indian Acoustics

Aristotle (384 – 322 BC) was perhaps the first to understand the generation and radiation of acoustic waves. In his treatise “On Sound and Hearing,” he wrote that sound takes place when bodies strike the air ... the air being contracted and expanded ... is carried forwards ... and that which is contiguous ... is carried onwards ... very far away ... . Admirers of antiquity see in this passage an exact account of the production and propagation of sound while others, such as Sir Francis Bacon (1561 – 1626), consider it only a vague notion and verbal generalization (Whewell, 1858). Bacon, in his work entitled, “The history and first inquisition of sound and hearing,” (Montagu, 1834) wrote, “The collision or thrusting of air which they will have to be the cause of sound, neither denotes the form nor the latent process of sound, but is a term of ignorance and of superficial contemplation.” Devey (1902), who edited the works of Bacon, reckons that Bacon held Aristotle’s work in low esteem and was referring to it in this statement.

Along with Aristotle, other BC acousticians who made eminently noteworthy contributions are Pythagoras (570 - 497 BC) who is well known to every student of mathematics, the Greek philosopher Chrysippus (240 BC), and the Roman architect-engineer Vitruvius (25 BC). The first major scientific discovery by Pythagoras was in the area of acoustics. Egyptian papyrus was introduced to Greece around 650 BC but there are no original sources regarding his work partly because the esoteric practices of the Pythagoreans (Eli Maor, 2007). It is widely believed that Pythagoras (and his successors) established an inverse relationship between the length of a string and its resonance frequency, explained that the frequency of vibration of the string is equal to the frequency of vibration of the surrounding air, and determined the ratios of lengths of strings which when plucked together create harmonious sounds. Vitruvius explained that “voice proceeds in breadth but also successively ascends in height” (Whewell, 1858); indicating that sound, in a 3D space, travels in outwardly spreading spherical waves. Chrysippus observed that water waves move away from a source but do not transport matter over large distances and was of the view that sound exhibits analogous behavior (Pierce, 1989). He also was of the view that the air motion generated by vibrating body sounding a single musical note is vibratory and of the same frequency as the body – a view not shared by Gassendi who was a contemporary of Galileo (17<sup>th</sup> century) and Marsenne.

Accounts of developments in acoustics made before recorded history are based

on mythology. In the 27<sup>th</sup> century BC, according to Chinese mythology, Ling-Lun, a minister of the Yellow Emperor Huangundi was commissioned to establish a standard pitch for music. He cut a bamboo stem between the nodes to make his fundamental note (approximately 410 Hz), resulting in the “Huang – zhong pipe.” It is interesting to note that the A above the middle C in a piano has a frequency of exactly 440 Hz. An analysis of the dimensions of the pipe which was approximately 10 cm long was presented recently (Xia *et al.*, 2006). Ling-Lun is also credited with a series of twelve standard pitch-pipes and bronze bells.

In India, as in other countries, there was an interest in ancient times in the acoustics of music and speech. The foundation of research in phonetics was first laid in India by the eminent Sanskrit grammarian Panini who experts say lived at some time between the 4th and 7th centuries BC. It has been claimed that very little was added, until recently, to Astadhyayi (meaning eight chapters) a treatise attributed to Panini (Vasu, 1891) that was written to lay down the rules for grammar and the correct enunciation of Vedic hymns and other Sanskrit texts. The Natya Shastra written during period between 200 BC and 200 AD is a treatise that covers theatre, dance, and music and gives details of the music and instruments of that period (Tarlekar, 1991).

### **1.3.2 Acoustics from the 17th to 19th Centuries**

The governing equations; and initial and boundary conditions for the acoustics of fluids and solids, were developed during this period. Earlier, concepts and some results were established. However, the development of mathematical equations that are presently used had to wait for the development of differential and integral calculus.

Mersenne, Hooke, and Newton (17<sup>th</sup> century); Chaldni, Bernoulli and Euler (18<sup>th</sup> century); and Sophie Germain, Lord Rayleigh and Helmholtz (19<sup>th</sup> century) are a few famous acousticians of this period. Many of these acousticians actually did their major work in other fields – Young (19<sup>th</sup> century) in optics, Helmholtz in medicine, physiology, and electricity; Rayleigh in many fields, including gases, electricity, and optics.

In 1636, Marin Mersenne, a French natural philosopher often referred as the ‘father of acoustics’ presented the first correct published account on vibration of strings. Mersenne observed in his *Harmonie Universelle* that the frequency of vibration is inversely proportional to the length of the string and directly proportional to the square root of the cross sectional area. In 1700, Sauveur calculated the resonance frequency of a stretched string and he suggested the term acoustics for the science of sound.



### ***1.3.2.1 Acoustics of Fluids***

The mathematical theory of sound propagation began with Issac Newton (1642-1727) whose *Principia* (1686) included a mechanical interpretation of sound as being pressure pulses transmitted through neighboring fluid particles. He also investigated the speed of water waves and speed of sound in air. He summed up his analysis saying that, if the Earth's atmosphere were considered homogeneous, it would have certain height; and the velocity of sound in air is equal to the velocity acquired by a heavy body when it falls through one half this height. This is equivalent to stating that the speed of sound is equal to the square root of the ratio of atmospheric pressure to the density. Newton's estimate for speed of sound is found to be only approximate, because he, in essence, assumed that acoustic vibration is an isothermal process. However, it was not until 1816 that Laplace explained that the process is adiabatic and derived the correct expression for the speed of sound in air (Whewell, 1858).

Efforts were also made to experimentally determine the speed of sound in water. John Candon measured the elasticity of water and Chaldni used this to determine the speed of sound in a number of liquids with accuracy similar to that obtained for water. The value of speed of sound in fresh water obtained by Chaldni is 1494 m/s. Chladni, using Newton's method, determined the speed in a number of gases such as oxygen and carbon dioxide that come close to currently accepted values.

In 1826 Colladon measured directly the speed of sound in waters of Lake Geneva. A bell was lowered into the water from one boat and Colladon, in another boat about 10 miles away, listened with an underwater listening tube. The time between a flash of light caused by an explosive connected to a mechanism that struck the bell and the underwater sound reaching Colladon was used to fairly accurately measure the speed of sound. His value of 1435 m/s at 8 deg C in fresh water is nearly equal to the value of 1439 m/s accepted at present (Beyer, 1999).

### ***1.3.2.2 Acoustics of Elastic Solids***

In 1678, Robert Hooke formulated the famous law of proportionality of stress and strain for elastic bodies which bears his name. This law forms the basis of the mathematical theory of elasticity. Bernoulli, Euler, Lagrange, Coulomb, and Young analyzed Hooke's law and Newton's expression for force and derived theoretical equations for strings, beams, thin rods, and curved bars. The principle of superposition of modes was first noted in 1747 by Bernoulli and proved by Euler in 1753.

In 1802, Ernest F.F. Chladni published *Die Akustik* with about 60% of the book dealing with experimental structural acoustics. He is famous for the vibration patterns that he studied by sprinkling fine sand on vibrating plates and analyzing the nodal lines to which the sand converged.

In 1808 the French Institut (Academy of Sciences) offered a prize for the development of a mathematical theory of elastic vibration that was consistent with the experimental results of Chladni. The prize of a medal of one kilogram gold was offered by Emperor Napoleon. The first deadline was set in 1811 but had to be extended to 1813 and again to 1815. Lagrange, Biot, Laplace, and Legendre were to be the judges and were not allowed to compete. Most mathematicians did not attempt to solve the problem because Lagrange had said that the mathematical methods were inadequate to solve it. Sophie Germain, however spent a lot of time attempting to derive a theory of elasticity collaborating with Navier and Poisson. After several attempts Sophie Germain won the prize in 1815 and her work was published in 1821. She derived the fourth order differential equation that governs the vibration of plates (Meleshko, 2003).

Navier was first to investigate the general equations of equilibrium and vibration of elastic solids in 1821. He used neither stress nor strain as done in continuum mechanics. Instead he used Newton's concept of corpuscular or molecular theory in which all matter is composed of discrete particles. However, he derived an expression for the component in any direction of all forces that act upon a displaced particle and the equation of motion in terms of displacement of the molecule (Bucciarelli and Dworsky, 1980). Cauchy developed the dynamical equation of motion for a solid in 1822. He used stress-strain relations to eliminate stress from the equation of dynamic equilibrium, and arrived at equations in terms of displacements. Poisson investigated the propagation of waves through an elastic solid and found two types of waves: longitudinal and transverse. He also developed an approximate theory for vibration of rods and solved the problem of radial vibrations of a sphere in 1828.

In 1876 Pochhammer obtained the frequency equation for the propagation of waves in rods according to the exact equations of elasticity. Chree carried out similar studies and obtained the same results in 1889. Pochhammer expressed solutions of the equations in cylindrical coordinates in terms of Bessel functions and his method successfully employed to spheres and cylinders.

### **1.3.3 Acoustics in the 20th and 21st Centuries**

The firm establishment of theoretical acoustics (Skudrzyk, 1971; Morse and Ingard, 1968; Pierce, 1989) and the development of analytical (Crighton *et al.*, 1992) and numerical methods in the 20th and 21st centuries to solve the governing equations and initial and boundary conditions developed in the earlier centuries resulted in a rapid increase in our understanding and use of acoustics. Concurrently, design and development of underwater electroacoustic transducers (Sherman and Butler, 2007; Stansfield, 1990) electronic instruments, and methods to analyze acoustic signals (Nielsen, 1991; Burdic, 1984) were developed and used to experimentally verify the theoretical models and discover new phenomena.

Heavy fluid-structure interaction, the subject of part of this thesis, was hardly studied in earlier centuries but is presented in 20th century books by Junger and Feit (1972), Fahy (1985), and others. The development of computers and software packages that make use of finite and boundary element methods [ATILA, PAFEC] has led to a much deeper understanding of acoustic phenomena and the design and development of acoustical systems.

## **1.4 MOTIVATION FOR RESEARCH**

Arrays of underwater electroacoustic transducers are used in the generation and reception of acoustic waves. Projectors arrays are used to increase the source level and hydrophone arrays are used to detect very faint signals that would otherwise be submerged in noise as well as to determine the direction of arrival of the waves.

The pressure field of individual transducers used as radiators is influenced by the characteristics of the transducer itself, fluid-structure interaction, the shape and size of the array, and the behavior of nearby transducers. It is difficult to determine by conducting experiments the relative significance of these various influences. Therefore, the radiation characteristics of arrays are studied in an effort to improve our understanding of why measured pressure fields are not equal to pressure fields computed after neglecting the above influences.

Hydrophones, used in receiver arrays, are individually tested in homogeneous water under free-field conditions but are actually used in heterogeneous environments with elastic structures that scatter the acoustic field. The performance of the arrays depends on the environment and the characteristics of the individual hydrophones. However, it is not easy to measure the deterioration in the performance of the arrays due

to various parts of the real environment. Therefore, the effect of the parts is analytically studied one at a time.

Very significant progress in the study of fluid-structure interaction and array analysis has taken place in the last few decades. However, these subjects are often studied by investigators interested in the physics of acoustics and mathematics of signal processing, respectively. In this thesis, both the subjects are studied as the performance of transducer arrays in real environments is of interest.

## **1.5 ORGANIZATION OF THE THESIS**

The introduction to the thesis and an overview of acoustics through the ages is presented in Chapter 1. A few acoustical terms used in the thesis are introduced, the problems studied are briefly stated, the motivation for the thesis is described, and the organization of the thesis is presented.

In Chapter 2 a method is presented to determine the pressure radiated by a radiation from a cylindrical array of transducers with infinite rigid cylindrical baffles. Analysis of omni-directional and directional radiation that appears to emanate from a plane whose normal is along the axis of the cylinder is presented.

In Chapter 3 the effect of scattering from a nearby elastic cylinder on the error in determining the direction of arrival of a plane wave is studied. The exact governing equations are used both for the cylinder and the fluid. The energy and cross-correlation methods are used to find the direction of arrival.

In Chapter 4 the effect of scattering of a plane wave by a fluid cylinder embedded in another infinite fluid on the performance of a phased circular array of hydrophones is studied. Ray theory is used to determine the interior pressure field when a plane acoustic wave is normally incident on an infinite fluid cylinder embedded in another fluid of infinite extent and the pressure field is then used to determine the directional response of a phased circular array.

Finally, in Chapter 5, the major conclusions are summarized and indications are presented regarding the research that might be done in the future to build upon the results of the present thesis.

### ACOUSTIC RADIATION FROM CYLINDRICAL TRANSDUCER ARRAYS

#### 2.1 INTRODUCTION

Cylindrical arrays of underwater electroacoustic transducers (Stansfield, 1990) can be used to radiate acoustic pressure that is omnidirectional in the azimuthal plane or appears to emanate from a planar array. They are often used in sonar systems because the directivity pattern does not change when the beam is steered in the azimuthal direction. In this chapter, an analytical method is presented to determine the omnidirectional far-field pressure radiated by a full array of pistons and the directional far-field pressure radiated by a sector of the array.

Methods used to study acoustic radiation from underwater structures can be extended to study arrays. Analytical methods have been used to study forced vibrations of fluid-loaded cylindrical shells. In the first step, the displacement on the surface is specified and used to determine the self and mutual radiation impedances (Stepanishen, 1978; Ebenezer and Stepanishen, 1991). In the second step, the force on the structure is specified and the non-uniform displacement of the fluid-loaded structure is determined by using the radiation impedances which embody all the effects of the fluid (Stepanishen, 1982; Stepanishen and Ebenezer, 1991). Then, in the third step, the displacement is used to determine the far-field pressure (Sherman, 1968).

The three-step approach can be extended, as follows, to develop an analytical model of a cylindrical array of transducers. The transducers are electrically driven by applying voltage. The displacement on the face of each transducer is approximately uniform because the face of the transducer is small with respect to a wavelength in water but depends, unless controlled, on the location of the transducer in the array. Therefore, in the first step, the self and mutual radiation impedances of pistons in an infinite rigid cylindrical baffle (Greenspom and Sherman, 1964; Yokoyama *et al.*, 2004) are determined. In the second step, the displacements of the radiating faces of the fluid-loaded transducers in response to the electrical excitation are determined by using the radiation impedances that embody all the effects of the surrounding water. The far-field radiated pressure due to the non-uniform displacement is of final interest and is determined in the third step.

Alternatively, numerical methods can be used to simultaneously solve the governing equations in the water and the transducers but these are not without difficulties. Lam (1992) analyzed an array of Tonpilz transducers. Benthien (1990) presented model and experimental results for a linear array of three flextensional transducers. He showed that the centre transducer will “take in” power at some frequencies – where the radiation resistance is negative.

It is not necessary to model the transducer if it is assumed that the displacement of each transducer is known. This assumption was made by Laird and Cohen (1952) who studied radiation from one piston source in an infinite rigid cylindrical baffle, Rolleigh *et al.* (1977) who compared the theoretical vertical beam pattern radiated by a cylindrical array with experimental results and suggested a method to suppress vertical side-lobes, and by Ebenezer (1998) who studied directional radiation from a sparse array of piston transducers used for underwater communication and obtained good agreement with experimental results. This assumption can be dropped if the displacement of each piston is calculated using steps one and two described above.

In this chapter, a method is presented to determine the pressure radiated by a cylindrical array of piston transducers with uniform displacement on the face of each transducer. It is assumed that the array is in an infinite, rigid, cylindrical baffle. In the present analysis, all the pistons in the same column or stave vibrate in-phase but the more general case of each piston vibrating with a different displacement can also be analyzed using the same method. First, an analysis of the pressure radiated by adjacent staves vibrating in-phase is presented primarily to introduce various definitions, sign conventions, and assumptions used later in the phased-array analysis. This analysis was first presented by Laird and Cohen (1952) and used by Rolleigh *et al.* (1977). Then, the effect of phase shading on the maximum pressure and the beam width are presented. Phase shading is used in directional transmission (George and Paulraj, 1985) to increase the on-axis pressure. The method of stationary phase is used to determine the far field pressure and numerical results are presented to illustrate the applications.

## **2.2 RADIATION FROM A CYLINDRICAL ARRAY**

Consider a cylindrical array of electroacoustic piston transducers as shown in Fig. 2-1. The radius of the array is  $a$ . There are  $M$  transducers in the circumferential direction and each subtends an angle  $2\pi/M$  at the centre. The height of the array is  $2L$  and there are  $N$  transducers in the vertical direction. It is assumed that the array is in an infinite,

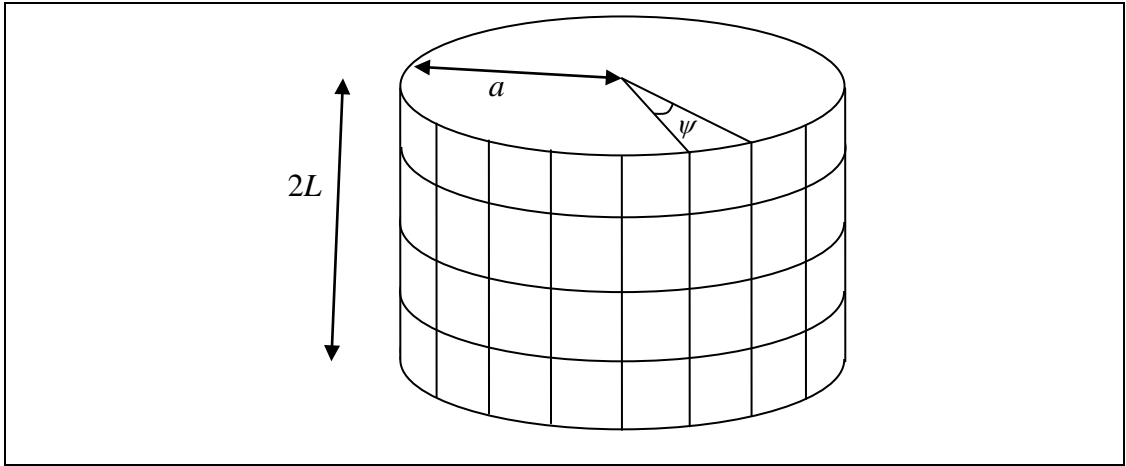


Fig. 2-1. Schematic of a cylindrical array of transducers. Each square on the curved surface of the cylinder represents the radiating face of one transducer. The radius and length of the array are  $a$  and  $2L$ , respectively. There are  $M$  transducers in the circumferential direction.  $\psi = 2\pi/M$  is the angle subtended by each stave at the centre. Each stave has  $N$  transducers in the vertical direction. It is assumed that the array is in an infinite, rigid, cylindrical baffle that is not shown.

rigid, cylindrical baffle. The density and speed of sound in the surrounding water are  $\rho$  and  $c$ , respectively.

### 2.2.1 In-phase radiation from transducers

Consider first the case where  $J \leq M$  adjacent staves vibrate uniformly with the same displacement and in-phase. Each stave consists of  $N$  transducers in the vertical direction.

The surface of the rigid baffle does not vibrate even though the vibration of the transducers causes acoustic waves in the surrounding water. Therefore, the radial component of displacement on the surface of the cylinder is expressed in the cylindrical co-ordinates  $(r, \phi, z)$  shown in Fig. 2-2 as

$$U(r, \phi, z) = \begin{cases} U_0; & |z| \leq L; r = a; |\phi| \leq \phi_0 \\ 0; & \text{otherwise} \end{cases} \quad (2-1)$$

where  $U_0$  is the amplitude and  $\phi_0 = \pi J / M$ . The term  $e^{-j\omega t}$  where  $t$  denotes time and  $\omega$  is the angular frequency is suppressed in all the equations for convenience. The radial

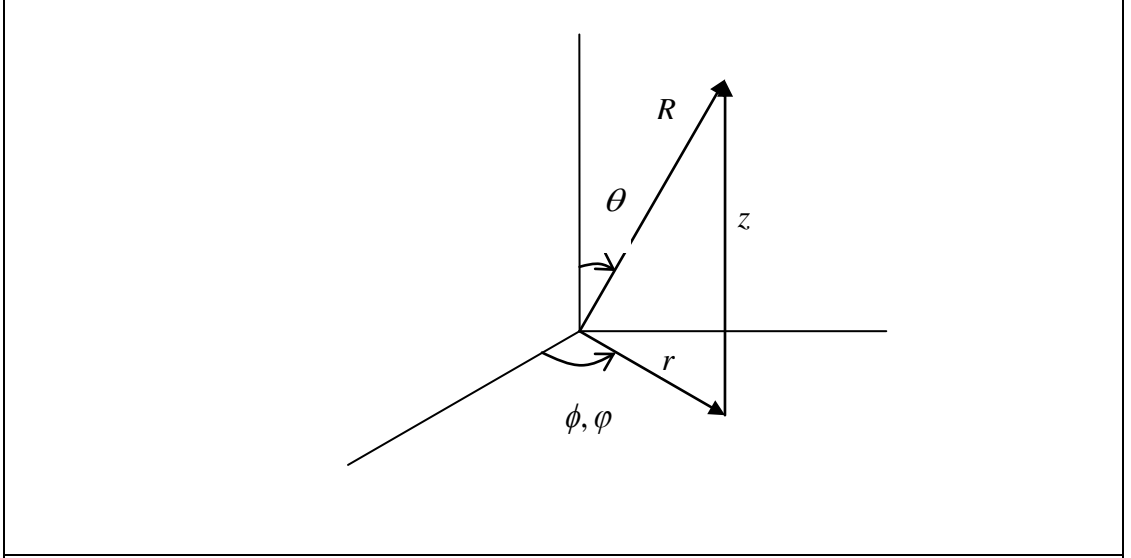


Fig. 2-2. The cylindrical coordinate system  $(r, \phi, z)$  and the spherical coordinate system  $(R, \theta, \phi)$  used in the analysis.

component of displacement on the surface of the transducers and the baffle is equal to the radial component of displacement in the water at  $r = a$  for all  $z$ . This continuity condition is used to determine coefficients in the solution to the Helmholtz wave equation that governs acoustic waves in fluids. The continuity condition can be satisfied at a large but finite number of points with various values of  $z$  on  $r = a$ . Alternatively, it can be satisfied in wavenumber – frequency space. The radial component of displacement is discontinuous at  $|z| = L$  because only the transducers vibrate and the baffle is rigid. Therefore, the second approach is used here.

A spatial Fourier transform pair is defined as:

$$\begin{aligned} \hat{H}(k_z) &= \int_{-\infty}^{\infty} H(z) e^{jk_z z} dz \\ H(z) &= \frac{1}{2\pi} \int_{-\infty}^{\infty} \hat{H}(k_z) e^{-jk_z z} dk_z \end{aligned} \quad (2-2)$$

where  $k_z$  is the wavenumber. Then, transforming Eq. (2-1) in the axial direction and expanding it using Fourier series in the  $\phi$  direction yields

$$\hat{U}(r, \phi, k_z) = 2U_0 \frac{\sin(k_z L)}{k_z} \sum_{n=0}^{\infty} a_n \cos(n\phi) \quad (2-3a)$$

where



$$a_n = \begin{cases} \phi_0 / \pi; n = 0 \\ 2 \sin(n\phi_0) / (n\pi); n = 1, 2, \dots \end{cases} \quad (2-3b)$$

The solution to the Helmholtz wave equation, in cylindrical coordinates, is expressed in wavenumber – frequency space as

$$\hat{P}(r, \phi, k_z) = \sum_{n=0}^{\infty} P_n(k_z) L_n(\beta r) \cos(n\phi) \quad (2-4a)$$

where

$$L_n(\beta r) = \begin{cases} H_n^{(1)}(\beta r); \beta \text{ real and positive, } k > 0 \\ H_n^{(2)}(\beta r); \beta \text{ real and negative, } k > 0 \\ K_n(\eta r); \eta^2 = -\beta^2, \beta \text{ imaginary} \end{cases} \quad (2-4b)$$

where  $P$  denotes pressure,  $\beta = (k^2 - k_z^2)^{0.5}$ ,  $k = \omega/c$  is the angular wave number,  $H_n^{(i)}(\cdot)$  is the  $n$ th order Hankel function of the  $i$ th kind, and  $K_n(\cdot)$  is the  $n$ th order modified Bessel function of the second kind. It is noted that the solution satisfies the Sommerfield radiation condition (Junger and Feit, 1972).

The radial displacement on the surface of the array is equal to the radial displacement in the water. It, therefore, follows that

$$\hat{U}(r, \phi, k_z) = \frac{-1}{\rho\omega^2} \frac{\partial \hat{P}(r, \phi, k_z)}{\partial r} \quad (2-5)$$

where the convention that extensional pressure is positive is used. Substituting Eqs. (2-3) and (2-4) in Eq. (2-5) yields

$$P_n(k_z) = -2\rho\omega^2 U_0 \frac{\sin(k_z L)}{k_z} \frac{a_n}{\beta L'_n(\beta a)}. \quad (2-6)$$

The pressure is then determined by substituting Eq. (2-6) in Eq. (2-4a) and evaluating the inverse Fourier transform:

$$P(r, \phi, z) = \frac{-\rho\omega^2 U_0}{\pi} \int_{-\infty}^{\infty} \frac{\sin(k_z L)}{k_z} \sum_{n=0}^{\infty} \frac{L_n(\beta r)}{\beta L'_n(\beta a)} a_n \cos(n\phi) e^{-jk_z z} dk_z \quad (2-7)$$

where prime denotes derivative with respect to the argument.

$P(r, \phi, z)$  should be an even function of  $z$  when  $U$  is an even function of  $z$ . This is seen to be the case when  $\hat{P}(r, \phi, k_z)$  is an even function of  $k_z$ . Therefore, it is assumed that  $\beta$  is real and positive when  $|k_z| < k$ . It then follows from Eqs. (2-7) and (2-4) that

$$\begin{aligned}
P(r, \phi, z) = & \frac{-\rho\omega^2 U_0}{\pi} X \\
& \left\{ \int_{-\infty}^{-k} \frac{\sin(k_z L)}{k_z} \sum_{n=0}^{\infty} \frac{K_n(\eta r)}{\eta K_n'(\eta a)} a_n \cos(n\phi) e^{-jk_z z} dk_z + \int_{-k}^k \frac{\sin(k_z L)}{k_z} \sum_{n=0}^{\infty} \frac{H_n^{(1)}(\beta r)}{\beta H_n^{(1)' }(\beta a)} a_n \cos(n\phi) e^{-jk_z z} dk_z \right. \\
& \left. + \int_k^{\infty} \frac{\sin(k_z L)}{k_z} \sum_{n=0}^{\infty} \frac{K_n(\eta r)}{\eta K_n'(\eta a)} a_n \cos(n\phi) e^{-jk_z z} dk_z \right\} \quad (2-8)
\end{aligned}$$

The pressure in the far-field is of primary interest. Using the large argument approximation for  $K_n(\eta r)$  and  $H_n^{(1)}(\beta r)$  yields

$$\begin{aligned}
P(r, \phi, z) = & \frac{-\rho\omega^2}{\pi} U_0 \sum_{n=0}^{\infty} a_n \cos(n\phi) X \\
& \left\{ \left( \frac{\pi}{2r} \right)^{0.5} \int_{-\infty}^{-k} \frac{\sin(k_z L)}{k_z} \frac{e^{-\eta r}}{\eta^{1.5} K_n'(\eta a)} e^{-jk_z z} dk_z + \left( \frac{2}{\pi r} \right)^{0.5} \int_{-k}^k \frac{\sin(k_z L)}{k_z} \frac{e^{j(\beta r - k_z z)}}{\beta^{1.5} H_n^{(1)' }(\beta a)} e^{-j(2n+1)\frac{\pi}{4}} dk_z \right. \\
& \left. + \left( \frac{\pi}{2r} \right)^{0.5} \int_{-k}^{\infty} \frac{\sin(k_z L)}{k_z} \frac{e^{-\eta r}}{\eta^{1.5} K_n'(\eta a)} e^{-jk_z z} dk_z \right\} \quad (2-9)
\end{aligned}$$

In the far field,  $r$  is very large and the first and third integrals in Eq. (2-9) are neglected because they contain exponentially decaying terms. The expression for pressure then reduces to

$$P(r, \phi, z) = \frac{-\rho\omega^2}{\pi} U_0 \left( \frac{2}{\pi r} \right)^{0.5} \sum_{n=0}^{\infty} a_n e^{-j(2n+1)\frac{\pi}{4}} \cos(n\phi) \int_{-k}^k \Gamma_n(r, \phi, z, k_z) dk_z \quad (2-10a)$$

where

$$\Gamma_n(r, \phi, z, k_z) = \frac{\sin(k_z L)}{k_z} \frac{e^{j(\beta r - k_z z)}}{\beta^{1.5} H_n^{(1)' }(\beta a)} \quad (2-10b)$$

and is evaluated by using the method of stationary phase. The primary contribution to the integral comes from  $k_z = \frac{kz}{\sqrt{r^2 + z^2}}$  and the approximation made by neglecting the first and third integrals in Eq. (2-9) is, therefore, justified. Finally, the pressure in the far field is expressed as

$$P(r, \phi, z) = \frac{j2\rho\omega^2 U_0}{\pi} \frac{\sin\left(\frac{kzL}{\sqrt{r^2 + z^2}}\right)}{\left(\frac{kz}{\sqrt{r^2 + z^2}}\right)} \frac{e^{jk\left(\frac{r^2 - z^2}{\sqrt{r^2 + z^2}}\right)}}{kr} \sum_{n=0}^{\infty} \frac{a_n e^{-jn\pi/2}}{H_n^{(1)' }\left(\frac{kra}{\sqrt{r^2 + z^2}}\right)} \cos(n\phi). \quad (2-11)$$

The pressure in the direction of the normal to the axis of the cylinder ( $z=0$ ) is of primary interest. In this direction, the above expression reduces to (Laird and Cohen, 1952)

$$P(r, \phi, z = 0) = \frac{j2\rho cL\omega U_0}{\pi r} e^{jkr} \sum_{n=0}^{\infty} a_n \frac{e^{-jn\pi/2}}{H_n^{(1)'}(ka)} \cos(n\phi). \quad (2-12)$$

Consider now the special case where all the transducer staves are vibrating in phase; i.e.  $J=M$  and  $\phi_0=\pi$ . This corresponds to omni-directional radiation in the azimuthal plane from the array. Substituting  $a_n = 0$  for  $n = 1, 2, \dots$  for this case and  $\phi = 0$  in Eq. (2-12) to determine the pressure in the direction of the normal to the surface of cylinder yields

$$P(r, \phi = 0, z = 0) = \frac{j2\rho cL\omega U_0}{\pi r} \frac{e^{jkr}}{H_0^{(1)'}(ka)}. \quad (2-13)$$

When  $ka$  is small, Eq. (2-13) reduces to

$$P(r, \phi = 0, z = 0) = \rho A_0 S \frac{e^{jkr}}{4\pi r}. \quad (2-14a)$$

where  $A_0 = -\omega^2 U_0$  is the acceleration on the surface and  $S$  is the surface area of the radiator. The expressions for far-field pressure on the axis of circular and rectangular pistons:

$$P(R, \pi/2, \phi) = \rho A_0 S \frac{e^{jkr}}{2\pi R}, \quad (2-14b)$$

and spheres

$$P(R, \pi/2, \phi) = \rho A_0 S \frac{e^{jkr}}{4\pi R}. \quad (2-14c)$$

are similar.  $S = 4\pi aL$  in Eq. (2-14a) and  $4\pi b^2$  in Eq. (2-14c) where  $b$  is the radius of the sphere. It is noted that the radiated pressure, at low frequencies, is independent of frequency and proportional to the uniform acceleration and surface area.

When  $ka$  is large, as is usually the case in arrays, Eq. (2-13) reduces to

$$P(r, \phi = 0, z = 0) = (1 + j) \sqrt{\frac{ac}{\pi}} \frac{\rho L \omega^{3/2} U_0}{r} e^{jkr}. \quad (2-15)$$

Eq. (2-15) shows that there is a  $20\log(2^{3/2}) = 9$  dB increase per octave in the radiated pressure when the displacement on the surface of the cylinder is independent of frequency. However, in transducers, the displacement on the surface will increase when

the frequency is less than the resonance frequency of the transducer and decrease after reaching a maximum. Therefore, Eq. (2-15) shows that the bandwidth of the transducer is increased in the upper sideband by the increase in the radiation efficiency of the cylindrical array.

### 2.2.2 Phased radiation from transducers in a sector

Consider now the case where the amplitude and phase of vibration of each stave is independently controlled but the displacement is uniform on the surface of each stave. This is done to simulate radiation from a rectangular array or generate a beam pattern with a desired shape in the azimuthal direction.

When  $J$  staves vibrate, the displacement on the surface of the cylinder is

$$U(a, \phi, z) = \sum_{m=1}^J U_m(a, \phi, z) \quad (2-16a)$$

where

$$U_m(a, \phi, z) = \begin{cases} A_m; & |\phi - \phi_m| \leq \phi_0; |z| \leq L \\ 0; & \text{otherwise} \end{cases} \quad (2-16b)$$

is the displacement of the  $m^{\text{th}}$  stave,  $A_m$  is complex and is used to control the amplitude and phase,  $\phi_m$  is the centre of the  $m^{\text{th}}$  stave, and  $\phi_0 = \pi / M$ .

Expanding the displacement in a Fourier series in the  $\phi$ -direction and using the Fourier transform in Eq. 2- (2) yields

$$\hat{U}(a, \phi, k_z) = \sum_{m=1}^J \hat{U}_m(a, \phi, k_z) \quad (2-17a)$$

where

$$\hat{U}_m(a, \phi, k_z) = 2A_m(\omega) \frac{\sin(k_z L)}{k_z} \sum_{n=0}^{\infty} [B_{mn} \cos(n\phi) + C_{mn} \sin(n\phi)], \quad (2-17b)$$

$$B_{mn} = \begin{cases} \phi_0; & n = 0 \\ \frac{\pi}{2} \cos(n\phi_m) \sin(n\phi_0); & n = 1, 2, \dots \end{cases}, \quad (2-17c)$$

and

$$C_{mn} = \begin{cases} 0; & n = 0 \\ \frac{2}{n\pi} \sin(n\phi_m) \sin(n\phi_0); & n = 1, 2, \dots \end{cases} \quad (2-17d)$$

The appropriate form of the solution to the Helmholtz wave equation, in cylindrical coordinates and wavenumber space is

$$\hat{P}(r, \phi, k_z) = \sum_{n=0}^{\infty} [P_n \cos(n\phi) + Q_n \sin(n\phi)] L_n(\beta r). \quad (2-18)$$

The coefficients  $P_n$  and  $Q_n$  are determined by using the displacement continuity condition at the interface between the cylinder and water in Eq. (2-5). Then, using Eq. (2-2) to determine the inverse Fourier transform of Eq. (2-18) yields

$$P(r, \phi, z) = \frac{-\rho\omega^2}{\pi} \int_{-\infty}^{\infty} \frac{\sin(k_z L)}{k_z} \sum_{n=0}^{\infty} \frac{L_n(\beta r)}{\beta L_n(\beta a)} \sum_{m=1}^J A_m(\omega) [B_{mn} \cos(n\phi) + C_{mn} \sin(n\phi)] e^{-jk_z z} dk_z. \quad (2-19)$$

Now consider the case where the phase of each stave is controlled to simulate radiation from a rectangular array. A top-view of the radiating sector of the cylindrical array is shown in Fig. 2-3 where the axis of the array passes through  $O$ . The  $J$  radiating staves are in the arc  $AB$ . Angle  $AOB$  is  $2\pi J/M$ . The centre of the radiating sector is  $C$  and angle  $AOC = \phi_c = \pi J/M$ . Let  $D$  be the centre of the  $m$ th stave. Then, angle  $AOD =$

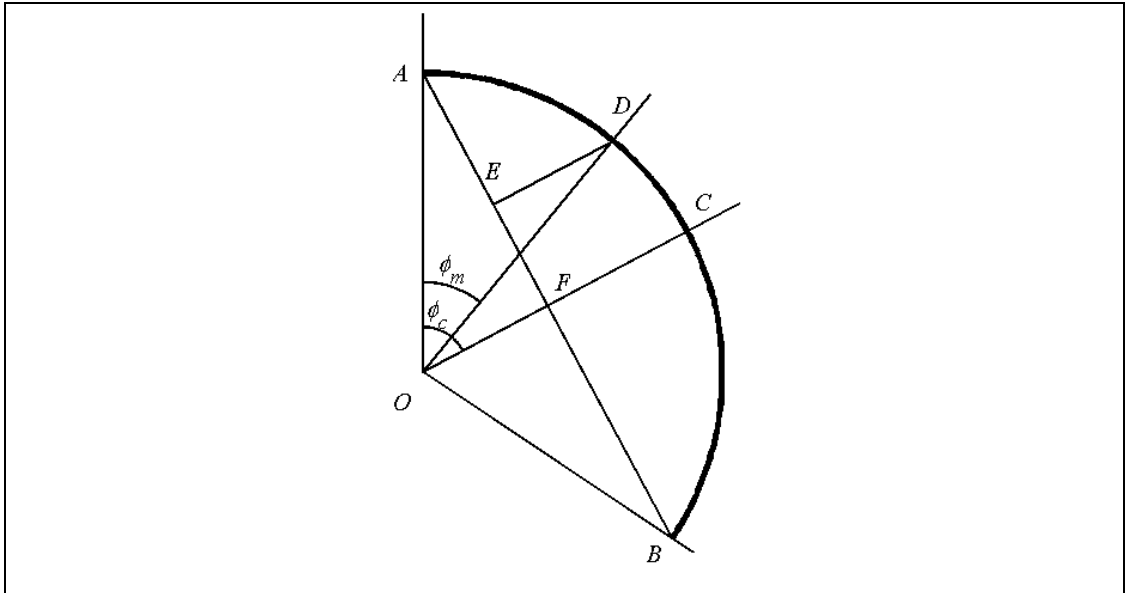


Fig. 2-3. Top-view of the radiating sector of a cylindrical array. The transducers in the arc  $ACB$  radiate. Each stave is delayed by an appropriate amount to simulate radiation from the chord  $AB$ . The delay applied to the  $m^{\text{th}}$  stave with centre at  $D$  is  $ED$ . An additional delay  $OF$  is applied to all the staves. Therefore, the total delay is  $a \cos(\phi_m - \phi_c)$ .

$$\phi_m = 2\pi(m - 0.5) / M .$$

In order to simulate radiation from a rectangular array whose width is equal to the chord  $AB$  and height is  $2L$ , a phase delay that corresponds to the distance  $ED$  is applied to the  $m$ th stave. For convenience, an additional delay that corresponds to the distance  $OF$  is applied to all the  $J$  staves. Therefore, the total delay applied to the  $m$ th stave corresponds to  $ED + OF = d_m = a \cos(\phi_m - \phi_c)$  and  $A_m = U_0 e^{jkd_m}$ .

Again, assuming that  $\beta$  is real and positive when  $|k_z| < k$ , and using the far field approximation yields

$$P(r, \phi, z) = \frac{-\rho\omega^2}{\pi} U_0 \sum_{m=0}^J e^{jkd_m} \sum_{n=0}^{\infty} [B_{mn} \cos(n\phi) + C_{mn} \sin(n\phi)] \times \quad (2-20)$$

$$\left\{ \int_{-\infty}^{-k} \frac{\sin(k_z L)}{k_z} \left( \frac{\pi}{2\eta r} \right)^{\frac{1}{2}} \frac{e^{-\eta r}}{\eta K_n^{(1)}(\eta a)} e^{-jk_z z} dk_z + \int_{-k}^k \frac{\sin(k_z L)}{k_z} \left( \frac{2}{\pi\beta r} \right)^{\frac{1}{2}} \frac{e^{j\left(\beta r - (2n+1)\frac{\pi}{4}\right)}}{\beta H_n^{(1)}(\beta a)} e^{-jk_z z} dk_z \right.$$

$$\left. + \int_{-k}^{\infty} \frac{\sin(k_z L)}{k_z} \left( \frac{\pi}{2\eta r} \right)^{\frac{1}{2}} \frac{e^{-\eta r}}{\eta K_n^{(1)}(\eta a)} e^{-jk_z z} dk_z \right\}$$

Neglecting the first and third integrals in Eq. (2-20), using the method of stationary phase, and observing that the primary contribution to the second integral in

Eq. (2-20) comes from  $k_z = \frac{kz}{\sqrt{r^2 + z^2}}$  yields

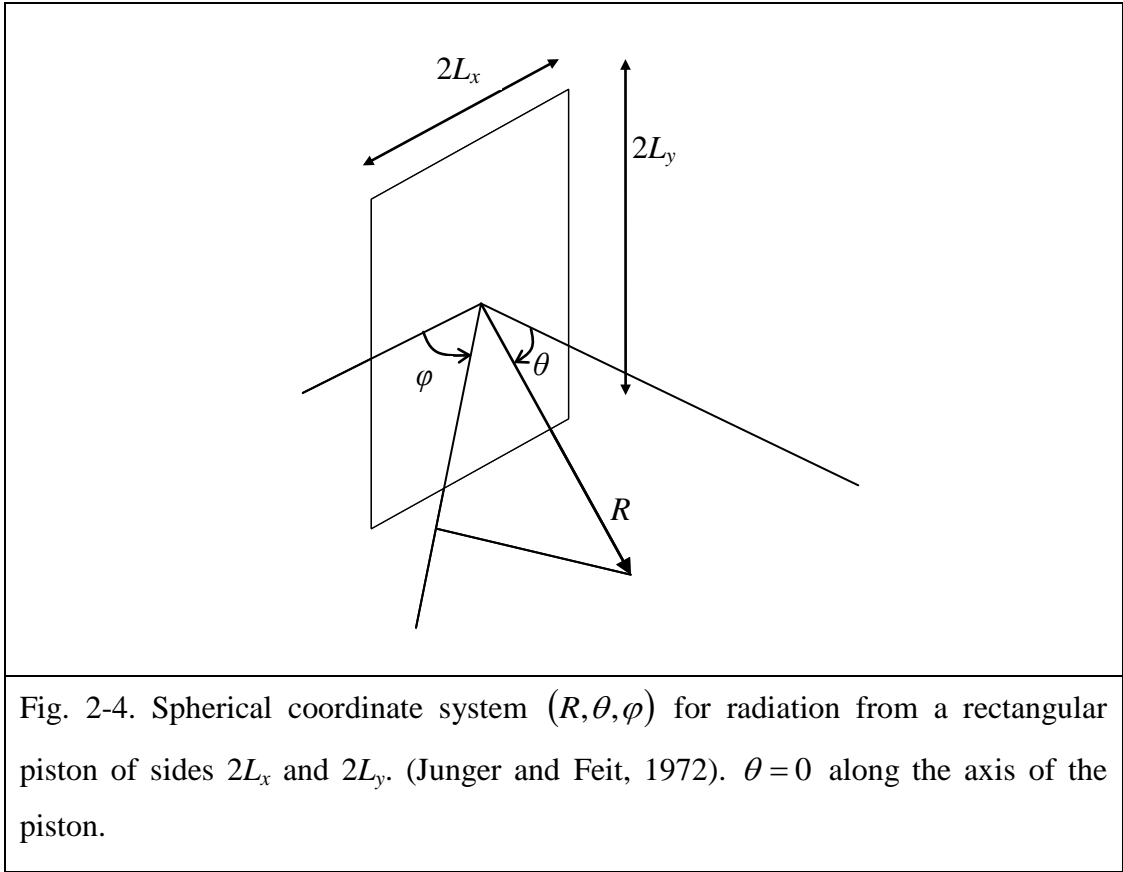
$$P(r, \phi, z) = \frac{j2\rho\omega^2 U_0}{\pi} \frac{e^{jk\left(\frac{r^2 - z^2}{\sqrt{r^2 + z^2}}\right)}}{kr} \frac{\sin\left(\frac{(kzL)}{\sqrt{r^2 + z^2}}\right)}{\left(\frac{(kz)}{\sqrt{r^2 + z^2}}\right)} \sum_{n=0}^{\infty} \frac{e^{-jn\pi/2}}{H_n^{(1)}\left(\frac{kra}{\sqrt{r^2 + z^2}}\right)} \sum_{m=1}^J [B_{mn} \cos(n\phi) + C_{mn} \sin(n\phi)] e^{jkd_m} \quad (2-21a)$$

In the direction of the normal to the axis of the cylinder ( $z=0$ ) and the pressure is expressed as

$$P(r, \phi, z = 0) = \frac{j2\rho\omega c L U_0}{\pi r} e^{jkr} \sum_{n=0}^{\infty} \frac{e^{-jn\pi/2}}{H_n^{(1)}(ka)} \sum_{m=1}^J [B_{mn} \cos(n\phi) + C_{mn} \sin(n\phi)] e^{jkd_m} . \quad (2-21b)$$

It is noted that the phased radiation only approximately simulates radiation from a rectangular piston because the vibration of each stave is in the radial direction and not in the direction along  $OC$  in Fig. 2-3.

The pressure (Junger and Feit, 1972) in the far-field of a rectangular piston, vibrating with uniform displacement  $U_0$ , in an infinite rigid baffle is also evaluated using



the method of stationary phase. It is expressed, in spherical coordinates  $(R, \theta, \varphi)$  shown in Fig. 2-4, as

$$P_p(R, \theta, \varphi) = \frac{-2\rho\omega^2 U_0}{\pi R} \frac{\sin(kL_x \sin \theta \cos \varphi)}{k \sin \theta \cos \varphi} \frac{\sin(kL_y \sin \theta \sin \varphi)}{k \sin \theta \sin \varphi} e^{jkR} \quad (2-22)$$

where  $2L_x$  is the width and  $2L_y$  is the height of the rectangular piston. The pressure along the axis of the piston is determined by using  $\theta = 0$  and reduces to Eq. (2-14b). The pressures radiated by the phased sector and the rectangular piston are compared in the next section.

### 2.3 NUMERICAL RESULTS AND DISCUSSIONS

Numerical results are presented for arrays *A* (Morris, 1984) and *B*. Details of the arrays are presented in Table 2-I. The radii of the arrays are chosen to illustrate the effect of the normalised operating frequency on the radiated patterns. The speed of sound in water is  $c = 1500$  m/s and the density of water is  $\rho = 1000$  kg/m<sup>3</sup>. After checking for convergence, all numerical results obtained using Eq. (2-21b) have been computed by replacing the infinite sum by the sum of the first 25 terms.

Table I. Characteristics of arrays

Array	Radius $a(\text{m})$	Length $2L(\text{m})$	No. of staves	Operating frequency (kHz)	Normalised operating frequency $ka$
A	0.365	0.635	30	10.5	16.1
B	0.4775	1	32	9, 7.5, 6	18, 15, 12

The stationary phase method is used to evaluate the integrals. The function  $\Gamma_n(r, \phi, z, k_z)$  in Eq. (2-10b) is shown in Fig. 2-5 to illustrate the rapid oscillations except near the stationary phase point:  $k_z = 0$ . The oscillations justify the assumption that the integral can be evaluated if the behaviour of the function near the stationary phase point is known.

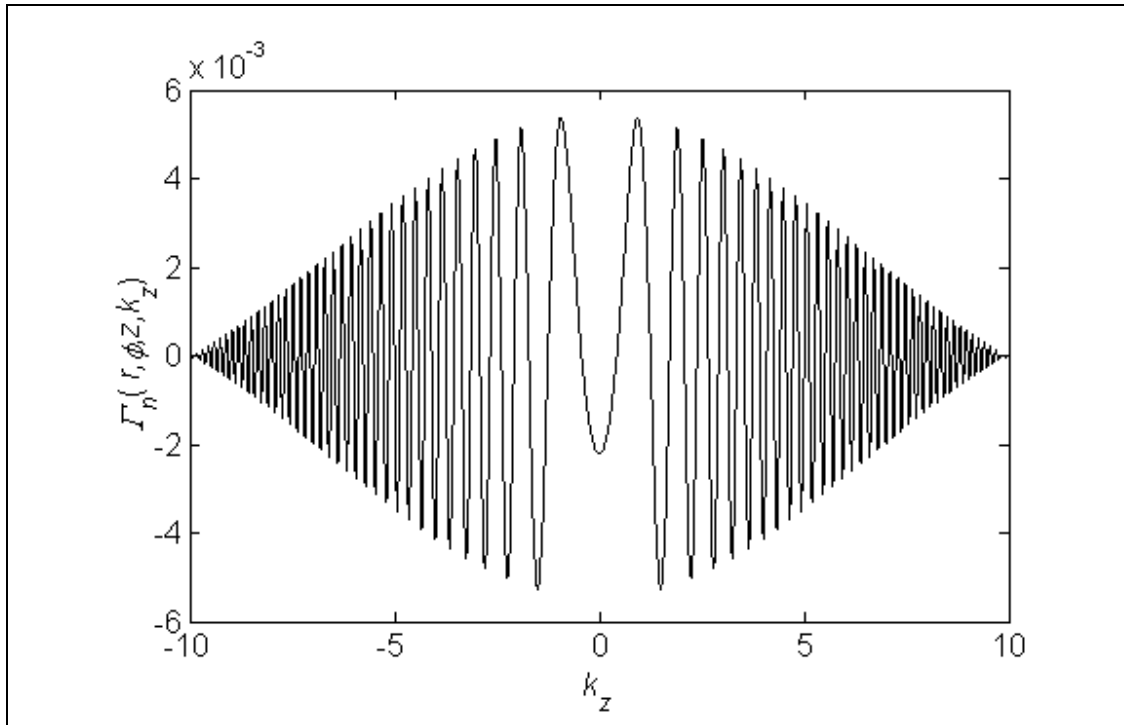


Fig. 2-5. The integrand  $\Gamma_n$ , in Eq. (2-10b), that is integrated using the method of stationary phase. It is shown for array A,  $f = 10.5$  kHz,  $n = 0$ ,  $r = 200$  m,  $z = 0$ , and  $\phi = 0$  to illustrate the rapid oscillations except near the stationary phase point:  $k_z = 0$ .



First, consider array A. The required source level (SL) of the array is specified to be 220 dB *re*  $\mu\text{Pa}$  @ 1 m in the omni-directional mode. It follows from Eq. (2-13) that the amplitude of displacement,  $U_0$ , is 0.996  $\mu\text{m}$ . It is useful to note that the hydrostatic pressure due to a 10 m water column is about  $10^5$  Pa which is the acoustic pressure corresponding to 220 dB *re*  $\mu\text{Pa}$ .

Consider, next, the case where only 9 of the 30 staves vibrate with the displacement required to generate 220 dB in the omni-directional mode. The staves in the sector vibrate in-phase and the radiation is directional. It follows from Eq. (2-12) that the source level on the axis of the sector is 221.4 dB. The directivity pattern for this case is shown in Fig. 2-6a. The maximum does not occur on the axis of the sector but at  $\pm 30$  deg. When the number of staves is increased to 11, the maxima occur at 0 deg and at  $\pm 40$  deg and the SL increases slightly to 221.5 dB as shown in Fig. 2-6b.

Consider, next, the case of phased radiation from 9 of the 30 staves in array A. The delays are chosen to simulate radiation from a rectangular piston. The displacement amplitude is again 0.996  $\mu\text{m}$ . The radiated pressure in the azimuthal plane is computed using Eq. (2-21b) and shown in Fig. 2-7 using a blue solid line. For comparison, the pressure radiated by a corresponding rectangular piston is computed using Eq. (2-22) and shown in Fig. 2-7 using a red dashed line. The piston is mounted in an infinite rigid baffle and vibrates with the same displacement. The length, 0.635 m, of the rectangular

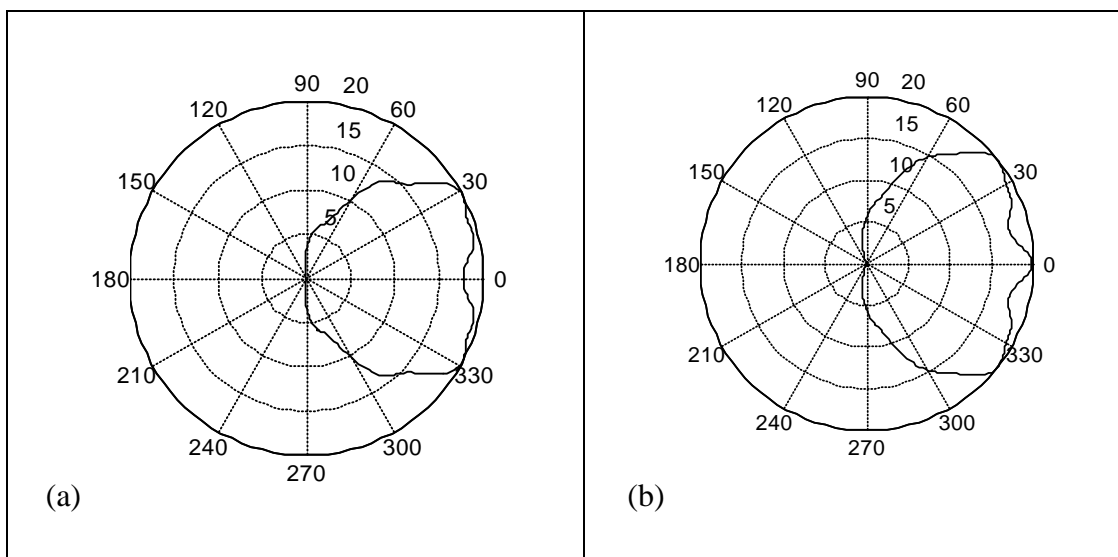


Fig. 2-6. Directivity patterns, in dB due to in-phase vibration of (a) nine and (b) eleven staves out of 30 staves in array A at 10.5 kHz.

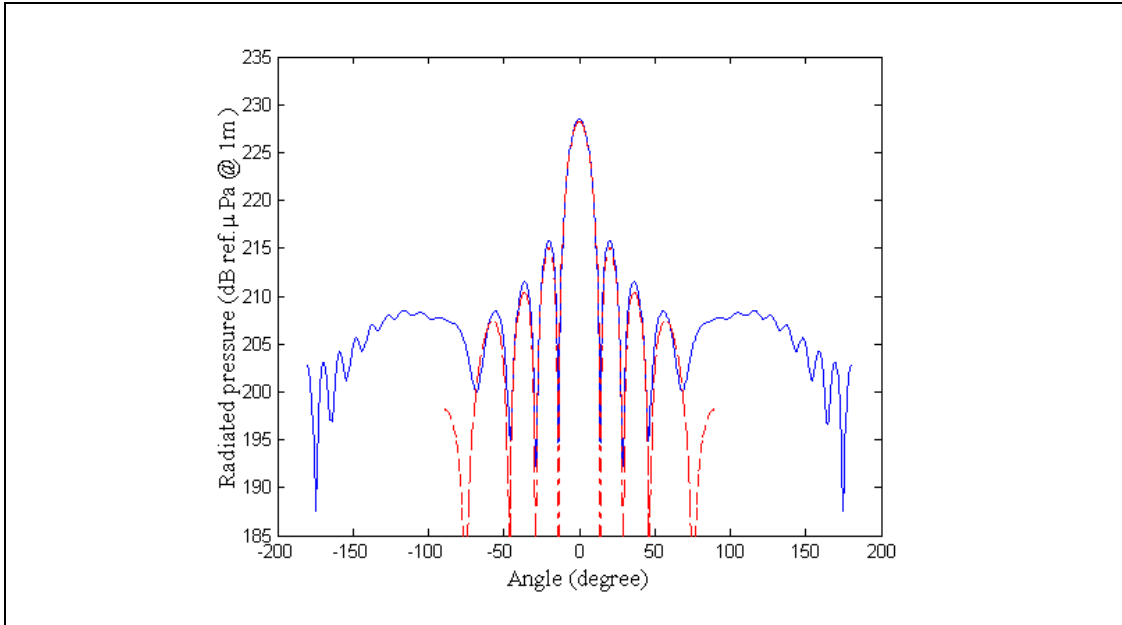


Fig. 2-7. Pressure radiated at 10.5 kHz by phased radiation of nine staves in array *A* (blue solid line) and a corresponding rectangular piston (red dashed line).

piston is equal to the length of the cylinder. Its width, 0.591 m, is equal to the length of the chord, *AB*, in Fig. 2-3. It is seen that the on-axis radiated pressure is 228.5 dB for the cylindrical sector and is a little more than the 228.2 dB radiated by the rectangular piston. The 3 dB beamwidths of the cylindrical sector and the piston are 12.15 deg and

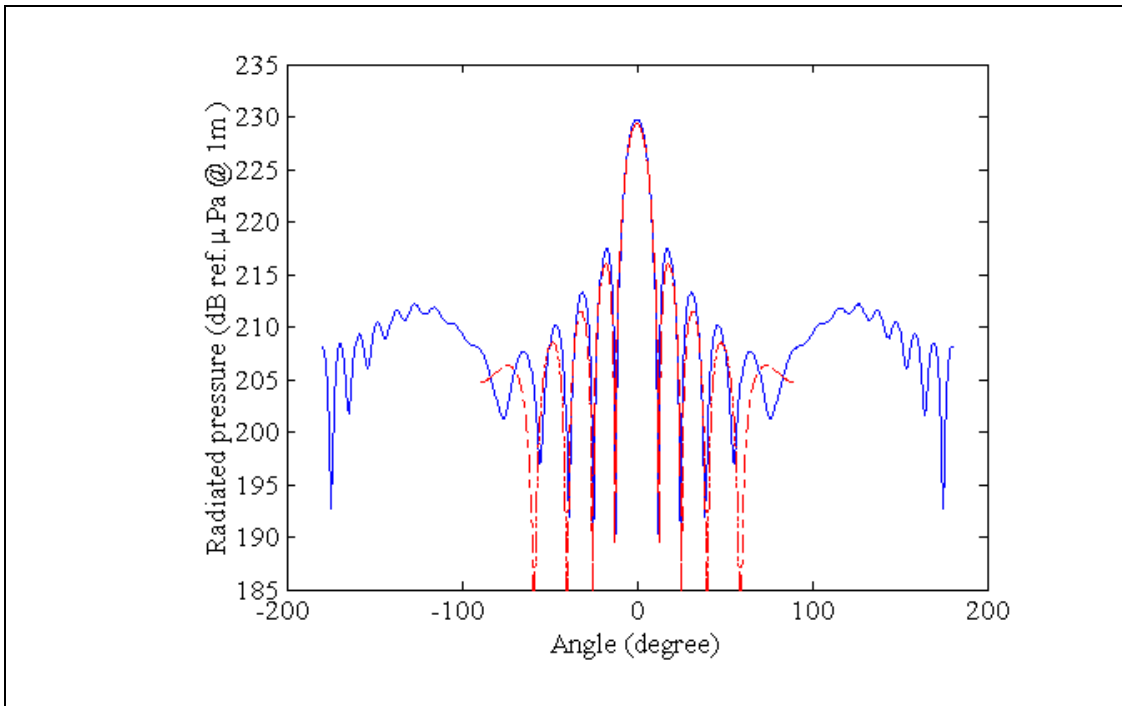


Fig. 2-8. Pressure radiated at 10.5 kHz by phased radiation of 11 staves in array *A* (blue solid line) and a corresponding rectangular piston (red dashed line).

12.3 deg, respectively. The main lobe of the cylindrical sector is a little wider and the side lobes are a little less than that of the piston. The piston does not radiate any energy behind the baffle but the sector radiates some energy in all directions.

Phased radiation by 11 staves in array *A* is shown in Fig. 2-8. The pressure on the axis is 229.8 dB and a little more than that radiated by 9 staves. The beamwidth decreases to 10.5 deg. The on-axis pressure and beamwidth for the corresponding piston are 229.3 dB and 10.9 deg, respectively.

Consider, next, radiation from array *B*. When the source level (SL) of the array is 220 dB *re*  $\mu\text{Pa}$  @ 1 m in the omni-directional mode, it follows from Eq. (2-13) that the amplitudes of displacement,  $U_0$ , are 0.697  $\mu\text{m}$ , 0.916  $\mu\text{m}$ , and 1.281  $\mu\text{m}$  at 9 kHz, 7.5kHz, and 6 kHz respectively. Consider, next, the case where only 11 of the 32 staves vibrate with the displacement required to generate 220 dB in the omni-directional mode. The staves in the sector vibrate in-phase and the radiation is directional. It follows from Eq. (2-12) that the source levels on the axis of the sector are 221.6 dB, 221.9 dB and 221.3 dB at 9 kHz, 7.5 kHz, and 6 kHz, respectively. The directivity patterns for these cases are shown in Figs. 2-9. When the radiation is at 9 kHz, the maximum occurs on the axis of the sector and also at  $\pm 40$  deg. When the radiation is at 7.5 kHz, the maximum occurs at  $\pm 28$  deg. When the radiation is at 6 kHz, the maximum does not occur on the axis of the sector but at  $\pm 18$  deg.

Consider, next, the phase radiation from array *B* at 9 kHz. The displacement amplitude required for generating omni-directional SL of 220 dB *re*  $\mu\text{Pa}$  @ 1m is 0.697  $\mu\text{m}$ . The on-axis pressure when 11 of the 32 staves vibrate in phase with this amplitude is 221.6 dB. The pressure due to phased radiation from 11 of the 32 staves designed to simulate radiation from a piston are shown in Fig. 2-10. The on-axis pressure is 229.8 dB. It is seen that the difference between the omni and phased radiation is 9.8 dB. The on-axis pressure radiated by the corresponding rectangular piston is 229.5 dB and is only a little lower than that radiated by the phased sector.

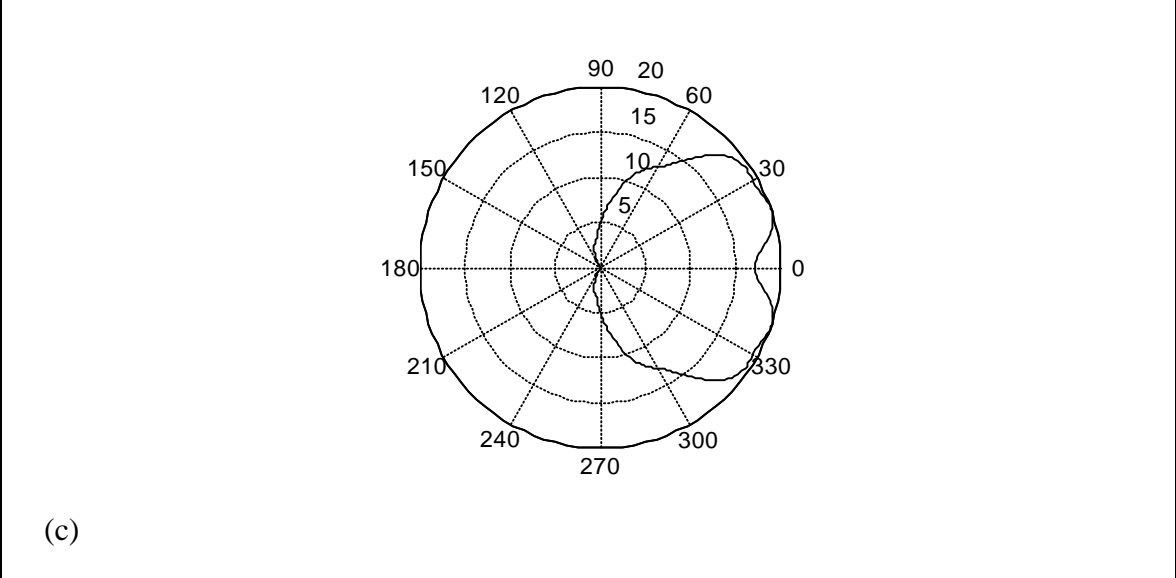
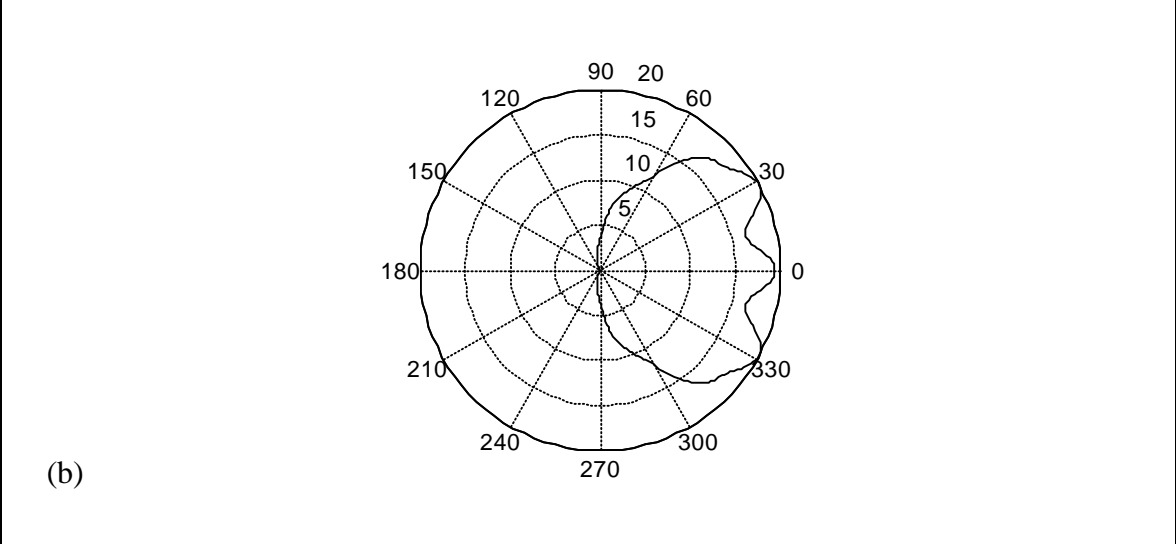
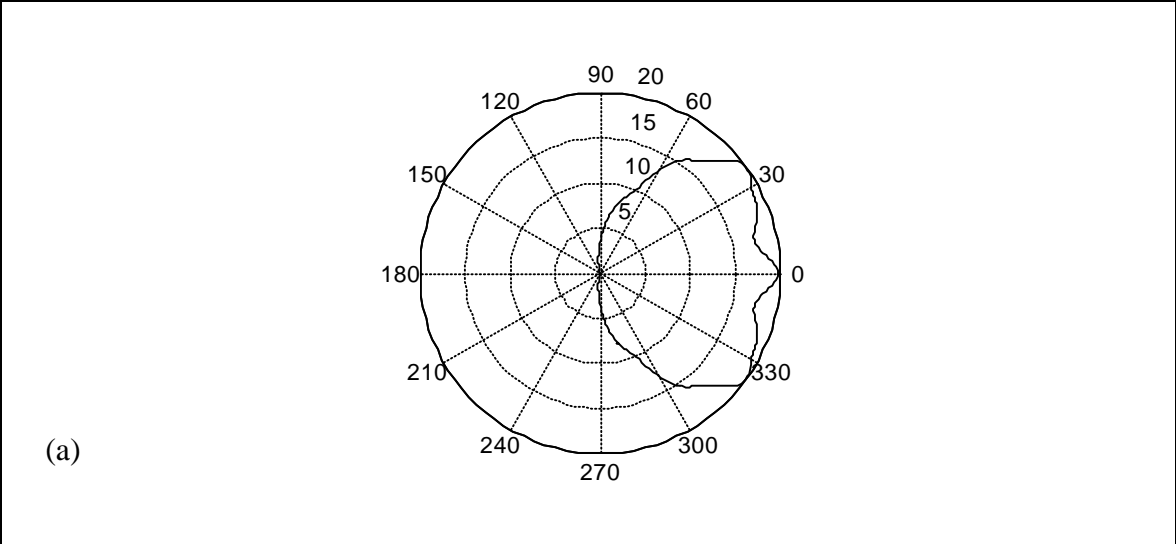


Fig. 2-9. Directivity patterns, in dB, due to in-phase vibration of 11 staves out of 32 staves in array *B* at a) 9 kHz, b) 7.5 kHz, and c) 6 kHz.

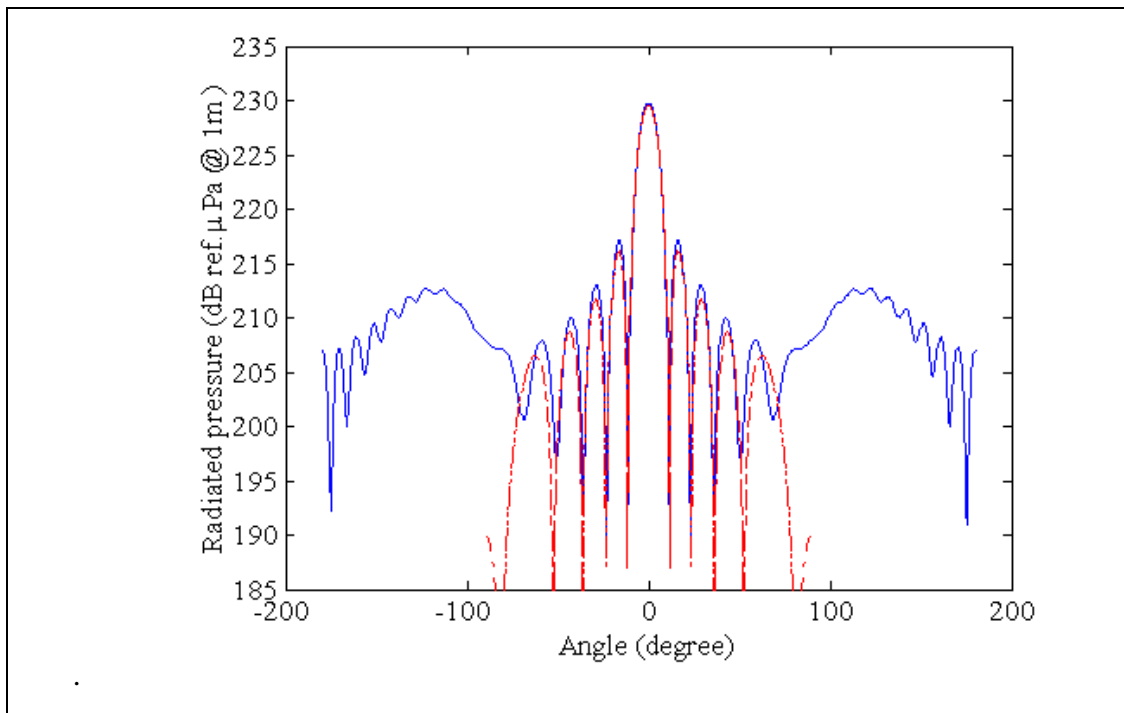


Fig. 2-10. Pressure radiated at 9 kHz by phased radiation of 11 staves in array *B* (blue solid line) and a corresponding rectangular piston (red dashed line).

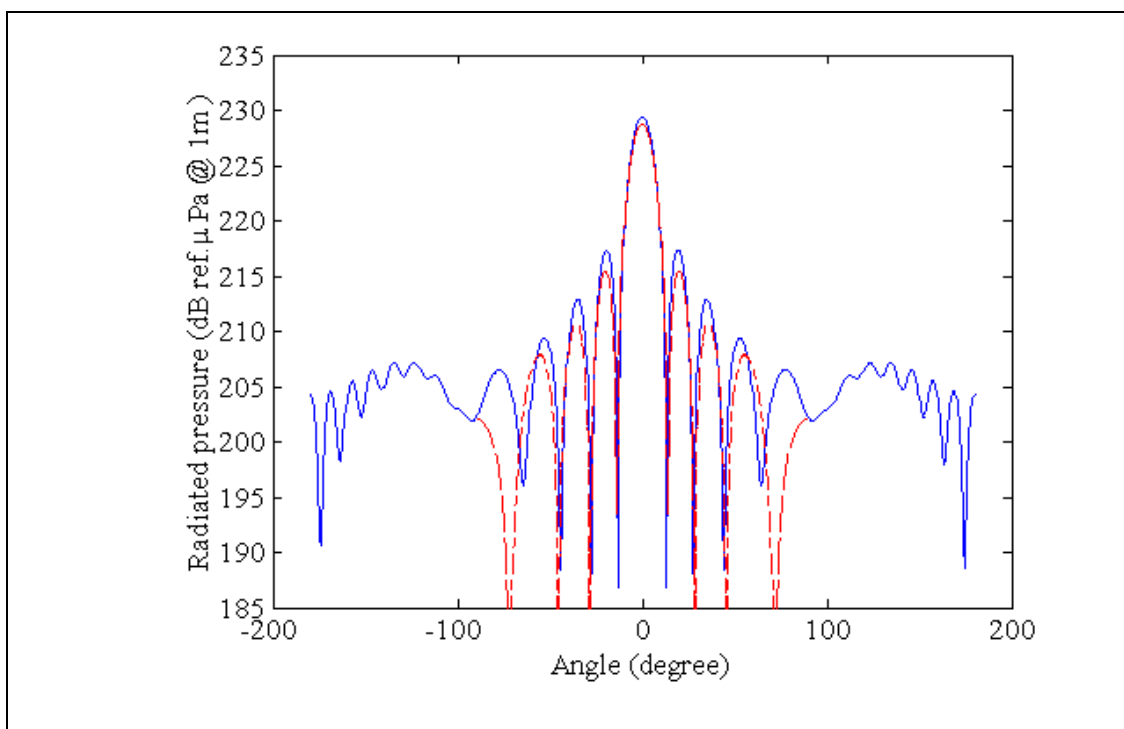


Fig. 2-11. Pressure radiated at 7.5 kHz by phased radiation of 11 staves in array *B* (blue solid line) and a corresponding rectangular piston (red dashed line).

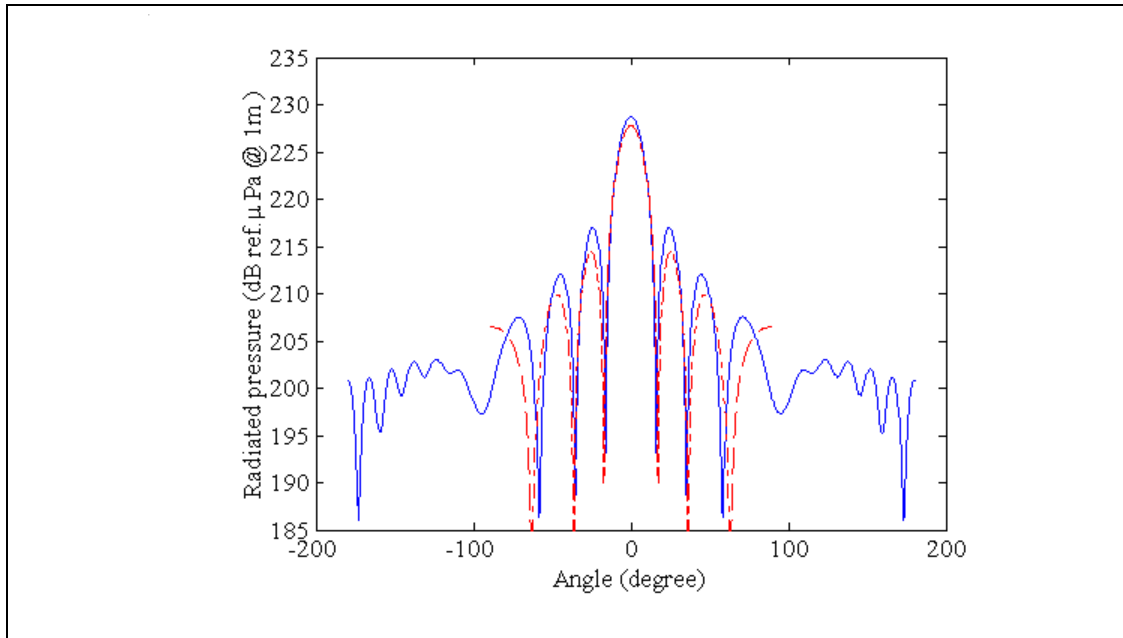


Fig. 2-12. Pressure radiated at 6 kHz by phased radiation of 11 staves in array *B* (blue solid line) and a corresponding rectangular piston (red dashed line).

Consider, next, radiation from array *B* at 7.5 kHz. The displacements required for generating omni-directional pressure of 220 dB *re*  $\mu\text{Pa}$  @ 1 m is 0.916  $\mu\text{m}$ . The on-axis pressure when 11 of the 32 staves vibrate in phase with this amplitude is 221.9 dB. The pressure due to phased radiation from 11 of the 32 staves designed to simulate radiation from a piston are shown in Fig. 2-11. The on-axis pressure is 229.4 dB and is nearly the same as the corresponding pressure for array *B*. The on-axis pressure radiated by the corresponding rectangular piston is 228.7 dB and is only a little lower than that radiated by the phased sector.

Consider, finally, radiation from array *B* at 6 kHz. The displacement amplitude required for generating omni-directional pressure of 220 dB is 1.281  $\mu\text{m}$ . The on-axis pressure when 11 of the 32 staves vibrate in phase with this amplitude is 221.3 dB. The pressure due to phased radiation from 11 of the 32 staves designed to simulate radiation from a piston is shown in Fig. 2-12. The on-axis pressure is 227.7 dB. The on-axis pressure radiated by the corresponding rectangular piston is 227.7 dB and is lower than that radiated by the phased sector.

Table 2-II. Displacements and on-axis pressures for the arrays

Array	<i>A</i>	<i>B</i>	<i>B</i>	<i>B</i>
Frequency (kHz)	10.5	9	7.5	6
Displacement ( $\mu\text{m}$ ) corresponding to 220 dB omni pressure in azimuth.	0.996	0.697	0.916	1.281
On-axis pressure due to phased radiation from sector (dB) with same displacement. 11 staves are excited.	229.8	229.8	229.4	228.7
On-axis pressure due to radiation into half-space from corresponding rectangular piston with same displacement (dB).	229.3	229.5	228.7	227.7

The displacements required to generate omni-directional pressure of 220 dB are summarized in Table 2-II. The on-axis pressures due to phased radiation with the same displacements are also shown. It is seen from the results for array *B* that the required displacement is higher at lower frequencies. As noted earlier, the on-axis pressure for the sector is only a little greater than that for the corresponding rectangular piston. This is due to the larger radiating area of the sector.

## 2.4 CONCLUSIONS

A method is presented to determine the omni-directional and directional far-field pressures radiated by cylindrical arrays of transducers. The transducers vibrate in the direction of the normal to the array surface and the effect of this is included in the model. Numerical results are presented for the array described by Morris (1984) operating at 10.5 kHz and another array operating at 9, 7.5, and 6 kHz.

Numerical results are used to show that the displacement on the surface of the array required to generate 220 dB *re*  $\mu\text{Pa}$  @ 1m in the omni-directional mode is of the order of 1 micron. Therefore, great care should be taken to ensure that there is no gap

between the components used to assemble transducers. Stansfield (1990) recommends the use of rigid adhesives at all joints.

The pressure generated by in-phase radiation of transducers in a sector is also analyzed. Numerical results show that the on-axis source level is about 221 dB when about one third of the array is radiating and the displacement is equal to that required to generate 220 dB in the omni directional mode. The maximum, in this case, does not always occur on the axis because the radiating surface is curved. This is in contrast to radiation from a planar piston radiator of any shape where the maximum always occurs on the normal to the plane because all points on the radiator are equidistant from a point at infinity and on the normal.

Phased radiation of the type used in directional transmissions is also analyzed. The amplitude of the displacement remains the same and the phase is controlled to approximately simulate radiation from a rectangular piston. The displacement is along the normal to the curved surface. The assumption that the radiator is in an infinite cylindrical baffle is used and it is, therefore, not necessary to assume that the power is radiated into a half-space. However, it is seen from Table 2-II that there is no significant difference between the on-axis pressure radiated by a cylindrical sector in an infinite cylindrical baffle and a rectangular piston in an infinite rigid planar baffle. This is also seen in Figs. 2-7, 2-8, 2-10 to 2-12 where the beam-width is nearly the same for the two cases and the pressure radiated in the rear sector is very small. The on-axis pressure radiated by the sector is a little greater than that radiated by the piston because of the slightly larger radiating area.



### ERROR IN FINDING DIRECTION OF ARRIVAL USING A LINEAR ARRAY DUE TO SCATTERING FROM AN ELASTIC CYLINDER

#### 3.1 INTRODUCTION

Sonar domes, with stiffeners, house acoustic transducer arrays that are used to determine the direction of arrival of nearly plane acoustic waves generated by distant sources. Scattering of the waves, by the stiffener, disturbs the pressure field and causes a difference between the actual and measured directions of arrival. The errors, when using energy and split beam correlation methods, in finding the direction of arrival (DOA), caused by the presence of a stiffener in the form of a circular elastic cylinder near a linear array of hydrophones, are investigated.

Characterization of arrays of hydrophones is done in free-field conditions with no boundaries or scatterers in the neighborhood of the array. However, arrays are installed inside a sonar dome that is often constructed using thin plates and stiffeners. Acoustic plane waves from distant sources are partly reflected by the thin plates. The transmitted waves are scattered by the stiffeners and reach the hydrophones. In some cases, the frequency of interest is such that the cross-section of the stiffener is comparable to the wavelength in water and the length of the stiffener is several times the wavelength. The presence of the effectively infinite cylinder causes significant changes in the magnitudes and phases of the pressures at the locations of the hydrophones in the array (Mathew *et al.*, 2010).

Scattering from various types of cylinders is studied. Morse and Ingard (1968) present the scattered pressure, displacement, and intensity fields when a plane wave is normally incident on a rigid infinite cylinder. Junger and Feit (1972) present the pressure field when a plane wave is normally incident on rigid finite and rigid infinite cylinders. Skudrzyk (1971) presents the pressure scattered from rigid and fluid cylinders. Faran (1951) presents the calculated and measured directivity of the pressure field scattered by an infinite elastic cylinder. Akay *et al.* (1993) present the scattering from fluid-filled concentric elastic cylindrical shells using exact equations of elasticity and modified Donnell's shell theory. The method of separation of variables and a Fourier series expansion in the circumferential direction are used in all the above investigations.

Scattering from cylindrical objects is studied when detection or imaging is of interest. Schock *et al.* (2001) present a sonar system with a linear array of projectors and a planar array of hydrophones that generates images of cylindrical pipes, cables, and ordnance buried below the seabed. Teutsch and Kellermann (2006) present modal array signal processing algorithms to find multiple acoustic sources using circular microphone arrays mounted on cylindrical baffles. They present the effect of the baffles on detection and localization.

Forward scattering is of interest when the target is passing between the source and the receiver but the scenario has been likened to looking into the sun because the pressure in the incident wave is higher than that in the scattered wave unless the target resonates. Recently, interest in the use of forward scattering for detection has revived, leading to measurements in tanks, marine environments, and theoretical calculations.

Ding (1997) presents experimental results obtained in a tank with objects between a 38 kHz source and a hydrophone. The transducers are 7.69 m apart. Measurements, done using long bursts, with and without a target to determine the scattered pressure, are in agreement with theoretical results. Bucaro *et al.* (2009) also present experimental results obtained by doing measurements in a tank using a cylindrical object of length 18 in and diameter 5 in as the target and a broad band pulse. The scattered pressures obtained by doing measurements with and without the target are in good agreement with theoretical results. The perpendicular distance between the source and the receiver line array is 4.7 m. They also propose a method that is useful for measurements in marine environments and does not require measurements with and without a target. Bucaro *et al.* (2011) later conducted experiments with a spherical shell of diameter 60 cm lying on the bottom of the Gulf of Mexico, used a wavenumber filter to remove the incident wave, and validated the method. Sabra *et al.* (2010) experimentally demonstrate using the 10 – 20 kHz band that a cylinder of length 2 m and diameter 36 cm towed across the line joining a vertical source array and a vertical receiver array can be detected even in the presence of noise. They use principal component analysis of the forward scattered field. The distance between the arrays is 160 m and the distance between the cylinder and the receiver array is 110 m.

Han *et al.* (2009) propose an algorithm for bearing and range estimation of a cylinder fully buried under the seabed. They consider the reflection and transmission of an acoustic wave at the water-sediment interface. They use one source, an array of hydrophones, and a multiple signal classification (MUSIC) method. Horiki and Newman

(2006) present a method to determine the direction of arrival of multiple electromagnetic signals after using an iterative method to remove the effects of nearby scatterers and mutual coupling between receivers.

In this chapter, the error in finding the direction of arrival of a plane wave due to scattering from a nearby infinite elastic cylinder is investigated. The cylinder is modeled using exact governing equations. Two classical signal processing methods are used in the study. In one method to determine the direction of arrival of the wave, often called energy method (Knight *et al.*, 1981; Waite, 1998), the array is virtually steered to various directions. When the wave-front is parallel to the virtual array, the outputs from all the hydrophones are in phase. When the wave is incident at an angle, the outputs are not in phase. Therefore, the sum of the outputs in the former case is greater than in the latter. It is concluded that the wave is arriving from a particular direction when the sum of the outputs of the hydrophones, when the array is steered to that direction, is greater than that when the array is steered to other directions. In another method, known as split beam correlation method (Knight *et al.*, 1981; Waite, 1998) the array is split into two half-arrays. The outputs from the hydrophones in each half-array are summed. The outputs from the half-arrays are then cross correlated. The time at which the split beam correlation is maximum is used to determine the direction of arrival. Numerical results are presented to illustrate the error in determining the direction of arrival because of the cylinder.

### 3.2 ACOUSTIC SCATTERING

Consider a linear array of uniformly spaced  $2H$  point hydrophones on the  $x$  axis of a  $(x, y, z)$  Cartesian coordinate system as shown in Fig. 3-1. The distance between adjacent hydrophones is  $d$ . The coordinates of the  $h$ th hydrophone are  $[x_h, 0, 0]$ ,  $h = 1, 2, \dots, 2H$  where  $x_h = (-2H+2h-1)d/2$ .

An infinite elastic isotropic circular cylinder of radius  $a$  is located in front of the array as shown in Fig. 3-1. The axis of the cylinder is parallel to the  $z$  axis. The centre of the cylinder is at  $(0, b, 0)$  where the perpendicular distance between the array and the axis of the cylinder is  $b$ . A plane acoustic harmonic wave is traveling at an angle  $\alpha$  to the  $y$  axis as shown in Fig. 3-1. It is scattered by the cylinder and the resulting wave is not plane at the array. It is of interest to determine the direction of arrival,  $\alpha$ , of the plane

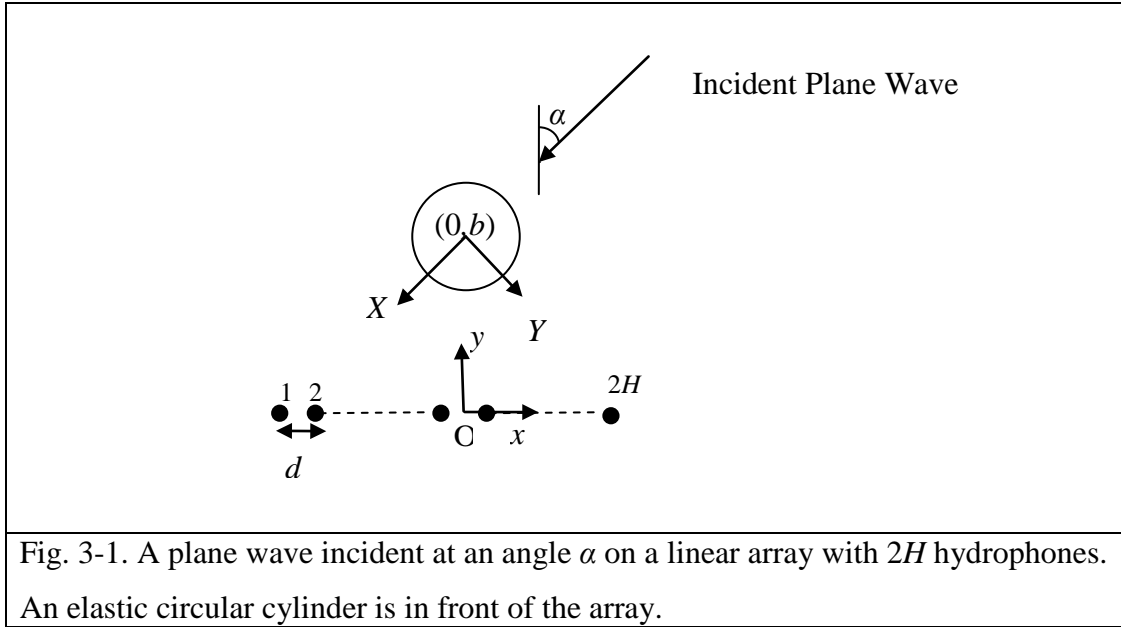


Fig. 3-1. A plane wave incident at an angle  $\alpha$  on a linear array with  $2H$  hydrophones. An elastic circular cylinder is in front of the array.

wave in the presence of the cylinder.

It is convenient to define another Cartesian coordinate system  $(X, Y, Z)$  with origin at the centre of the cylinder, i.e., at  $(0, b, 0)$  in the  $(x, y, z)$  coordinate system. The  $X$  axis is such that the incident plane wave is traveling along the  $+X$  axis.

The pressure due to the plane wave of unit amplitude is expressed in the  $(X, Y, Z)$  coordinate system as,

$$\hat{p}_i(t) = \hat{P}_i(\omega)e^{-j\omega t} = P_0 e^{j(kX - \omega t)} \quad (3-1)$$

where  $\hat{\phantom{x}}$  denotes that the function is expressed in the  $(X, Y, Z)$  coordinate system,  $P_0$  is the amplitude of the wave,  $k = \omega / c$  is the wavenumber,  $\omega = 2\pi f$  is the angular frequency,  $t$  is the time,  $f$  is the frequency, and  $c$  is the speed of sound in water.

It is convenient to define a cylindrical coordinate system  $(r, \theta, Z)$  with origin at the origin of the  $(X, Y, Z)$  coordinate system to analyze scattering and determine the pressure at the hydrophone locations. The  $Z$  axis is the same in both these coordinate systems. In the cylindrical coordinate system, Eq. (3-1) is expressed as

$$P_i(\omega) = P_0 e^{jkr \cos \theta} \quad (3-2)$$

where  $X = r \cos \theta$  and  $Y = r \sin \theta$ . The time dependence factor  $e^{-j\omega t}$  is suppressed for convenience here and in many other equations.

Using a relationship among the exponential, the trigonometric, and the Bessel functions, Eq. (3-2) is expressed as (Morse and Ingard, 1968)

$$P_i(\omega) = P_0 \sum_{n=0}^{\infty} \varepsilon_n j^n J_n(kr) \cos n\theta \quad \varepsilon_n = \begin{cases} 1 & n=0 \\ 2 & n>0 \end{cases} \quad (3-3)$$

where  $J_n(\cdot)$  is the  $n$ th order Bessel function of the first kind.

The infinite plane wave is traveling along the normal to the axis of the cylinder. Therefore, there is no displacement in the axial direction and there can be no dependence on  $z$  and this is a plane-strain case. The stress-strain relations of the cylinder are expressed as

$$\begin{bmatrix} \tau_{rr}(\omega) \\ \tau_{r\theta}(\omega) \\ \tau_{\theta\theta}(\omega) \end{bmatrix} = \begin{bmatrix} \lambda + 2\mu & 0 & \lambda \\ 0 & \mu & 0 \\ \lambda & 0 & \lambda + 2\mu \end{bmatrix} \begin{bmatrix} S_{rr}(\omega) \\ S_{r\theta}(\omega) \\ S_{\theta\theta}(\omega) \end{bmatrix} \quad (3-4)$$

where  $\tau_{rr}(\omega)$ , and  $\tau_{\theta\theta}(\omega)$  are the normal components of stress in the radial and tangential directions and  $\tau_{r\theta}(\omega)$  is the shear component of stress respectively. The components of strain have similar definitions.  $\lambda$  and  $\mu$  are Lamé's constants and are defined as  $\lambda = Y\sigma/(1+\sigma)(1-2\sigma)$  and  $\mu = Y/2(1+\sigma)$  where  $Y$  and  $\sigma$  are the Young's modulus and Poisson ratio respectively. The strain-displacement relations are

$$[S_{rr}(\omega), S_{r\theta}(\omega), S_{\theta\theta}(\omega)] = \left[ \frac{\partial U(\omega)}{\partial r}, \frac{\partial V(\omega)}{\partial r} - \frac{V(\omega)}{r} + \frac{1}{r} \frac{\partial U(\omega)}{\partial \theta}, \frac{1}{r} \frac{\partial V(\omega)}{\partial \theta} + \frac{U(\omega)}{r} \right] \quad (3-5)$$

where  $U(\omega)$  and  $V(\omega)$  are the radial and tangential displacements of the cylinder, respectively. The equations of dynamic equilibrium are (Sokolnikoff, 1956)

$$\begin{aligned} \frac{\partial \tau_{rr}(\omega)}{\partial r} + \frac{1}{r} \frac{\partial \tau_{r\theta}(\omega)}{\partial \theta} + \frac{\tau_{rr}(\omega) - \tau_{\theta\theta}(\omega)}{r} &= -\rho_1 \omega^2 U(\omega) \\ \frac{\partial \tau_{r\theta}(\omega)}{\partial r} + \frac{1}{r} \frac{\partial \tau_{\theta\theta}(\omega)}{\partial \theta} + \frac{2\tau_{r\theta}(\omega)}{r} &= -\rho_1 \omega^2 V(\omega) \end{aligned} \quad (3-6)$$

where  $\rho_1$  is the density of the elastic cylinder.

Substituting Eqs. (3-4) and (3-5) in Eq. (3-6) yields the following exact equations of motion:

$$\begin{aligned} (\lambda + 2\mu) \left[ \frac{\partial^2 U}{\partial r^2} + \frac{1}{r} \frac{\partial U}{\partial r} - \frac{1}{r^2} U \right] + \left( \frac{\lambda + \mu}{r} \right) \frac{\partial^2 V}{\partial r \partial \theta} - \left( \frac{\lambda + 3\mu}{r^2} \right) \frac{\partial V}{\partial \theta} + \frac{\mu}{r^2} \frac{\partial^2 U}{\partial \theta^2} &= -\rho_1 \omega^2 U \\ \left( \frac{\lambda + \mu}{r} \right) \frac{\partial^2 U}{\partial r \partial \theta} + \left( \frac{\lambda + 3\mu}{r^2} \right) \frac{\partial U}{\partial \theta} + \mu \left[ \frac{\partial^2 V}{\partial r^2} + \frac{1}{r} \frac{\partial V}{\partial r} - \frac{1}{r^2} V \right] + \left( \frac{\lambda + 2\mu}{r^2} \right) \frac{\partial^2 V}{\partial \theta^2} &= -\rho_1 \omega^2 V \end{aligned} \quad (3-7)$$

where the argument  $\omega$  is suppressed for convenience. The solution to these equations are expressed in the form (Faran, 1951)

$$U(\omega) = \sum_{n=0}^{\infty} \left[ \frac{nA_n}{r} J_n(k_2 r) - B_n k_1 J_n'(k_1 r) \right] \cos n\theta \quad (3-8a)$$

$$V(\omega) = \sum_{n=0}^{\infty} \left[ \frac{nB_n}{r} J_n(k_1 r) - A_n k_2 J_n'(k_2 r) \right] \sin n\theta \quad (3-8b)$$

where  $A_n, B_n$  are unknown coefficients to be determined and prime denotes the derivative with respect to the argument,  $k_1 = \omega/c_1$  and  $k_2 = \omega/c_2$ , and  $c_1 = [(\lambda + 2\mu)/\rho_1]^{0.5}$  and  $c_2 = (\mu/\rho_1)^{0.5}$  are the speeds of compressional and shear waves in the cylinder, respectively. Substituting Eqs. (3-5) and (3-8) in Eq. (3-4) yields the components of stress:

$$\tau_{rr}(\omega) = \left\{ 2\mu \sum_{n=0}^{\infty} \left[ \frac{nA_n k_2}{r} J_n'(k_2 r) - B_n k_1^2 J_n''(k_1 r) - \frac{nA_n}{r^2} J_n(k_2 r) \right] + \lambda k_1^2 \sum_{n=0}^{\infty} B_n J_n(k_1 r) \right\} \cos n\theta \quad (3-9a)$$

$$\tau_{r\theta}(\omega) = \mu \left\{ \sum_{n=0}^{\infty} \left[ \frac{-n^2 A_n}{r^2} J_n(k_2 r) + \frac{2nB_n}{r} k_1 J_n'(k_1 r) - \frac{2nB_n}{r^2} J_n(k_1 r) - A_n k_2^2 J_n''(k_2 r) + \frac{A_n}{r} k_2 J_n'(k_2 r) \right] \sin n\theta \right\} \quad (3-9b)$$

where " denotes the second derivative with respect to the argument. The radial component of displacement in the incident wave, associated with the pressure in Eq. (3-3), is expressed as

$$U_i(\omega) = \frac{1}{\rho\omega^2} \frac{\partial P_i(\omega)}{\partial r} = \frac{P_0 k}{\rho\omega^2} \sum_{n=0}^{\infty} \varepsilon_n j^n J_n'(kr) \cos n\theta \quad (3-10)$$

where  $\rho$  is the density of water.

The incident plane wave scatters in all directions. The scattered outgoing wave is a solution to the Helmholtz wave equation and must be symmetrical about  $\theta=0$ . Therefore, the scattered pressure is expressed as (Faran, 1951)

$$P_s(\omega) = \sum_{n=0}^{\infty} C_n H_n^{(1)}(kr) \cos(n\theta) \quad (3-11)$$

where  $H_n^{(1)}(\cdot)$  is the Hankel function of the first kind of order  $n$  and the factors  $C_n$  are coefficients to be determined. The radial component of displacement associated with this wave is

$$U_s(\omega) = \frac{1}{\rho\omega^2} \frac{\partial P_s(\omega)}{\partial r} = \frac{k}{\rho\omega^2} \sum_{n=0}^{\infty} C_n H_n^{(1)}(kr) \cos n\theta \quad (3-12)$$

At the interface between the elastic cylinder and the surrounding water, the radial component of displacement and pressure in water are equal to the radial components of displacement and stress in the elastic cylinder respectively. Therefore,

$$P_i(\omega) + P_s(\omega) = -\tau_{rr}(\omega) \quad \text{at } r=a, \quad (3-13a)$$

and

$$U_i(\omega) + U_s(\omega) = U(\omega) \quad \text{at } r=a. \quad (3-13b)$$

Further, at the surface of the elastic cylinder the tangential component of shear stress must vanish. Therefore,

$$\tau_{r\theta}(\omega) = 0 \quad \text{at } r=a. \quad (3-13c)$$

Substituting Eq. (3-3), (3-8) – (3-12) in the boundary condition Eqs. (3-13) yields

$$[F][A_n \ B_n \ C_n]^T = [G] \quad (3-14)$$

for the  $n^{\text{th}}$  mode where

$$[F] = \begin{bmatrix} 2\mu n[(k_2 a)J_n'(k_2 a) - J_n(k_2 a)] & (k_1 a)^2[\lambda J_n(k_1 a) - 2\mu J_n''(k_1 a)] & a^2 H_n^{(1)}(ka) \\ -nJ_n(k_2 a) & (k_1 a)J_n'(k_1 a) & \frac{ka}{\rho\omega^2} H_n^{(1)}(ka) \\ k_2 a J_n'(k_2 a) - (k_2 a)^2 J_n''(k_2 a) - n^2 J_n(k_2 a) & 2n[(k_1 a)J_n'(k_1 a) - J_n(k_1 a)] & 0 \end{bmatrix} \quad (3-15a)$$

and

$$G = \begin{bmatrix} -P_0 \varepsilon_n(j)^n a^2 J_n(ka) \\ -\left(\frac{P_0 ka}{\rho\omega^2}\right) \varepsilon_n(j)^n J_n'(ka) \\ 0 \end{bmatrix} \quad (3-15b)$$

where  $[\ ]^T$  denotes the transpose of a matrix. Solving Eq. (3-15) for  $C_n$  and using it in Eq. (3-11) yields the scattered pressure and the total pressure  $P(\omega) = P_i(\omega) + P_s(\omega)$ .

For the special case of a rigid cylinder the displacement on the surface is zero. Therefore,

$$U_i(\omega) + U_s(\omega) = 0 \quad \text{at } r=a. \quad (3-16)$$

Substituting Eqs. (3-10) and (3-12) in Eq. (3-16) yields

$$C_n = \begin{cases} \frac{-P_0 J_1(ka)}{H_1^{(1)}(ka)} & n = 0 \\ -2P_0 j^n \left\{ \frac{J_{n-1}(ka) - J_{n+1}(ka)}{H_{n-1}^{(1)}(ka) - H_{n+1}^{(1)}(ka)} \right\} & n > 0 \end{cases} \quad (3-17)$$

and the scattered pressure is determined using Eq. (3-11).

In the cylindrical coordinate system, the  $h$ th hydrophone is at  $(r_h, \theta_h, 0)$  where

$$r_h^2 = b^2 + x_h^2 \quad (3-18a)$$

and

$$\theta_h = \alpha + \tan^{-1}(x_h / b) \quad (3-18b)$$

where  $x_h = (-2H + 2h - 1)d / 2$  is the location of the  $h$ th hydrophone. Therefore, at the location of the  $h$ th hydrophone, the incident pressure,  $P_i^h(\omega)$ , is obtained using Eq. (3-3) and expressed as

$$P_i^h(\omega) = P_0 \sum_{n=0}^{\infty} \varepsilon_n j^n J_n(kr_h) \cos(n\theta_h), \quad \varepsilon_n = \begin{cases} 1 & n = 0 \\ 2 & n > 0 \end{cases}, \quad (3-19a)$$

and the scattered pressure,  $P_s^h(\omega)$ , is obtained using Eq. (3-11) and expressed as

$$P_s^h(\omega) = \sum_{n=0}^{\infty} C_n H_n^{(1)}(kr_h) \cos(n\theta_h). \quad (3-19b)$$

Then, they are used to determine the total pressure

$$P^h(\omega) = P_i^h(\omega) + P_s^h(\omega) \quad (3-19c)$$

at the location of the  $h$ th hydrophone.

### 3.3 ERROR IN FINDING DIRECTION OF ARRIVAL (DOA)

The pressures at the hydrophone locations in the linear array are measured and used to compute the DOA of the incident plane wave. The elastic cylinder in the neighborhood of the array disturbs the pressure field and causes a difference between the actual and computed directions of arrival. The errors in finding the DOA, when using two classical, data-independent, signal processing methods, called energy and split beam correlation methods, are investigated.

In practice, errors are caused by ambient and self noise, errors in the positions of the hydrophones, non-identical hydrophones and electronic components, the curvature of the dome, and the presence of stiffeners. The total error should preferably be less than



0.3 degree and the error due to the curved dome including stiffeners should be less than 0.1 degree. Here, the error due the presence of a stiffener alone is investigated.

In practical applications, due to the presence of noise, it is possible to only estimate the direction of arrival. Further, in most cases, the exact location of the source of the acoustic waves and the correct direction of arrival are not known and it is, therefore, not possible to determine the error in finding or estimating the direction of arrival. Under some controlled conditions, the location of the source can be measured (with some error) using radar or other methods and the approximate error in finding the direction of arrival using acoustic methods can be determined. However, in most cases, this approximate error is the sum of the errors due to several factors mentioned earlier. In an acoustic tank, the angle between the normal to the array and the line joining the source to the centre of the array can be measured – but only by using very sophisticated and accurate equipment. Therefore, it is convenient to study the error due to one of the factors (stiffener) using theoretical models.

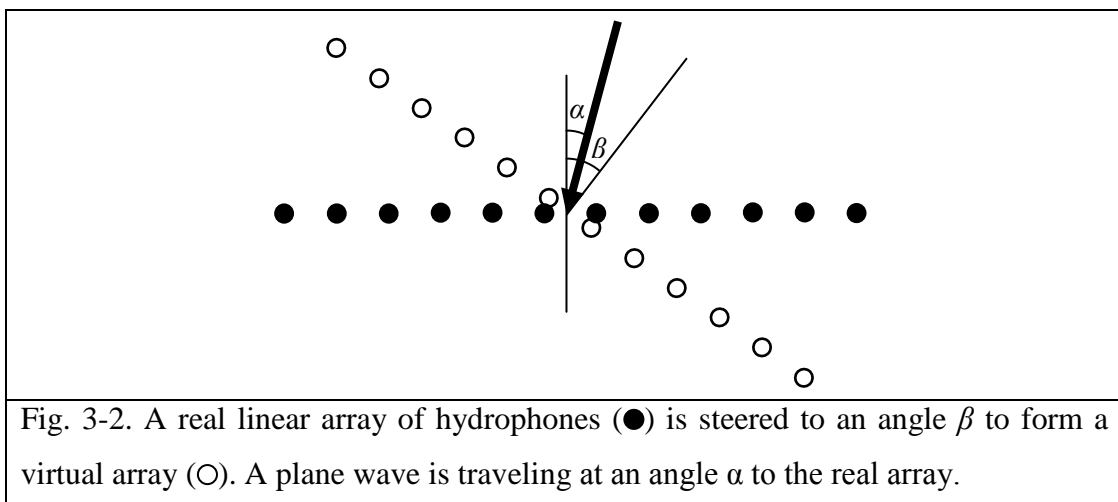
### 3.3.1 Energy Method

In the energy method (Knight *et al.*, 1981; Waite, 1998), virtual hydrophones are created by using delays at the outputs of the hydrophones and a beam is formed by adding (or summing) the outputs from the virtual hydrophones. When a sinusoidal wave is incident on the array, the array voltage output,  $v_e(\beta, t)$ , is expressed as

$$v_e(\beta, t) = M \sum_{h=1}^{2H} \text{Re} [P^h(\omega) e^{-j\omega(t-\Delta_h)}] \quad (3-20a)$$

where  $P^h(\omega)e^{-j\omega t}$  is the pressure at the location of the  $h$ th hydrophone,

$$\Delta_h = x_h \sin \beta / c \quad (3-20b)$$



is the delay for the  $h$ th hydrophone,  $P^h(\omega)e^{-j\omega(t-\Delta_h)}$  is pressure at the location of the  $h$ th virtual hydrophone and  $M$  is the receiving acoustic sensitivity of each hydrophone expressed in V/Pa. The array voltage output can be computed by using the pressures at the hydrophone locations in any convenient coordinate system and  $P^h(\omega)$  in Eq. (3-20a) can be replaced by either  $\hat{P}^h(\omega)$  or  $\tilde{P}^h(\omega)$  where  $\tilde{\phantom{x}}$  denotes that the function is expressed in the  $(x,y,z)$  coordinate system. The method is known as the energy method because neither phase nor time difference is used to determine the DOA; and, in practice, for each  $\beta$ , the square of the output from the array is integrated over time.

When a plane wave is traveling at an angle  $\beta$  to the normal to the array, and there is no cylinder, the delays in Eq. (3-20b), in effect, simulate hydrophones on a linear array that is at an angle  $\beta$  to the real array, as shown in Fig. 3-2. Therefore, the pressures at the simulated-hydrophone locations are equal in magnitude and phase, and the summed output from the array is  $2H$  times the output from each hydrophone.

However, when a plane harmonic wave is incident at an angle  $\alpha$  as shown in Fig. 3-2, and there is no cylinder, and the delays in Eq. (3-20b) are used, the virtual hydrophones lie on a straight line that is at an angle to the wavefront. Therefore, the phases of pressures at the simulated-hydrophone locations are not equal, and the sum of the hydrophone outputs is less than  $2H$  times the output from each hydrophone. Substituting, in Eq. (3-20a), the pressures at the hydrophone locations obtained by using the expression

$$\tilde{P}_i(\omega) = \exp(-jkx \sin \alpha - jky \cos \alpha) \quad (3-21)$$

for the incident pressure, yields

$$v_e(\beta, t) = M \cos(\omega t) \frac{\sin[Hkd(\sin \alpha - \sin \beta)]}{\sin[kd(\sin \alpha - \sin \beta)/2]} \quad (3-22)$$

Eq. (3-22), for the special case of  $\alpha = 0$ , is presented in several textbooks.

The array is virtually steered to various directions by gradually changing the value of  $\beta$  in Eq. (3-20b) and finding the value of  $\beta$ ,  $\beta_e$ , at which the array output is maximum. In the absence of the cylinder, it is seen, from Eq. (3-22) as well as from earlier statements, that the amplitude of  $v_e(\beta, t)$  has a local maximum when all the virtual hydrophones in the array lie on the same wavefront, or equivalently, when the array is steered to the direction from which the wave is coming, i.e., for  $\beta_e = \alpha$ . When a

scatterer, for example an elastic cylinder, is in the neighbourhood of the array, and it is not possible to annul the effect of its presence, it is concluded that the plane wave is coming from the measured direction  $\beta_e$ . However, if the plane wave is actually coming from the  $\alpha$  direction then the error in finding the direction of arrival is  $\beta_e - \alpha$ .

### 3.3.2 Split Beam Correlation Method

In the second method, known as split beam correlation method, the linear array is split into two half-arrays: the hydrophones 1, 2...  $H$  are in the first half array and the hydrophones  $H+1$ ,  $H+2$ , ...  $2H$  are in the second half array. The array is steered in exactly the same way as done when using the energy method and the delay in Eq. (3-20b) is used. Then, the outputs from the hydrophones in the two half arrays are summed separately to obtain  $v_1(\beta, t)$  and  $v_2(\beta, t)$ , and their cross-correlation

$$v_1(\beta, t) * v_2(\beta, t) = \int_{-\infty}^{\infty} v_1(\beta, t) v_2(\beta, t - \tau) dt \quad (3-23)$$

is computed where \* denotes split beam correlation and  $\tau$  is the correlation time. The cross-correlation has only one maximum, at  $\tau = \tau_0$ , when the incident wave is aperiodic, and the direction of arrival of the plane wave is determined by using  $\tau_0$ .

When a sinusoidal wave is incident on the array, the outputs from the left-half and right-half arrays are expressed as

$$v_1(\beta, t) = M \sum_{h=1}^H \text{Re} \left[ P^h(\omega) e^{-j\omega(t-\Delta_h)} \right] \quad (3-24a)$$

and

$$v_2(\beta, t) = M \sum_{h=H+1}^{2H} \text{Re} \left[ P^h(\omega) e^{-j\omega(t-\Delta_h)} \right], \quad (3-24b)$$

respectively, where  $v_1(\beta, t) + v_2(\beta, t) = v_e(\beta, t)$ . In general, the outputs from the two half arrays are expressed in the form

$$v_1(\beta, t) = A_1 \cos[\omega(t - \tau_1)] \quad (3-25a)$$

and

$$v_2(\beta, t) = A_2 \cos[\omega(t - \tau_2)] \quad (3-25b)$$

When a plane harmonic wave is incident at an angle  $\alpha$  as shown in Fig. 3-2, and there is no cylinder, substituting in Eq. (3-24) the plane-wave pressures at the

hydrophone locations obtained by using Eq. (3-21), yields

$$v_1(\beta, t) = M \cos\left[\omega t - kHd(\sin \alpha - \sin \beta)/2\right] \frac{\sin[Hkd(\sin \alpha - \sin \beta)/2]}{\sin[kd(\sin \alpha - \sin \beta)/2]} \quad (3-26a)$$

and

$$v_2(\beta, t) = M \cos\left[\omega t + kHd(\sin \alpha - \sin \beta)/2\right] \frac{\sin[Hkd(\sin \alpha - \sin \beta)/2]}{\sin[kd(\sin \alpha - \sin \beta)/2]} \quad (3-26b)$$

Then, comparing Eqs. (3-25) with Eqs. (3-26) yields  $\tau_1 = Hd(\sin \alpha - \sin \beta)/(2c)$  and  $\tau_2 = -Hd(\sin \alpha - \sin \beta)/(2c)$ .

When a wave with period  $T$  is incident on the array, the infinite number of maxima that occur in the cross-correlation have the same period,  $T$ , and one maximum occurs at

$$\tau_0 = \tau_1 - \tau_2 = Hd(\sin \alpha - \sin \beta)/c = \Delta\phi/c \quad (3-27)$$

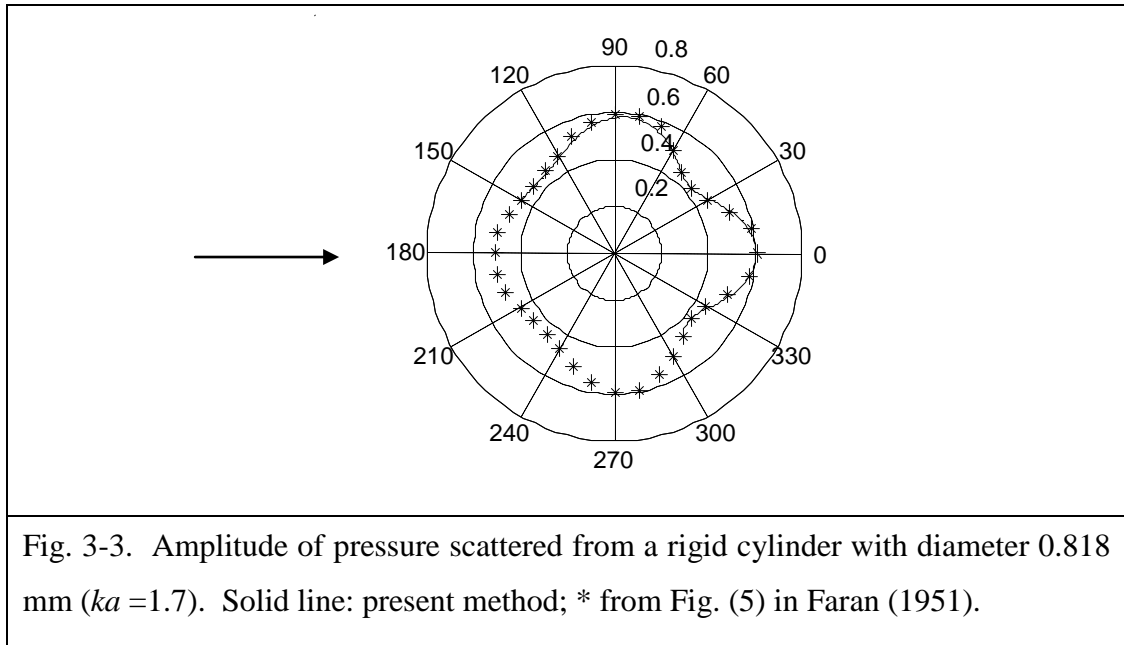
where  $\Delta\phi$  is the phase difference between the outputs  $v_1$  and  $v_2$ . If the split beams are steered to nearly the direction from which the wave is incident, then  $\beta \approx \alpha$  and  $|\tau_0| \leq T/2$ . In practice, the energy method is used to find  $\alpha$  and  $\tau_0$  is determined by computing the cross-correlation or measuring the phase difference. Then, substituting the known value of  $\beta$  and the computed value of  $\tau_0$  in Eq. (3-27) yields the computed DOA:

$$\alpha_c = \sin^{-1}\left[\tau_0 c/(dH) + \sin(\beta)\right] \quad (3-28)$$

When there is no cylinder,  $\alpha_c = \alpha$  and there is no error in finding the DOA. When the cylinder is present, substituting the expressions for the pressures at the hydrophone locations in Eq. (3-19) in Eq. (3-24) yields the outputs from the half arrays that are used to determine  $\tau_0$ . Then, substituting the values of  $\tau_0$  and the value of  $\beta$  used to compute the delays, in Eq. (3-28) yields the computed DOA,  $\alpha_c$ . The error in finding the DOA is  $\alpha_c - \alpha$

### 3.4 NUMERICAL RESULTS AND DISCUSSIONS

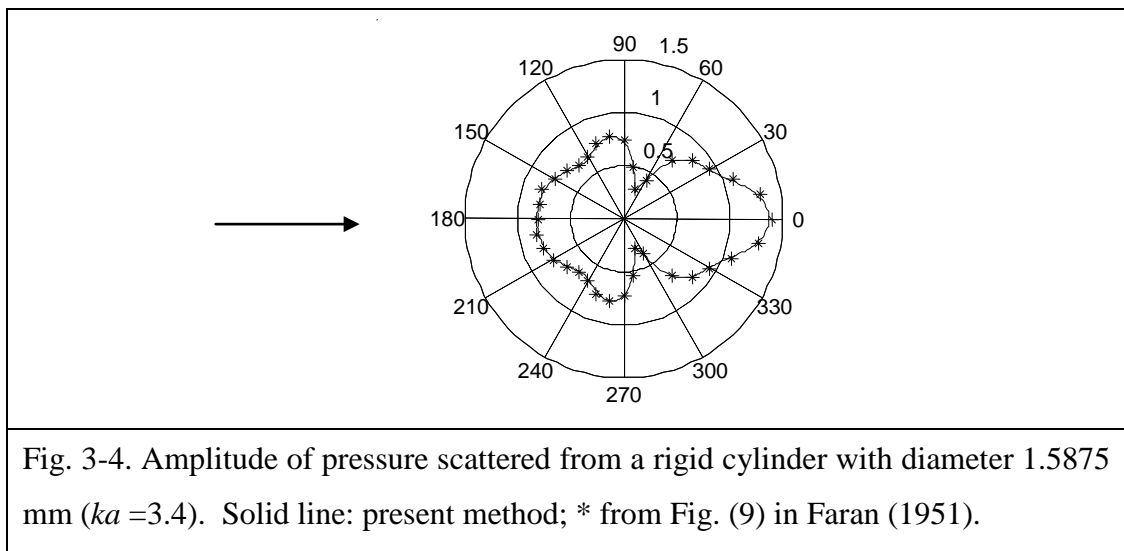
In the first sub-section, the pressures scattered by rigid and elastic cylinders of various dimensions are computed and compared with those presented by Faran (1951).



Then, total pressures at hydrophone locations are presented. In the second sub-section, the errors in the DOA computed using two methods are presented.

### 3.4.1 Scattered and Total Pressure

The computed normalized scattered pressure patterns for rigid cylinders of various dimensions and values of  $ka$  are first shown. These are computed using Eq. (3-11) and the coefficients  $C_n$  in Eq. (3-17). The incident wave is coming from the direction  $\theta = 180^\circ$  and is indicated by an arrow in each figure. Results are shown for rigid cylinders of diameter 0.818 mm ( $ka = 1.7$ ), 1.5875 mm ( $ka = 3.4$ ) and 2.3495 mm ( $ka = 5$ ) in Figs. 3-3, 3-4, and 3-5 respectively when plane wave is incident approximately at 1 MHz. There is very good agreement with the values obtained by digitizing Figs. 5, 9 and 13 in Faran (1951).



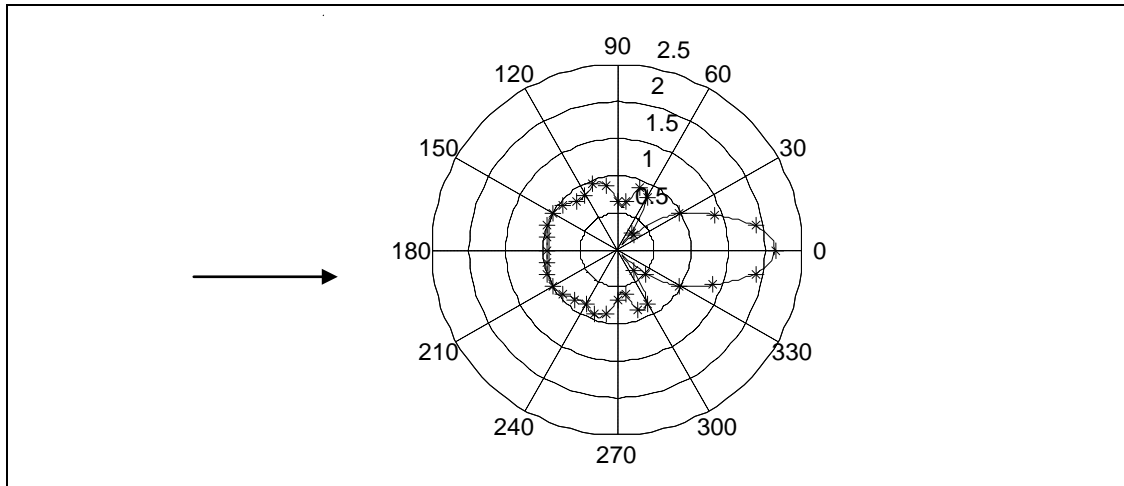


Fig. 3-5. Amplitude of pressure scattered from a rigid cylinder with diameter 2.3495 mm ( $ka=5$ ). Solid line: present method; \* from Fig. (13) in Faran (1951).

The amplitudes of pressures scattered by various elastic cylinders, computed at 1 MHz using Eq. (3-11) and the coefficients  $C_n$  in Eq. (3-14) are shown in Figs. 3-6 to 3-8 using solid lines. Results obtained from Figs. 4, 7 and 12 of Faran (1951) are shown using asterisks. Results are shown in Fig. 3-6 for a steel cylinder with Young's modulus,  $Y$ , equal to 200 GN/m<sup>2</sup>, Poisson's ratio,  $\sigma$  equal to 0.28,  $\rho=7700$  kg/m<sup>3</sup>,  $ka = 1.7$ , and  $k_1a = 0.45$ ; and in Fig. 3-7 for a copper cylinder with  $Y = 119$  GN/m<sup>2</sup>,  $\sigma = 1/3$ ,  $\rho=8900$  kg/m<sup>3</sup>,  $ka = 3.4$ , and  $k_1a = 1.08$ . The amplitude of scattered pressure from aluminum cylinder is shown in Fig 3-8 which corresponds to  $ka = 5$ ,  $Y= 70$  GN/m<sup>2</sup>,  $k_1a=1.17$ ,  $\sigma=1/3$ , and  $\rho=2700$  kg/m<sup>3</sup> for aluminum.

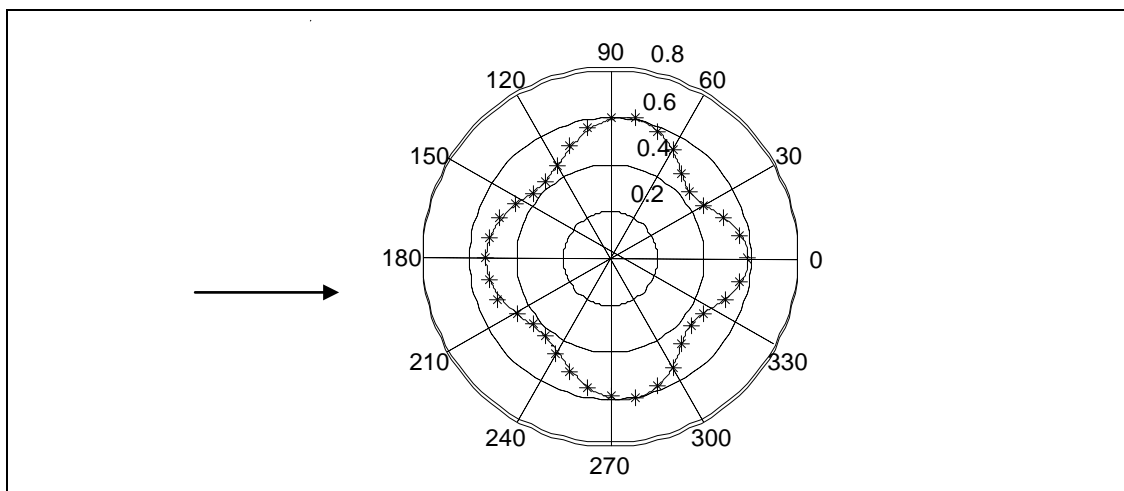


Fig. 3-6. Amplitude of pressure scattered at 1 MHz from a steel cylinder with diameter 0.813 mm. Solid line: present method; \* from Fig. (4) in Faran (1951).

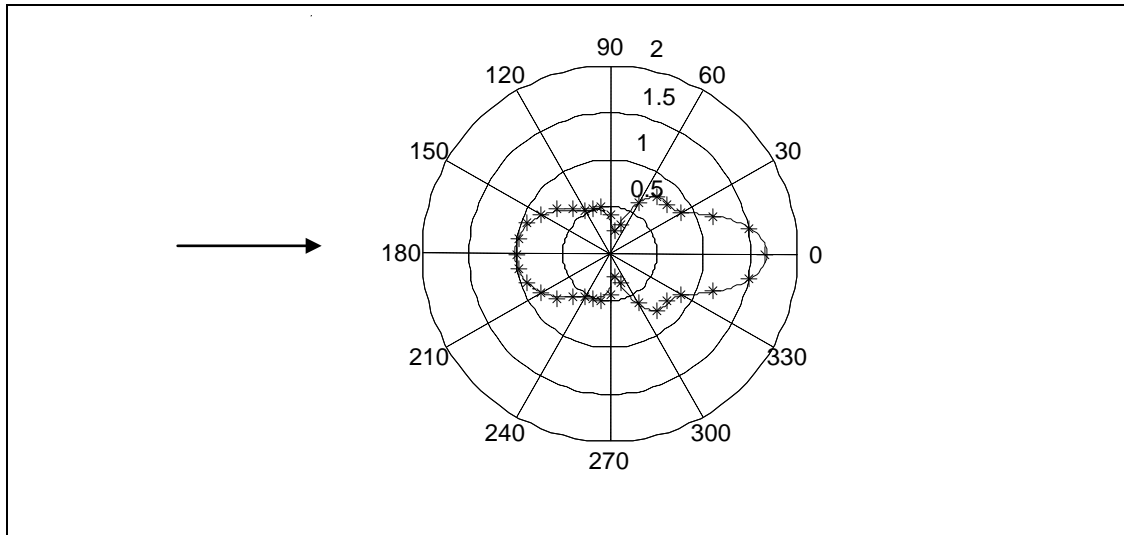


Fig. 3-7. Amplitude of pressure scattered at 1 MHz from a copper cylinder with diameter 1.588 mm. Solid line: present method; \* from Fig. (7) in Faran (1951).

Numerical results are presented to illustrate quantitatively the error in finding the direction of arrival by using the energy and split beam correlation methods. Results are presented for a Titanium (Ti) cylinder of diameter 36 mm. The Young's modulus, Poisson's ratio, and density of Ti are  $115 \text{ GN/m}^2$ , 0.3, and  $4450 \text{ kg/m}^3$ , respectively.  $P_0=1$ . The effects of number of hydrophones in the array,  $2H$ ; the distance between the array and the cylinder,  $b$ ; and the frequency,  $f$ , of the incident wave on the scattered pressure and the error in the DOA are illustrated. Unless otherwise specified, the plane wave is incident on the array from broadside, i.e.,  $\alpha = 0$ .

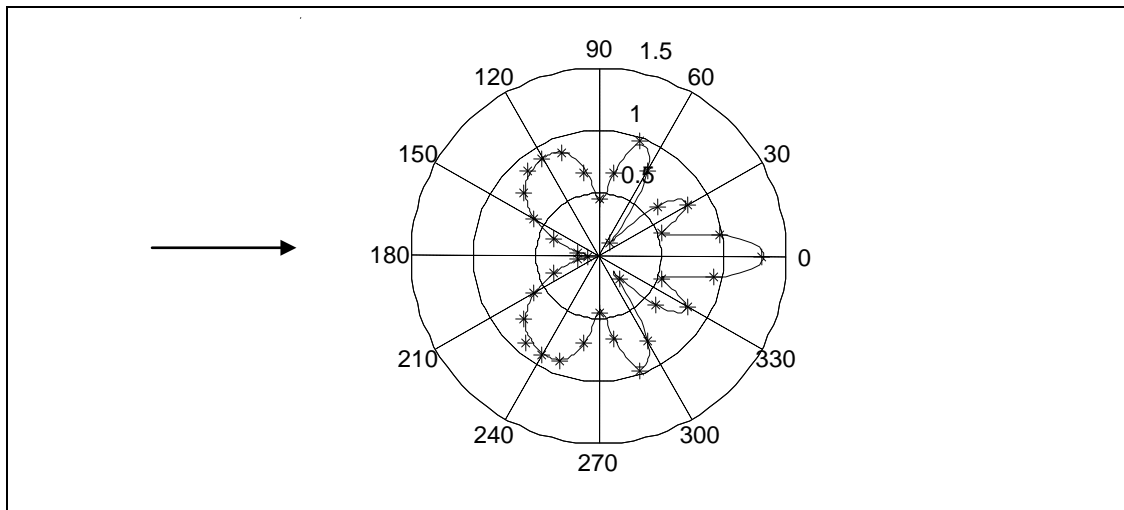


Fig. 3-8. Amplitude of pressure scattered from an aluminum cylinder with diameter 2.349 cm at 1 MHz. Solid line – computed using present method; \* from Fig. (12) in Faran (1951).

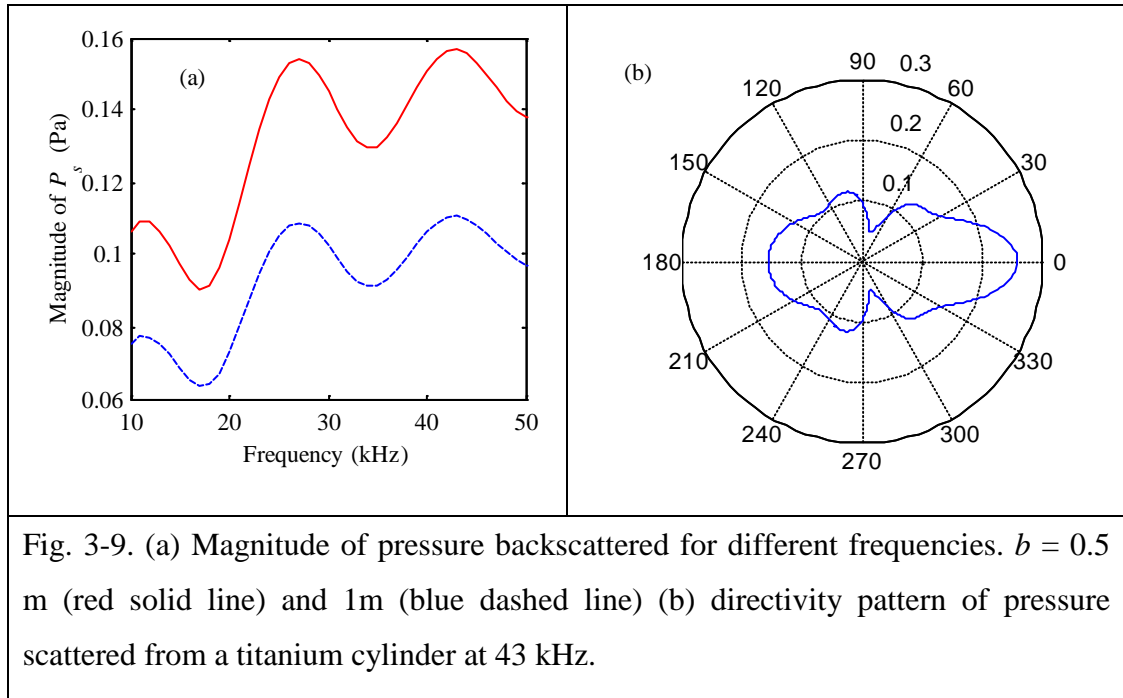


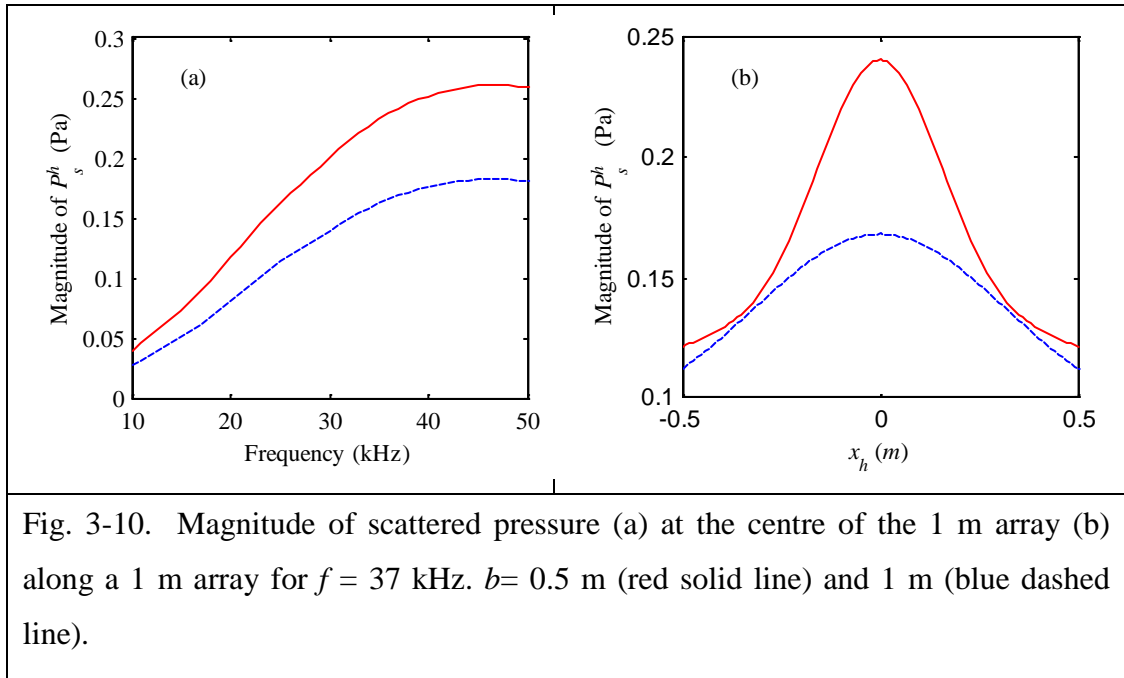
Fig. 3-9. (a) Magnitude of pressure backscattered for different frequencies.  $b = 0.5$  m (red solid line) and 1m (blue dashed line) (b) directivity pattern of pressure scattered from a titanium cylinder at 43 kHz.

The magnitude of the pressure scattered from the Ti cylinder is shown in Fig. 3-9. In Fig. 3-9a, the pressure scattered along the  $\theta = 180$  deg direction, computed using Eq. (3-11) and the solution to Eq. (3-14), is shown at distances of  $b = 0.5$  m and 1 m using a red solid line and a blue dashed line, respectively. This pressure is often called the back scattered pressure. There are local maxima in the back scattered pressure at 11, 27, and 43 kHz. The directivity of the scattered pressure at 43 kHz is shown in Fig. 3-9b. It is seen that there is strong angular dependence indicating that hydrophones in an array will experience considerably different pressures.

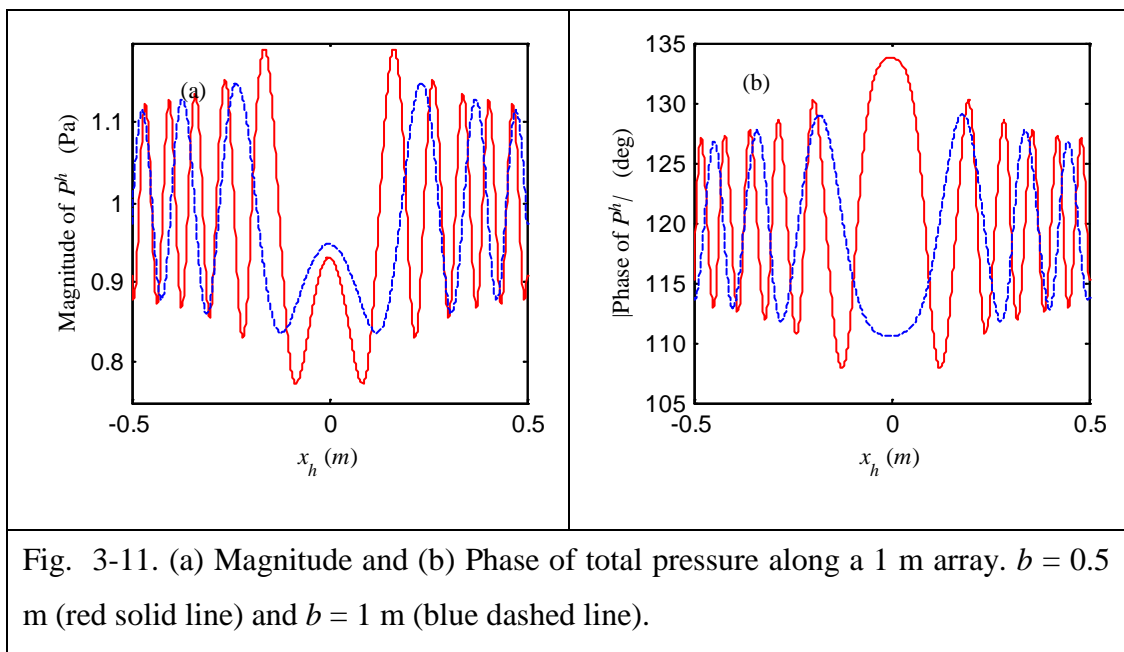
In Fig. 3-10, the scattered pressure, computed using the solution to Eq. (3-14), and Eq. (3-19b), are shown for  $b = 0.5$  m and 1 m using a red solid line and a blue dashed line, respectively. In Fig. 3-10a, the magnitude of scattered pressure is shown at the centre of the 1 m array as a function of frequency. The magnitude of scattered pressure increases as frequency increases and reaches a peak at about 47 kHz. It decreases when the distance,  $b$ , to the array increases. In Fig. 3-10b, the magnitude of scattered pressure is plotted along a 1 m array with uniform spacing, at  $f = 37$  kHz. The frequency corresponds to normalized frequencies of  $ka = 2.8$  and  $k_1a = 0.71$ . The maximum in the magnitude of scattered pressure occurs at the centre of the array – the point on the array that is closest to the cylinder.

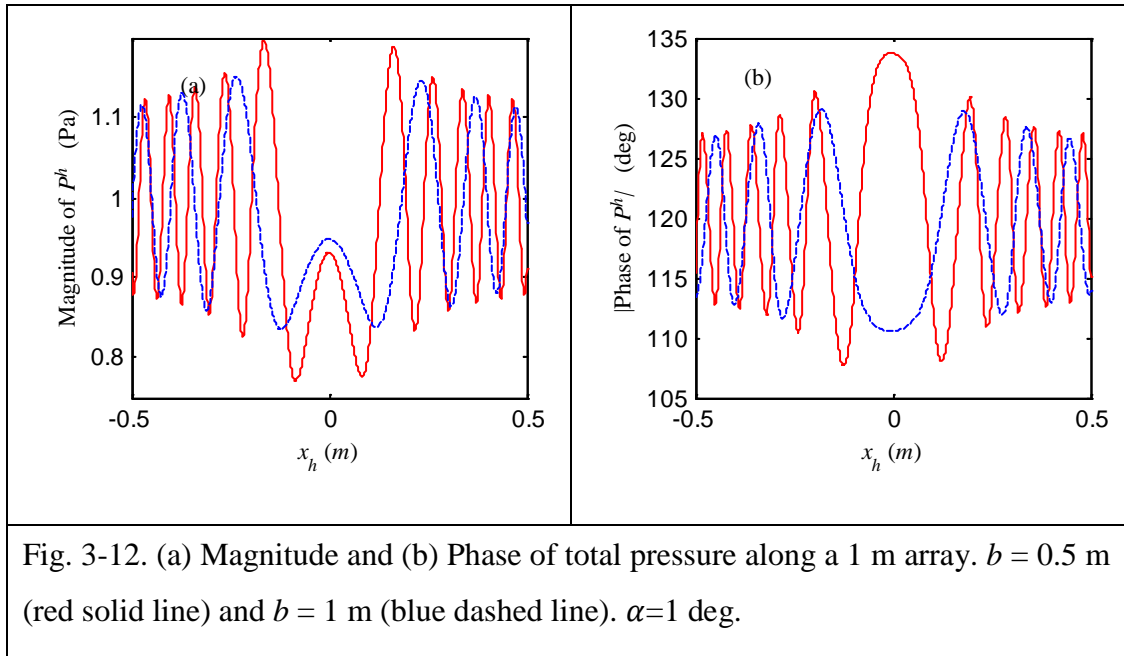
In Fig. 3-11, the magnitude and phase of total pressure, computed using the solution to Eq. (3-14) and Eq. (3-19), are shown at  $f = 37$  kHz along a 1 m array for  $b =$



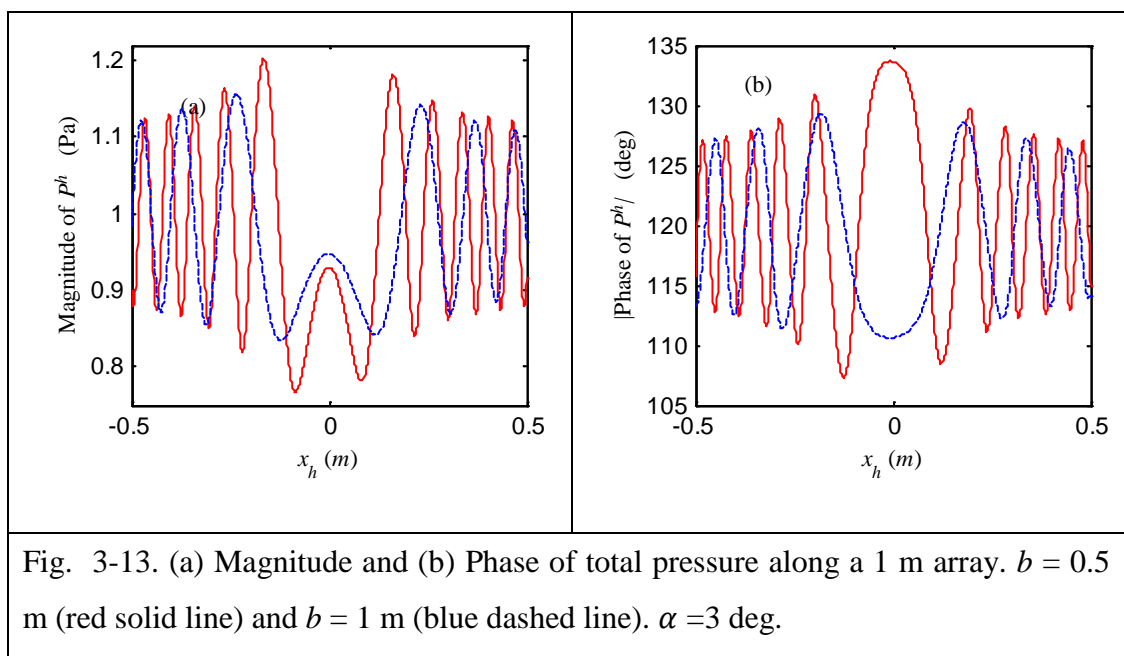


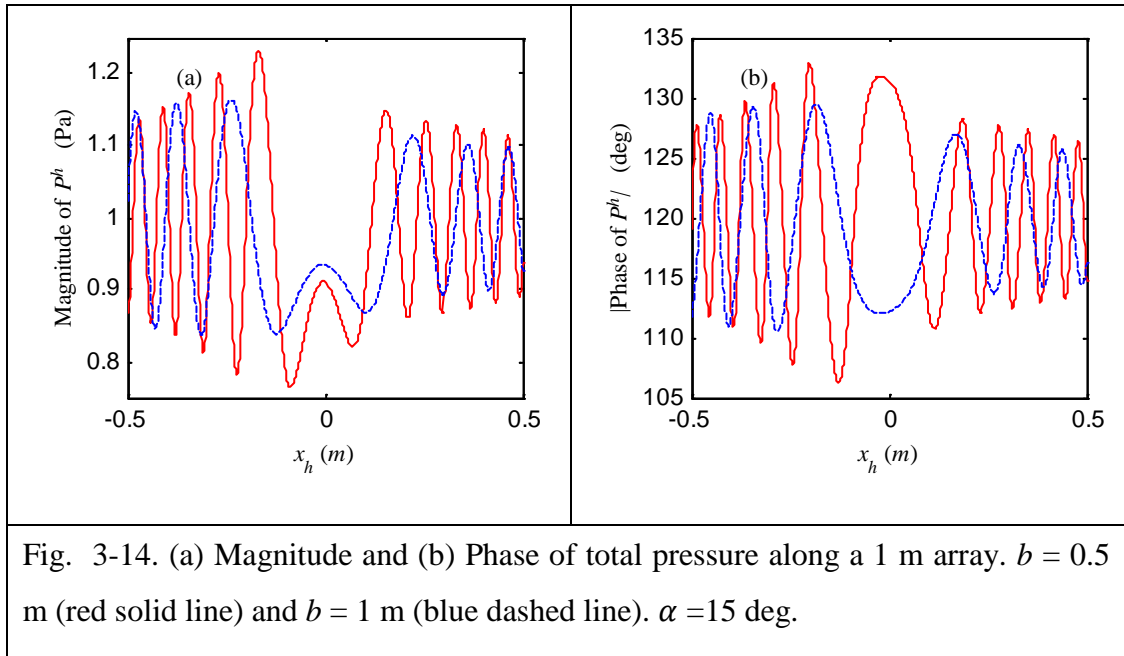
0.5 m and 1 m, using solid and blue dashed lines, respectively. For  $b = 0.5$  m, the magnitude of the pressure varies by about  $\pm 21\%$  and the phase varies by about  $\pm 13$  deg. Even when the distance to the cylinder is doubled, i.e.,  $b = 1$  m, the corresponding changes are quite large and about  $\pm 15\%$  and  $\pm 10$  deg. This is not very surprising because the magnitude of the scattered pressure varies as  $r^{-0.5}$ . The large variations indicate that the error in finding the direction of arrival (DOA) is to be studied. If there were no cylinder, the magnitude would be one and the phase would be exactly the same at all points on the array.



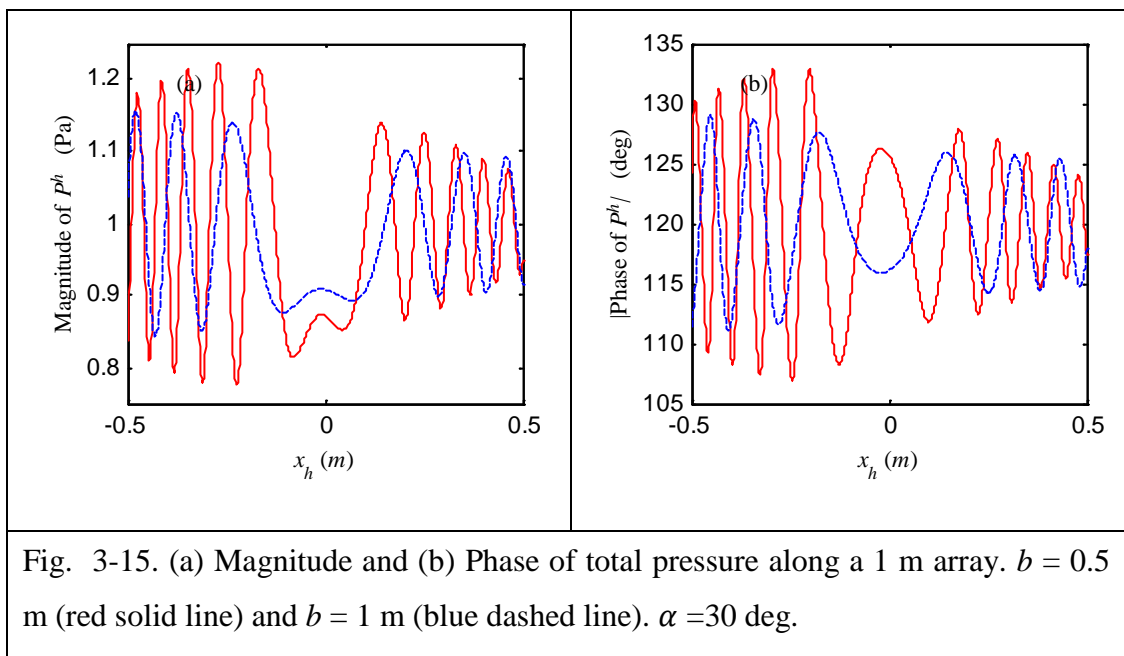


In Fig. 3-12, the magnitude and phase of total pressure, computed using the solution to Eq. (3-14) and Eq. (3-19), are shown at  $f = 37$  kHz along a 1 m array for  $b = 0.5$  m and 1 m, using solid and blue dashed lines, respectively when the angle between the incident wave and the normal to the array is  $1^\circ$ , i.e.,  $\alpha = 1$ . For  $b = 0.5$  m, the magnitude of the pressure varies by about  $\pm 21.5\%$  and the phase varies by about  $\pm 13$  deg and for,  $b = 1$  m, the corresponding changes are about  $\pm 16\%$  and  $\pm 9$  deg respectively. Similar results are presented in Fig. 3-13 for  $\alpha = 3$ .





In Fig. 3-14, the magnitude and phase of total pressure, computed using the solution to Eq. (3-14) and Eq. (3-19), are shown at  $f = 37$  kHz along a 1 m array for  $b = 0.5$  m and 1 m, using solid and blue dashed lines, respectively when the angle between the incident wave and the normal to the array is  $15^\circ$ , i.e.,  $\alpha = 15$  deg. For  $b = 0.5$  m, the magnitude of the pressure varies by about  $\pm 23.5\%$  and the phase varies by about  $\pm 13$  deg and for,  $b = 1$  m, the corresponding changes are about  $\pm 16.5\%$  and  $\pm 9$  deg respectively. It is observed that the variation in magnitude and phase of the pressure is more in the left half array than the right half array.



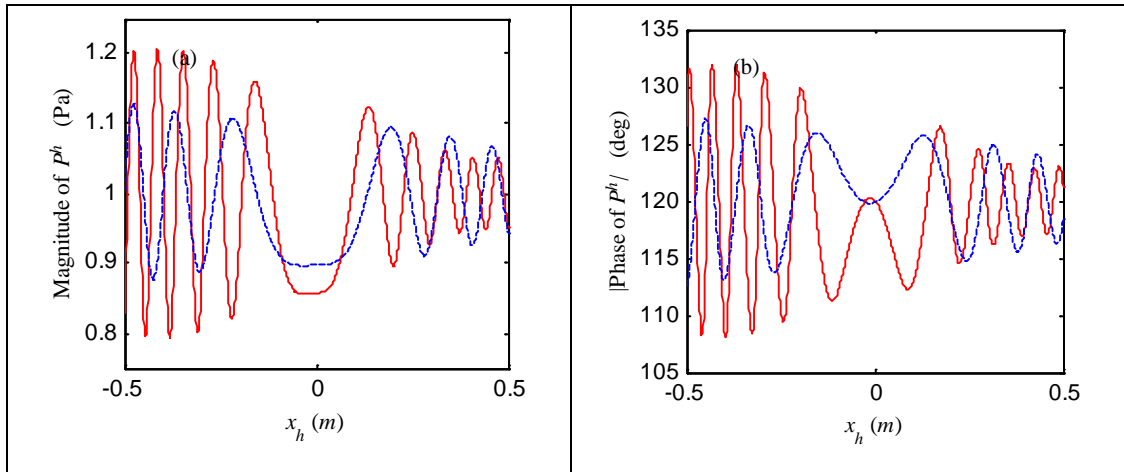


Fig. 3-16. (a) Magnitude and (b) Phase of total pressure along a 1 m array.  $b = 0.5$  m (red solid line) and  $b = 1$  m (blue dashed line).  $\alpha = 45$  deg.

In Fig. 3-15, the magnitude and phase of total pressure, computed using the solution to Eq. (3-14) and Eq. (3-19), are shown at  $f = 37$  kHz along a 1 m array for  $b = 0.5$  m and 1 m, using solid and blue dashed lines, respectively when the incident wave is incident at an angle  $30^\circ$  on the array, i.e.,  $\alpha = 30$  deg. Here also the deviation in magnitude and phase of the pressure is more in the left half array than the right half array.

In Fig. 3-16, the magnitude and phase of total pressure, computed using the solution to Eq. (3-14) and Eq. (3-19), are shown at  $f = 37$  kHz along a 1 m array for  $b = 0.5$  m and 1 m, using solid and blue dashed lines, respectively when the plane wave is incident at an angle  $45^\circ$  on the array, i.e.,  $\alpha = 45$  deg. Here also the deviation in magnitude and phase of the pressure is more in the left half array than the right half array.

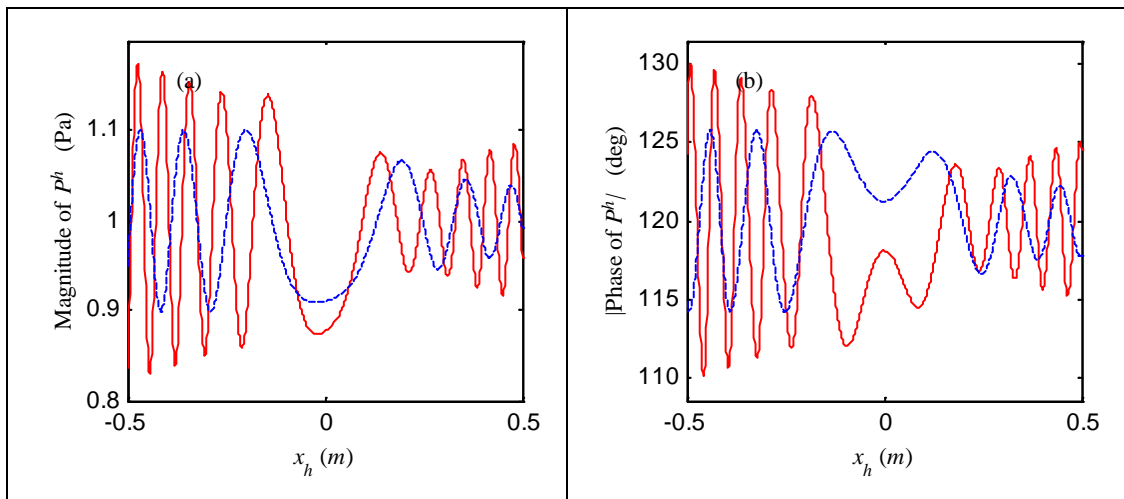


Fig. 3-17. (a) Magnitude and (b) Phase of total pressure along a 1 m array.  $b = 0.5$  m (red solid line) and  $b = 1$  m (blue dashed line).  $\alpha = 60$  deg.

In Fig. 3-17, the magnitude and phase of total pressure, computed using the solution to Eq. (3-14) and Eq. (3-19), are shown at  $f = 37$  kHz along a 1 m array for  $b = 0.5$  m and 1 m, using solid and blue dashed lines, respectively when the plane wave is incident at an angle  $60^\circ$  on the array, i.e.,  $\alpha = 60$  deg. Here also the deviation in magnitude and phase of the pressure is more in the left half array than the right half array.

### 3.4.2 Error in DOA

Numerical results are now presented for the error in finding direction of arrival using an array with 60 identical hydrophones. The hydrophones are spaced  $\lambda/2$  apart ( $\approx 20$  mm) where  $\lambda$  is the wavelength in water of a 37 kHz wave. The length of the array is  $\approx 1.2$  m. The angle of incidence is varied in steps of 0.1 deg and the beam is steered in steps of 0.001 deg. The error in finding the direction of arrival, due to the presence of a Titanium cylinder of diameter 36 mm, is shown in Fig. 3-18 for  $b = 0.5$  m, 1 m, and 1.5 m using solid, dashed, and dash-dot lines, respectively. This corresponds to normalized frequencies of  $kb \approx 77.5, 155, 232.5$  when  $b=0.5$ m, 1m, 1.5m respectively. The errors obtained using the energy method (Sec. 3.1), the split beam correlation method (Sec. 3.2) with beam steered to broadside ( $\beta=0$ ), and the split beam correlation method with beam steered to  $\alpha$  are shown in Figs. 3-18a, 3-18b and 3-18c, respectively.

When  $\alpha = 0$  deg, the error is zero because of symmetry. It is seen from the data presented in 3-18a that, for some small values of  $\alpha$ , ( $\alpha < 10$ ), the error is often greater when  $b = 1.5$  m than it is when  $b = 0.5$  or 1 m. This is not surprising because of two characteristics of the pressure field – seen in Fig. 3-11 to 3-17 – when the array is further from the cylinder. One, the region near  $x = 0$ , in which the total pressure is lower than the incident pressure, is wider. Two, the oscillations along the length of the array are fewer. These characteristics will result in less-nearly-perfect cancellation of the scattered pressure when the outputs from the hydrophones are summed. However, when the array is very very far away from the cylinder, the scattered pressure is negligible and the error in finding the DOA tends to zero. The maximum errors, in Fig. 3-18a, are about 0.057 deg, 0.036 deg, and 0.031 deg for  $b=0.5$  m, 1 m, and 1.5 m, respectively. It is also seen from Fig. 3-18a and 3-18b that the error, when the spit beam correlation method with beam steered to broadside is used, varies very rapidly with  $\alpha$  and is, for some values of

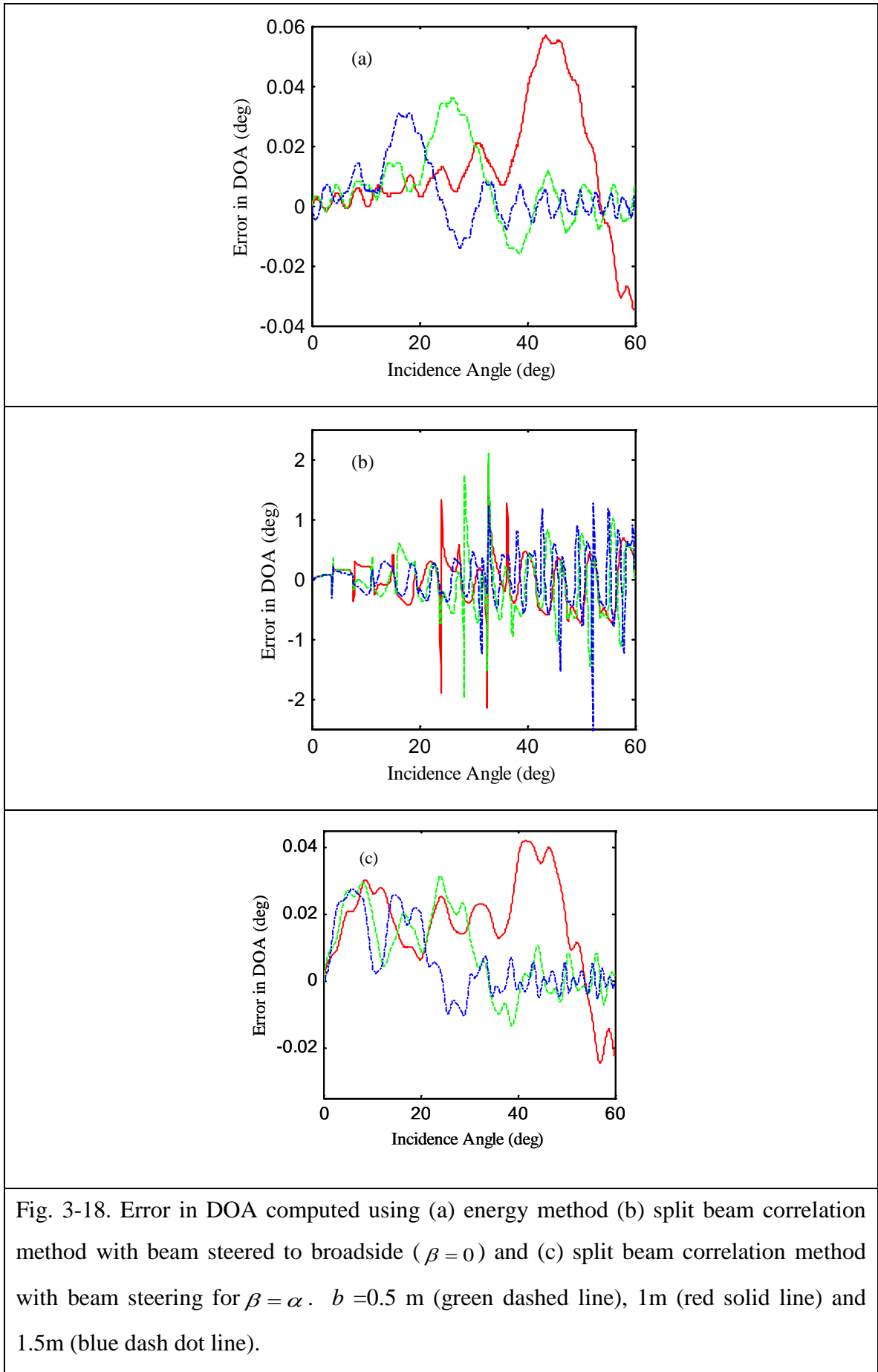


Fig. 3-18. Error in DOA computed using (a) energy method (b) split beam correlation method with beam steered to broadside ( $\beta = 0$ ) and (c) split beam correlation method with beam steering for  $\beta = \alpha$ .  $b = 0.5$  m (green dashed line), 1m (red solid line) and 1.5m (blue dash dot line).

$\alpha$ , more than 100 times the error when the energy method is used. In practice, the error cannot be determined because the correct DOA is not known. However, the error in finding the DOA can be significantly reduced, in some cases, by averaging the DOA over  $\beta$ . The error, when the split beam correlation method with beam steered to  $\alpha$ , is shown in Fig 3-18c for  $\beta = \alpha$ . The error is much less than that in Fig. 3-18b for the case of beam steered to broadside but, for most values of  $\alpha$ , greater than that obtained by using the energy method and shown in Fig. 3-18a. Therefore, it is concluded that there is no significant advantage in using the split beam correlation method with beam steered to  $\alpha$  to find the DOA. However, this is to be reviewed when noise is present (Carter, 1981).

The errors in the DOA when using the split beam correlation method with beam steered to neighborhood of  $\alpha$  are shown in Figs. 3-19a and 3-19b for  $\alpha = 1$  deg and 3 deg, respectively. They are shown for  $b = 0.5$  m, 1 m, and 1.5 m. It is seen that the error does not always decrease when  $b$  increases. On the contrary, it is seen from Fig. 3-19b that the error increases when  $\beta < \alpha$  and  $b$  increases. This is not surprising in view of the earlier observations based on Figs. 3-11 to 3-17. The split beam correlation method is often used for tracking after detection using the energy method. However, here it is seen from Fig. 3-18a and 3-19a that the error when using the energy method is much less than that when using the split beam correlation method with beam steered to  $\alpha$ .

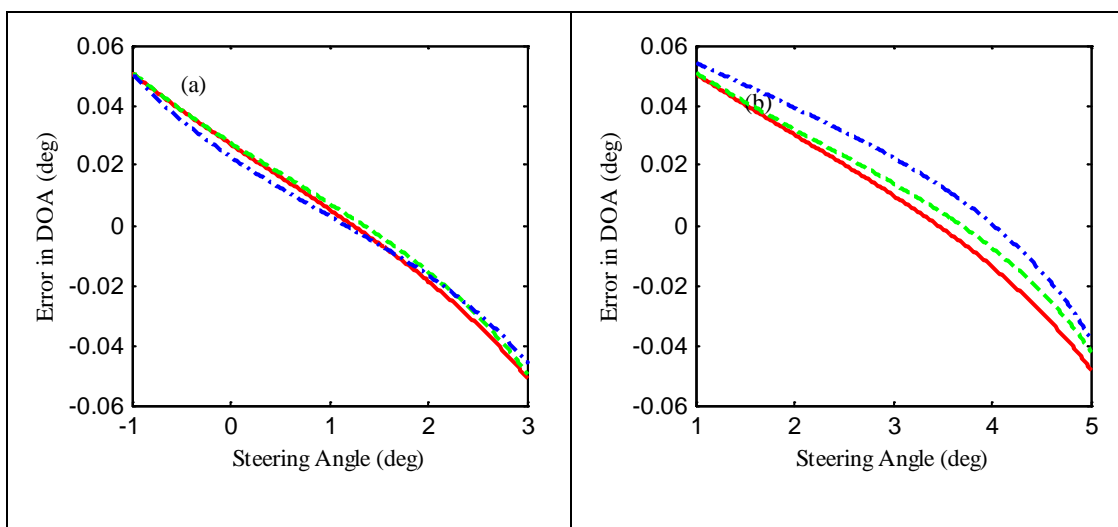


Fig. 3-19. Error in DOA due to cross correlation method with beam steered to neighborhood of  $\alpha$  as a function of steering angles when a plane wave is incident at (a)  $1^\circ$  and (b) at  $3^\circ$ .  $b = 0.5$  m (green dashed line), 1m (red solid line) and 1.5m (blue dash dot line).

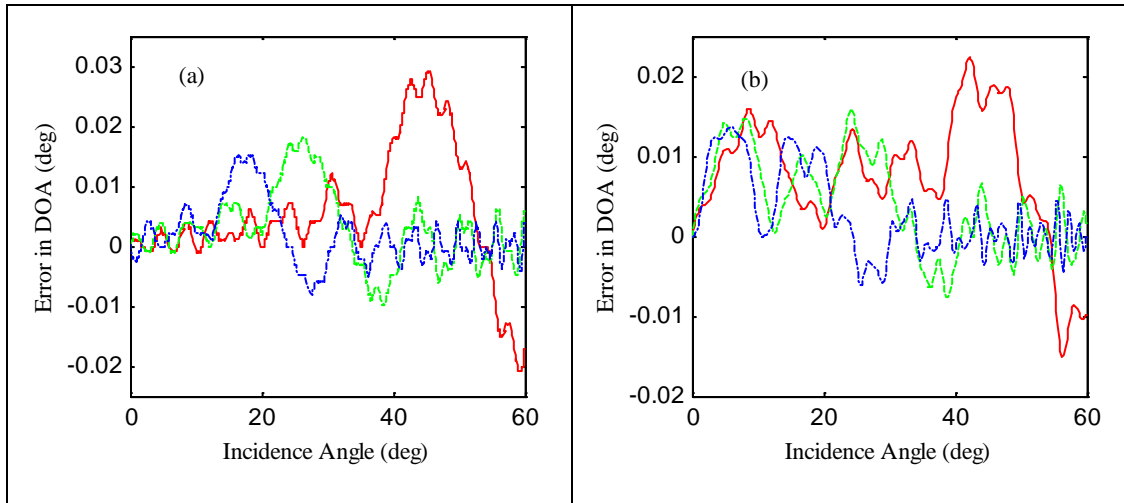


Fig. 3-20. Error in DOA computed using (a) energy method and (b) split beam correlation method (with beam steered to  $\alpha$ ).  $b = 0.5$  m (green dashed line), 1m (red solid line) and 1.5m (blue dash dot line). 24 mm diameter cylinder is in front of the array.

The errors in finding the DOA using the energy method and the cross correlation method with beam steered to  $\alpha$ , due to the presence of a 24 mm diameter ( $a = 12$  mm) Titanium cylinder are shown in Figs. 3-20a and 3-20b, respectively. It is seen by comparing the errors in Figs. 3-20a and 3-20b with the errors in Figs. 3-18a and 3-18c, respectively, for  $a = 18$  mm, that the error in finding the DOA using either method varies approximately as  $a^{7/4}$  for all the values of  $\alpha$  and  $b$  considered here.

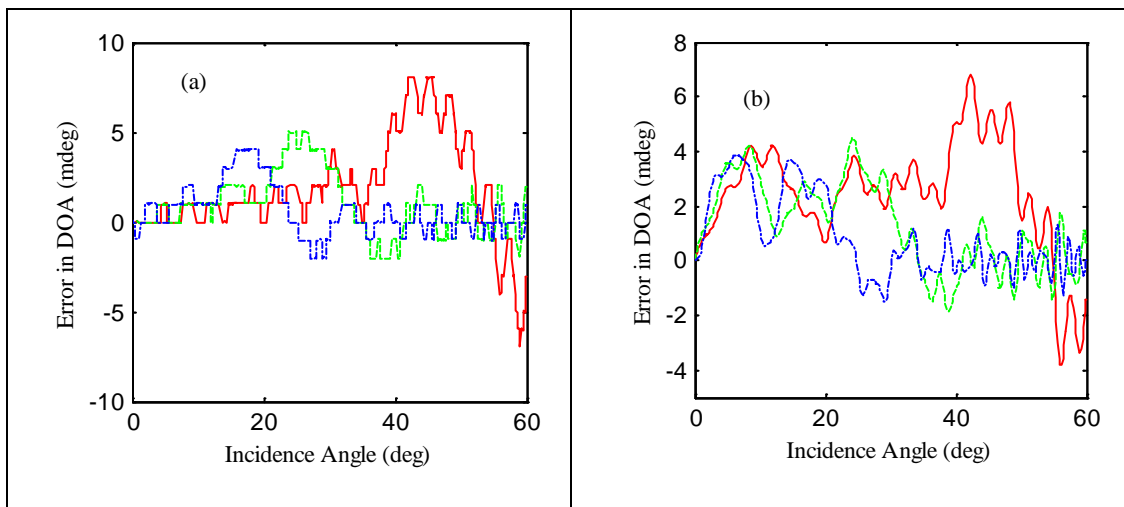
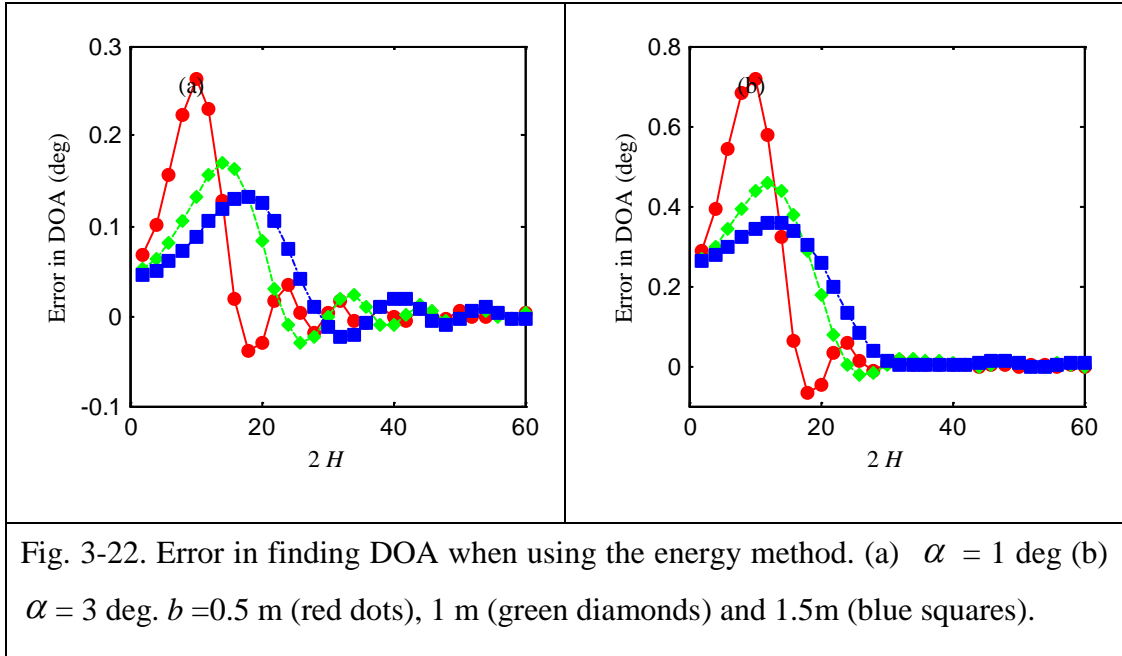


Fig. 3-21. Error in DOA computed using (a) energy method and (b) split beam correlation method (with beam steered to  $\alpha$ ).  $b = 0.5$  m (green dashed line), 1m (red solid line) and 1.5m (blue dash dot line). 12 mm diameter cylinder is in front of the array.





The errors in finding the DOA using the energy method and the cross correlation method with beam steered to  $\alpha$ , due to the presence of a 12 mm diameter ( $a = 6$ mm) Titanium cylinder are shown in Figs. 3-21a and 3-21b, respectively. Errors calculated for  $a = 6$  mm shown in Fig. 3-21 are also in agreement with the approximation made in the Fig. 3-20. For all the cases considered, the error when using the split beam correlation method with beam steered to  $\alpha$ , is greater than the error when using the energy method for small values of  $\alpha$ , ( $\alpha < 10$ ), and lesser for large values of  $\alpha$ .

Finally, the error in finding the DOA by the energy method due to the presence of the cylinder is shown in Fig. 3-22 as a function of number of hydrophones in the array the for  $b = 0.5$  m,  $b = 1.0$  m and  $b = 1.5$  m. The linear array has hydrophones that are spaced uniformly at  $\lambda/2$  when a plane wave is incident at a frequency of  $f = 37$  kHz. The errors, for  $\alpha = 1$  deg and 3 deg are shown using red dots, green diamonds and blue squares, respectively. In both cases, the error initially increases when  $H$  increases and initially decreases when  $b$  increases. When  $H$  is increased further, the error oscillates about zero.

### 3.5 CONCLUSIONS

The errors in finding the direction of arrival of a plane wave due to scattering from a nearby infinite elastic cylinder computed using the energy method and the split beam correlation method are investigated. The effect of the elastic cylinder in front of the

array on the pressures at the hydrophone locations when a plane wave is incident is investigated first. The magnitude and phase of the pressure has large variations along the 1m array. The error in estimating the direction of arrival of the acoustic wave depends on this variation and the method used to process the signal.

The error when using the split beam correlation method without beam steering is, in some cases, about 100 times the error when using the energy method and changes very rapidly for some angles of incidence. The error due to the cross correlation method with beam steered to  $\alpha$  is less than that with beam steered to broadside ( $\beta = 0$ )

For small angles of incidence ( $\alpha < 10$ ), the error in finding the DOA using the energy method is less than that using the cross correlation method with beam steered to  $\alpha$ . In most cases, for small angles of incidence, the error in finding the DOA does not decrease when the distance between the cylinder and the array increases. In all the cases, the error initially increases when the number of hydrophones in the array increases. When the number of hydrophones is greater than 20 (and the length of the array is greater than 10 times the wavelength) the error oscillates about zero when the number of hydrophones is increased. The error in finding the DOA using the energy method and the split beam correlation method with beam steered to  $\alpha$ , varies approximately as  $\alpha^{7/4}$ . Considering only the effect of the stiffener, it is better, overall, to use the energy method than the split beam correlation method with beam steered to  $\alpha$ .

## Chapter 4

### DIRECTIONAL RESPONSE OF A CIRCULAR ARRAY IN AN EMBEDDED FLUID CYLINDER

#### 4.1 INTRODUCTION

Arrays of hydrophones are housed within sonar domes to protect them and to prevent the flow of water directly over them (Waite, 2002). The arrays are used to detect acoustic waves radiated by distant sources and determine the direction of arrival of the nearly plane waves. The thickness of the dome is invariably much less than the radius of curvature of the dome and often much less than the wavelength in water at the frequency of interest (Warren, 1988). However, the curvature of the dome gives rise to convergence or divergence of the acoustic waves that are incident on it. In this chapter, a quantitative understanding of how well ray theory can be used to determine the directional response of a hydrophone array in a sonar dome is studied by using the theory to analyze a canonical problem. Specifically, ray theory is used to determine the interior pressure field when a plane acoustic wave is normally incident on an infinite fluid cylinder embedded in another fluid of infinite extent as shown in Fig. 4-1. The pressure field is then used to determine the directional response of a phased circular array.

Methods based on ray theory are suitable for acoustic analysis of sonar domes. Acoustic and hydrodynamic considerations are used to design the shape of the sonar dome (Loeser, 1981). The dome is usually doubly curved and has absorbing internal structures. Further, the normalized frequency  $ka$ , where  $k$  is the acoustic wavenumber in the water and  $a$  is the radius of curvature of the dome, is usually much greater than one. Therefore, the interior pressure field cannot be easily determined using analytical or numerical methods. Moreover, the surface of the dome and the internal structures are designed such that only one or at most a few rays – called eigenrays – in an incident plane wave pass through any point within the dome. Therefore, ray theory is used in the present analysis.

Domes used in ships are filled with fresh water and pressurized using an overhead tank. The speed of sound in fresh water is less than that in sea water. However, the speeds of both types of stress waves in the dome are often greater than that in sea water. Therefore, on entry into the interior water, the rays may converge or diverge. In

this chapter, the effect of this spreading is studied using interior fluids with sound speed greater than, and less than, that in the exterior fluid. The approach can be extended to include the effect of the dome material.

The pressure field inside the cylinder is determined using ray theory and the results are quantitatively validated by comparing them with those obtained using the method of separation of variables and series solutions. The latter method is used to study scattering from rigid cylinders and spheres (Morse and Ingard, 1968; Junger and Feit, 1972), fluid spheres (Anderson, 1950; Foote, 2007), fluid cylinders (Skudrzyk, 1971; Alemer *et al.*, 1986), solid elastic cylinders and spheres (Faran Jr., 1951) fluid-filled, concentric, elastic cylinders (Akay *et al.*, 1993) , and absorbing cylinders (Mitri *et al.*, 2004). Results are often presented as a function of  $ka$  where  $k$  is the acoustic wavenumber of the exterior fluid and  $a$  is the radius of the scatterer. At low frequencies, the method is very convenient but the primary limitation of the method is that it cannot be applied to several other geometries of interest. Further, at high frequencies, where  $ka$  is much greater than one, a very large number of terms is required for the series solution to converge. However, high frequencies and other geometries are of interest in many practical applications.  $ka$  is approximately 20 when the frequency is 5 kHz and the radius of the scatterer is 1 m as well as when the frequency is 1 MHz and the radius of the scatterer is 5 mm. Further, the method of separation of variables cannot be easily used to analyze domes because of the shape of the dome and the presence of internal surfaces.

Other methods are used even at low frequencies when the geometry does not permit use of the method of separation of variables. However, these methods are often validated by comparing the results obtained for cylinders or spheres with those obtained using the method of separation of variables. Boag *et al.* (1988) use fictitious filament sources to study the scattered cross section of fluid cylinders with arbitrary cross section. The number of sources required for convergence increases when the frequency or radius increases. Numerical results are presented for a circular cylinder with  $ka$  up to approximately 10. Chandra and Thompson (1992) also study a plane wave incident on an embedded fluid cylinder. The densities of the inner and outer fluids are the same but the speeds of sound in them are different. They use Pade approximants to improve the convergence of the Neumann series that is used to solve an integral equation. They present accurate numerical results for the interior and exterior pressure fields at  $ka = 2$ .

It is known that, in general, ray theory is accurate at very high frequencies. However, at frequencies that are not very high and in cases where there are several

eigenrays or caustics in the neighbourhood, it is to be determined – as done in this chapter – whether the use of ray theory yields results that are sufficiently accurate by comparing the results with those obtained using some other method that is known to be accurate at low frequencies. The comparison is best done for a canonical problem that can be solved by using both methods.

Ray theory is used by Clay and Medwin (1977) who present a method that yields exact results at all frequencies when applied to reflection and transmission of a plane wave obliquely incident on a multi-layered fluid with planar interfaces. In this method, the total pressure is expressed as a sum of pressures due to rays that are partially reflected and partially transmitted at each interface. Marston and Langley (1983) use ray theory to study acoustic backscattering from a fluid sphere. They present results for  $ka = 100$  and  $1000$  and compare them with those obtained using the method of separation of variables and series solutions. Marston (1992, 1997) has extensively used geometrical acoustics and physical acoustics (Bowman *et al.*, 1969) to study a variety of problems. Stanton *et al.* (1993a, 1993b) use a model with only 2 rays to study backscattering from elongated objects such as cylinders and prolate spheroids with low acoustic contrast. They use a heuristic phase term, and compare results for  $ka$  up to 10 with the series solution.

Another method that is used at high frequencies is based on the method of separation of variables and the Sommerfeld-Watson transformation. Brill and Uberall (1970) use this method to study the portion of a high-frequency plane wave that is transmitted through a fluid cylinder embedded in an infinite fluid. The transmitted wave is expressed as a sum of waves that are reflected 0, 1, 2, 3, ... times within the cylinder – where there are  $n$  waves that are reflected  $n$  times within the cylinder. Numerical results are presented for  $ka = 100$ . Rumerman (1991) uses this method and the Kirchhoff thin shell theory to study scattering from an elastic cylindrical shell. He uses the residue theory and the Sommerfeld-Watson transformation to convert the expression for backscattered pressure from a modal sum to a contour integral. The integral is shown to have contributions from specular reflection, waves that circumnavigate the shell, and certain poles. Including all the contributions is shown to yield results that are in good agreement with those obtained using modal analysis for  $1.5 < ka < 20$ .

A different high frequency method is used by Bruno *et al.* (2004) who study scattering from rigid bodies using a boundary integral formulation and present results for a cylinder with  $ka$  varying from one to 100,000. They express the surface pressure as the

product of a slowly varying amplitude and a highly oscillatory exponential. Then, they use a localized integration method that is related to the method of stationary phase. They present results for scattering from a rigid cylinder with  $ka$  varying from 1 to  $10^5$ .

Other authors use, at high frequencies, the Kirchhoff approximation for an integral equation formulation or improvements based on it. Medwin and Clay (1998) provide details of a method to use the Kirchhoff approximation, convert the Kirchhoff integral equation to an integral expression, and determine the scattered pressure. Schneider (2003) summarizes the results for scattering from a submarine obtained by using several methods and briefly discusses the limitations of using the Kirchhoff approximation in the integral equation formulation.

Junger (1982) presents a method to study scattering from a rigid body of revolution characterized by a radius that varies along the length of the body. He assumes that it scatters sound as though each circular element is a part of an infinite cylinder of the same radius. This is less restrictive than the Kirchhoff approximation in which it is assumed that scattering occurs as though each element is a part of an infinite plane. He presents results for a prolate spheroid that are in good agreement with those obtained using a T-matrix approach in the low frequency Rayleigh region as well as the mid frequency resonance region. In the high frequency Kirchhoff region, the results are in good agreement with those obtained using the Kirchhoff approximation. Ye *et al.* (1997) extend the method and apply it to scattering from fluid prolate spheroids.

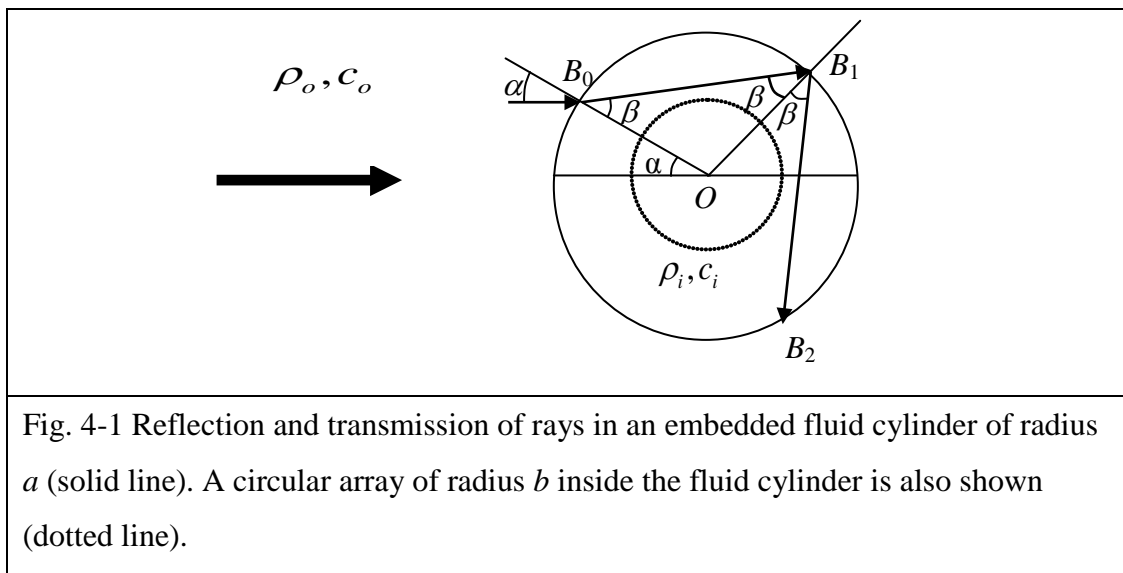
In another high frequency approach, the scattered pressure is expressed as a series with the terms containing negative integer powers of the wavenumber (Bowman *et al.*, 1969; Kravtsov and Orlov, 1993; Kaufman *et al.*, 2002). The series is known variously as Debye series and Luneburg-Kline series. Retaining only the first term in this series and making an approximation yields eikonal and transport equations that can also be derived using geometrical acoustics (Kinsler *et al.*, 1982). Other approximate solutions with fractional powers of the wavenumber are used in the geometric theory of diffraction and in the study of caustics.

In this chapter, a high-frequency ray-acoustics method is presented and used to determine the interior pressure field when a plane wave is normally incident on a fluid cylinder embedded in another infinite fluid. The geometrical and physical acoustics (Bowman *et al.*, 1969) approximations are used. Geometrical acoustics is used to determine the pressure when the rays diverge or converge. The physical acoustics or Kirchhoff approximation for scattering is also used: the reflection and transmission of

each ray when it meets a curved interface is assumed to occur as if it is from an infinite plane interface that is tangent to the interface (Medwin and Clay, 1998). The method is of interest because it can be extended to study the interior pressure field for other bodies with shapes that are not suitable for using the method of separation of variables. It is shown using numerical results that the pressure field computed using this method is in good agreement with that computed using the method of separation of variables. The output from a sector of a circular array of hydrophones in the embedded cylinder is computed and compared with the output from an array in an infinite homogenous fluid. These outputs are of interest as they are used to determine the direction of arrival of the wave. The error in estimating the direction of arrival depends on the signal processing method also.

#### 4.2 DIRECTIONAL RESPONSE OF HYDROPHONE ARRAY

Consider a high-frequency plane wave traveling along the positive  $x$  axis as shown in Fig. 4-1. It is incident on a fluid cylinder of radius  $a$  and infinite length embedded in an outer fluid. The axis of the cylinder lies on the  $z$  axis. Therefore, there is no variation in the pressure field along the axis of the cylinder and only the  $(x,y)$  Cartesian coordinates and  $(r,\theta)$  polar coordinates are used. The densities of the inner and outer fluids are  $\rho_i$  and  $\rho_o$ , respectively; and the speeds of sound in the fluids are  $c_i$  and  $c_o$ , respectively. Following convention, the density ratio  $\rho_i / \rho_o$  and sound-speed ratio  $c_i / c_o$  are defined as  $g$  and  $h$ , respectively. The non-dimensional frequency,  $ka$ , where  $k$  is the wavenumber in the exterior fluid is much greater than one.

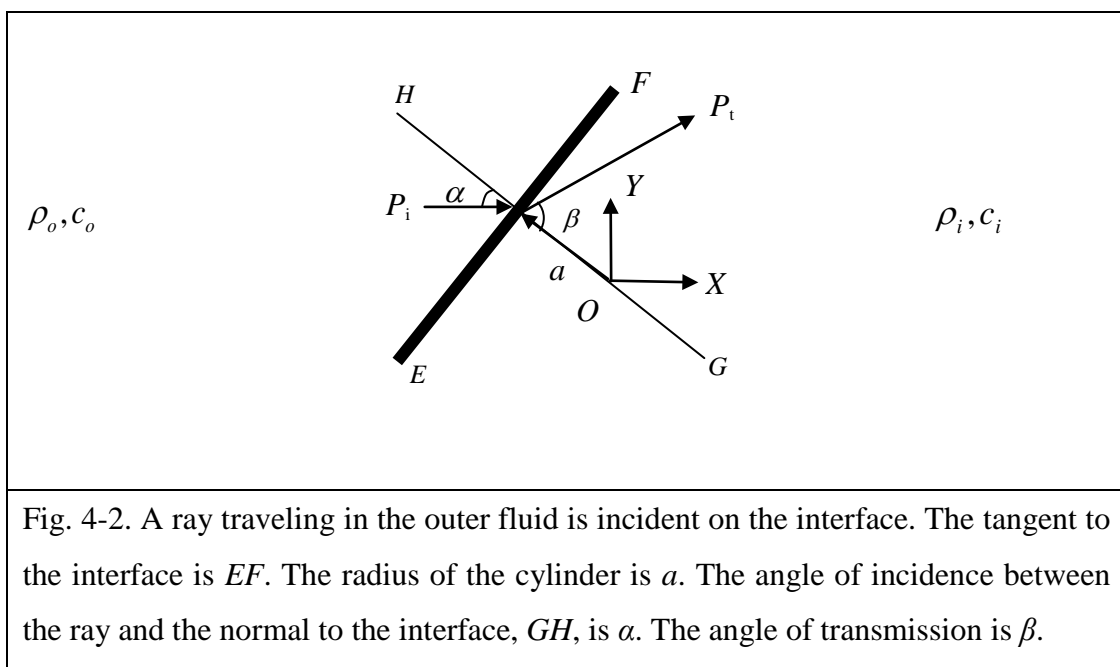


Consider next  $2H$  equispaced point hydrophones. They are on the perimeter of a circle of radius  $b$  with centre at the origin where  $b < a$ . The outputs from  $2J$  adjacent hydrophones in one sector are delayed and summed to simulate a linear array where  $J$  is typically approximately equal to  $H/3$ .  $2H$  such linear arrays are simulated by using  $2H$  sectors where, for example, hydrophones 1 to  $2J$  form sector 1, hydrophones 2 to  $2J+1$  form sector 2, and so on. The effect of the embedded fluid cylinder on the outputs from the simulated linear arrays is of interest.

The outputs from the hydrophones depend on the pressure field inside the embedded cylinder. An expression for the interior pressure field is presented. It is derived here by using expressions for transmission and reflection coefficients, pressure variation due to divergence and convergence of rays inside a cylinder, and methods to trace rays and determine which rays will pass through a particular point of interest. The interior pressure field computed using ray theory is shown to be quite accurate even in the neighborhood of caustics. It is then used to determine the outputs from the simulated linear arrays.

#### 4.2.1 Incident ray in the outer fluid

Consider a ray traveling in the outer fluid in a direction perpendicular to the axis of the cylinder and incident on the fluid cylinder as shown in Fig. 4-1. The incident and transmitted rays are at angles  $\alpha$  and  $\beta$ , respectively to the local normal to the surface of the cylinder where  $\alpha$  is specified and  $\beta$  is determined by using Snell's law. The pressure due to the transmitted ray is of interest.





It is assumed that the physical acoustics or Kirchhoff approximation (Medwin and Clay, 1998) is valid and that the transmission coefficient is equal to that when a ray (or plane wave) is incident on a plane interface that separates the two fluids. The plane interface is tangential to the cylinder at the point of incidence. Therefore, consider a ray traveling along the  $X$  axis and incident on an inclined surface,  $EF$ , separating two semi-infinite fluids as shown in Fig. 4-2. The normal to the surface,  $GH$ , passes through the origin. The distance,  $a$ , between the origin and the surface, along the normal, is equal to the radius of the cylinder.

The pressure due the incident ray of unit amplitude is  $P_{i0}(x, y, \alpha) = \exp(-jk_o x)$  where  $\omega$  is the angular frequency and  $k_o = \omega/c_o$  is the wave number in the outer fluid. The time factor,  $\exp(+j\omega t)$ , where  $t$  denotes time is suppressed for convenience. The pressure due to the transmitted ray, neglecting spreading effects that are included later, is expressed as

$$\bar{P}_{t0}(x, y, \alpha) = T_{oi}(\alpha) \exp[j(k_o d_{oi} - k_i d_{ot})]. \quad (4-1a)$$

Here, the overbar indicates that the pressure is due to a unit wave in the exterior fluid, the subscript 0 indicates that the ray has not been reflected at a concave interface, and

$$T_{oi}(\alpha) = (2\rho_i c_i \cos \alpha) / (\rho_i c_i \cos \alpha + \rho_o c_o \cos \beta) \quad (4-1b)$$

is the transmission coefficient (Medwin and Clay, 1998) when a plane wave is obliquely incident on a plane interface that includes the origin and separates two semi-infinite fluids,  $\alpha$  and  $\beta$  are the angles that the incident and transmitted waves, respectively make with the normal to the interface,  $k_i = \omega/c_i$  is the wave number in the inner fluid,  $d_{oi} = a \cos \alpha$  is the additional distance that the wave in Fig. 4-2 has to travel before the wavefront reaches the origin, and  $d_{ot}$  is the distance between a field point  $M_0(x, y)$  and  $B_0(\alpha)$  where  $B_0(\alpha) = (-a \cos \alpha, a \sin \alpha)$  is the point at which ray is incident on the fluid cylinder. This expression for  $\bar{P}_{t0}$  can also be obtained by using wave theory (Mathew and Ebenezer, 2009) and  $d_{ot} = (x + a \cos \alpha) \cos(\beta - \alpha) + (y - a \sin \alpha) \sin(\beta - \alpha)$ .

#### 4.2.2 Incident ray in the inner fluid

The ray that is transmitted into the embedded cylinder is reflected when it meets the interface at  $B1$  as shown in Fig. 4-1. The ray is traveling at an angle  $\beta$  to the normal

as shown in Fig. 4-1 and explained in the next sub-section. The ray that is transmitted to the outer fluid travels to infinity and does not re-enter the cylinder. Only the reflected ray is of interest.

It is again assumed that the Kirchhoff approximation is valid. Therefore, consider the wave of unit pressure amplitude in Fig. 4-3 that is incident on an inclined interface EF separating two semi-infinite fluids. The wave is traveling in a fluid of density  $\rho_i$  and speed of sound  $c_i$ . The normal to the interface, GH, forms an angle  $\gamma_1$  with the x axis. As shown in Fig. 4-3, the ray is traveling at an angle  $\beta$  to the normal and at an angle  $\gamma_1 - \beta$  to the x axis and is expressed as  $P_{i1}(x, y, \alpha) = \exp\{-jk_i[x \cos(\gamma_1 - \beta) + y \sin(\gamma_1 - \beta)]\}$ .

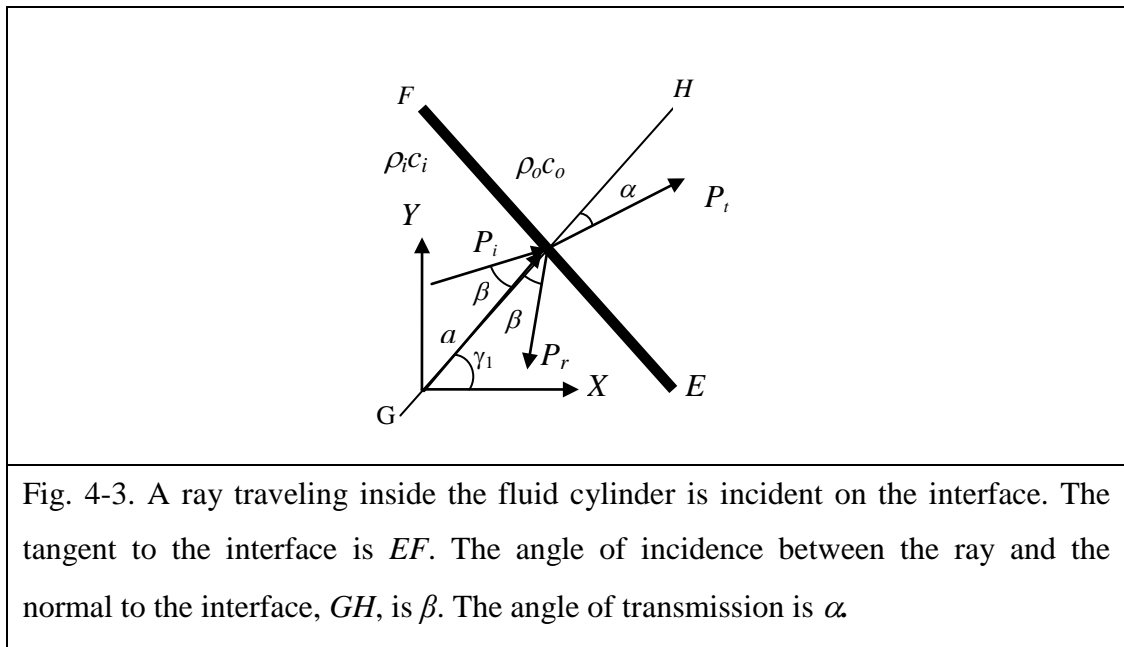
The pressure due to the reflected ray, corresponding to the unit incident ray and neglecting spreading effects that are included later, is expressed as

$$\hat{P}_{r1}(x, y, \alpha) = R_{io}(\alpha) \exp[-jk_i(d_{1i} - d_{1r})] \quad (4-2a)$$

where the hat over the pressure indicates that the pressure is due to a unit wave in the interior fluid, the subscript 1 indicates that the ray has been reflected once at a concave interface, and

$$R_{io}(\alpha) = (\rho_o c_o \cos \beta - \rho_i c_i \cos \alpha) / (\rho_o c_o \cos \beta + \rho_i c_i \cos \alpha) \quad (4-2b)$$

is the reflection coefficient when a plane wave is obliquely incident on a plane interface that includes the origin and separates two semi-infinite fluids,  $\beta$  and  $\alpha$  are the angles



that the incident and transmitted waves, respectively make with the normal to the interface,  $d_{1i} = a \cos \beta$  is the additional distance that the wavefront in Fig. 4-3 has travelled after it has passed through the origin, and  $d_{1r}$  is the distance between a field point  $M_1(x, y)$  and  $B_1(\alpha) = (a \cos \gamma_1, a \sin \gamma_1)$ . This expression for  $\hat{P}_{r1}$  can also be obtained by using wave theory (Mathew and Ebenezer, 2009) and  $d_{1r} = (x - a \cos \gamma_1) \cos(\gamma_1 + \beta) + (y - a \sin \gamma_1) \sin(\gamma_1 + \beta)$ .

The pressure due to the ray reflected once at a concave interface, corresponding to the unit ray traveling in the exterior fluid and incident on the fluid cylinder, neglecting only spreading effects that are included later, is expressed as

$$\begin{aligned} \bar{P}_{r1}(x, y, \alpha) &= \hat{P}_{r1}(x, y, \alpha) \bar{P}_{t0}(x, y, \alpha) / P_{i1}(x, y, \alpha) \\ &= T_{oi}(\alpha) R_{io}(\alpha) \exp[j(k_o a \cos \alpha + k_i \{x \cos(\gamma_1 + \beta) + y \sin(\gamma_1 + \beta) - 3a \cos \beta\})] \end{aligned} \quad (4-3)$$

where, as shown later,  $\gamma_1 = 2\beta - \alpha$ .

In general, the pressure due to the ray reflected  $q$  times at a concave surface, ( $q \geq 1$ ), corresponding to the unit ray traveling in the exterior fluid and incident on the fluid cylinder, neglecting spreading effects, is expressed as

$$\hat{P}_{rq}(x, y, \alpha) = R_{io}(\alpha) \exp[-jk_i(d_{qi} - d_{qr})] \quad (4-4)$$

where  $d_{qi}$  is the additional distance that the wavefront has travelled after it has passed through the origin, and  $d_{qr}$  is the distance between a field point  $M_q(x, y)$  and  $B_q(\alpha) = (a \cos \gamma_q, a \sin \gamma_q)$ .

The pressure due to the ray reflected  $q$  times at a concave interface, corresponding to the unit ray traveling in the exterior fluid and incident on the fluid cylinder, neglecting only spreading effects, is expressed recursively as

$$\begin{aligned} \bar{P}_{rq}(x, y, \alpha) &= \hat{P}_{rq}(x, y, \alpha) \bar{P}_{r(q-1)}(x, y, \alpha) / P_{iq}(x, y, \alpha) \\ &= T_{oi}(\alpha) R_{io}^q(\alpha) \exp[j(k_o a \cos \alpha + k_i \{x \cos(\gamma_q + \beta) + y \sin(\gamma_q + \beta) - (2q+1)k_i a \cos \beta\})] \end{aligned} \quad (4-5)$$

where  $P_{iq}(x, y, \alpha) = \exp\{-jk_i[x \cos(\gamma_q - \beta) + y \sin(\gamma_q - \beta)]\}$  is the pressure in the unit incident ray and it is shown later that  $\gamma_q = \pi - [\alpha + q(\pi - 2\beta)]$ .

### 4.2.3 Ray tracing inside the fluid cylinder

The path of each ray that enters the cylinder is of interest. Some rays will undergo total internal reflection in the exterior fluid. Each ray that enters the cylinder is reflected

and transmitted each time it encounters the interface between the two fluids. Of these, only the reflected ray is of interest because the transmitted ray travels to infinity and does not re-enter the cylinder.

Consider a ray in the exterior fluid that is incident on the cylinder such that the angle between the ray and the normal to the surface of the cylinder at the point of incidence is  $\alpha$  as shown in Fig. 4-1. It is incident on the cylinder at the point  $B_0(\alpha) = (-a \cos \alpha, a \sin \alpha)$  in Cartesian coordinates. It is assumed that the surface of the cylinder is locally plane and the expressions derived in the earlier section are used. Therefore, the amplitude of pressure in the ray that is transmitted into the cylinder is  $T_{oi}$ .

The transmitted ray travels at an angle  $\beta$  to the normal to the interface as shown in Figs. 4-1 and 4-2. Let  $O$  be the centre of the cross-section of the cylinder. The axis of the cylinder passes through it. Let  $B_1$  be the point at which the ray transmitted into the cylinder meets a concave interface for the first time. It is seen from Fig. 4-1 and the isosceles triangle  $B_0OB_1$  that  $\angle B_0B_1O = \beta$  and  $\angle B_0OB_1 = \pi - 2\beta$ . A ray from  $B_0$  to  $B_1$  is labeled as an  $n = 0$  ray because it has only been transmitted at a convex interface but not reflected at a concave interface.

The chords traversed by several traveling  $n = 0$  rays that have just entered the cylinder are shown in Fig. 4-4a and in Fig. 4-4b for the cases when  $g=h= 1.1$  and when  $g=h= 0.9$  respectively. Total internal reflection occurs when the angle of incidence is greater than the critical angle,  $\theta_c = \sin^{-1}(c_o / c_i)$  that in this case is 65.38 deg for the case where  $g=h= 1.1$ . The  $n=0$  rays reaches everywhere inside the fluid cylinder when  $h>1$  while there are regions inside the fluid cylinder where there are no  $n=0$  rays when  $h<1$ .

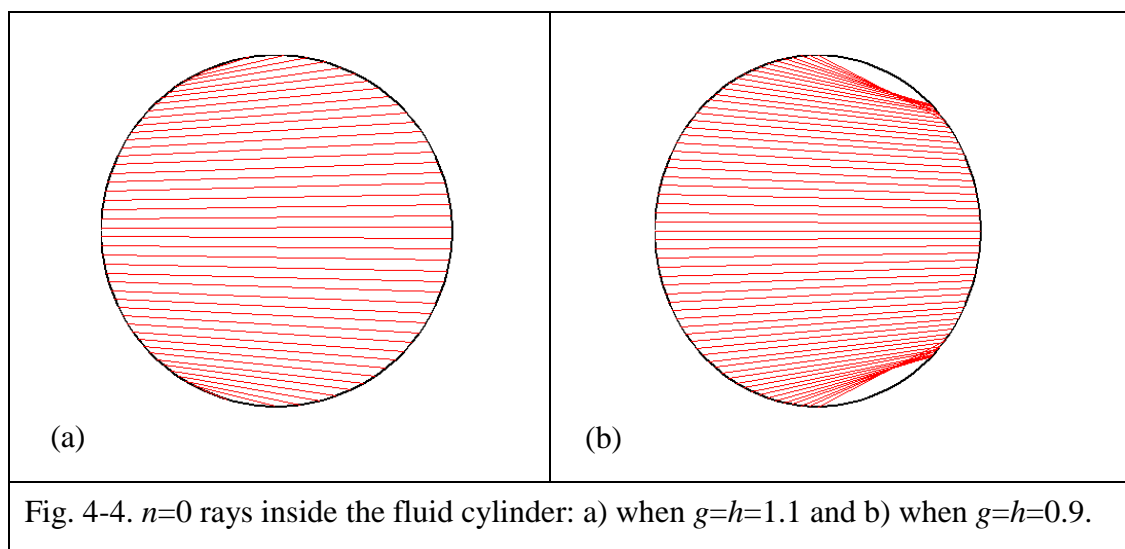


Fig. 4-4.  $n=0$  rays inside the fluid cylinder: a) when  $g=h=1.1$  and b) when  $g=h=0.9$ .

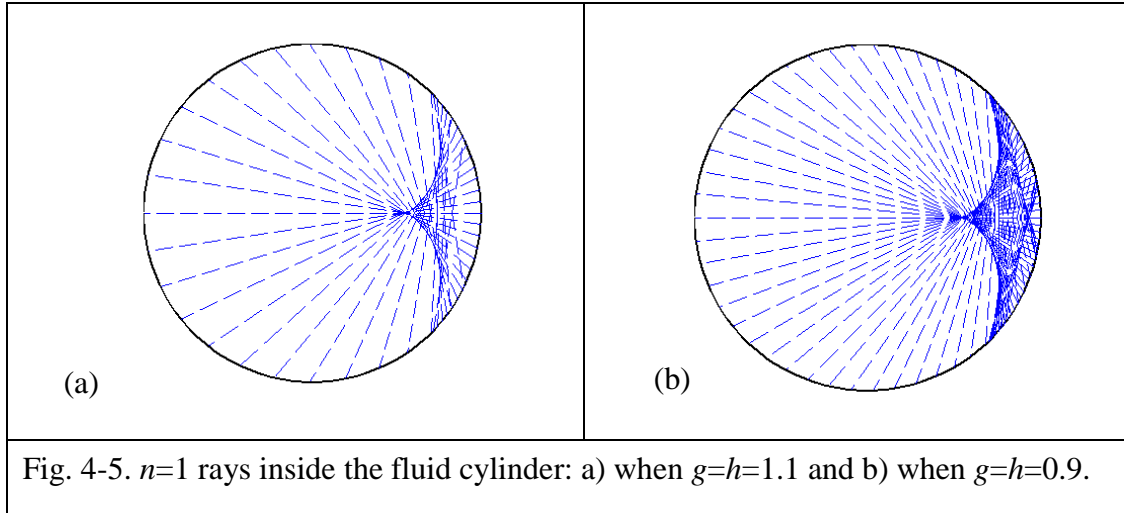


Fig. 4-5.  $n=1$  rays inside the fluid cylinder: a) when  $g=h=1.1$  and b) when  $g=h=0.9$ .

The chords traversed by  $n = 1$  rays after one internal reflection at a concave interface are shown in Fig. 4-5a and Fig. 4-5b for the cases when  $g=h= 1.1$  and when  $g=h= 0.9$ , respectively. Only one  $n=1$  ray reaches most parts of the cylinder. However, there is a region in which there are three  $n=1$  rays. When an  $n = 1$  ray meet the concave interface again an  $n = 2$  ray is reflected, and so on.

#### 4.2.4 Divergence, Convergence, and Caustics

The plane wave that is traveling along the  $x$  axis and incident on the fluid cylinder is considered to consist of an infinite number of parallel rays. Each ray, in the  $z = 0$  plane, that is incident on the cylinder, is incident at a unique angle  $\alpha$ . The paths of neighboring rays that are parallel in the exterior fluid are of interest. When  $c_i > c_o$ , the rays diverge after entering the cylinder. However, if  $c_i < c_o$ , the rays converge and some of them intersect within the cylinder, and then diverge. Irrespective of whether  $c_i > c_o$  or  $c_i < c_o$ , the rays that are traveling within the cylinder are reflected at the concave interface and then converge. Some of them intersect at a caustic (Kravtsov and Orlov, 1993) within the cylinder whereas others intersect at an imaginary point outside the cylinder. After intersection, they diverge. The details are of interest.

Consider a ray in the exterior fluid incident at an angle  $\alpha$  to the local normal to the surface as shown in Fig. 4-1. It meets the cylinder at  $B_0(\alpha) = (-a \cos \alpha, a \sin \alpha)$  and later at  $B_1(\alpha) = [a \cos(2\beta - \alpha), a \sin(2\beta - \alpha)]$ . Consider, next, an adjacent ray incident at an angle  $\alpha^+ = \alpha + d\alpha$ . It meets the cylinder at  $B_0(\alpha^+)$  and  $B_1(\alpha^+)$ . The slopes of the chords  $B_0(\alpha)B_1(\alpha)$  and  $B_0(\alpha^+)B_1(\alpha^+)$  are  $m_0(\alpha)$  and  $m_0(\alpha^+)$ , respectively. The chords meet, in  $(x,y)$  coordinates, at the focal point

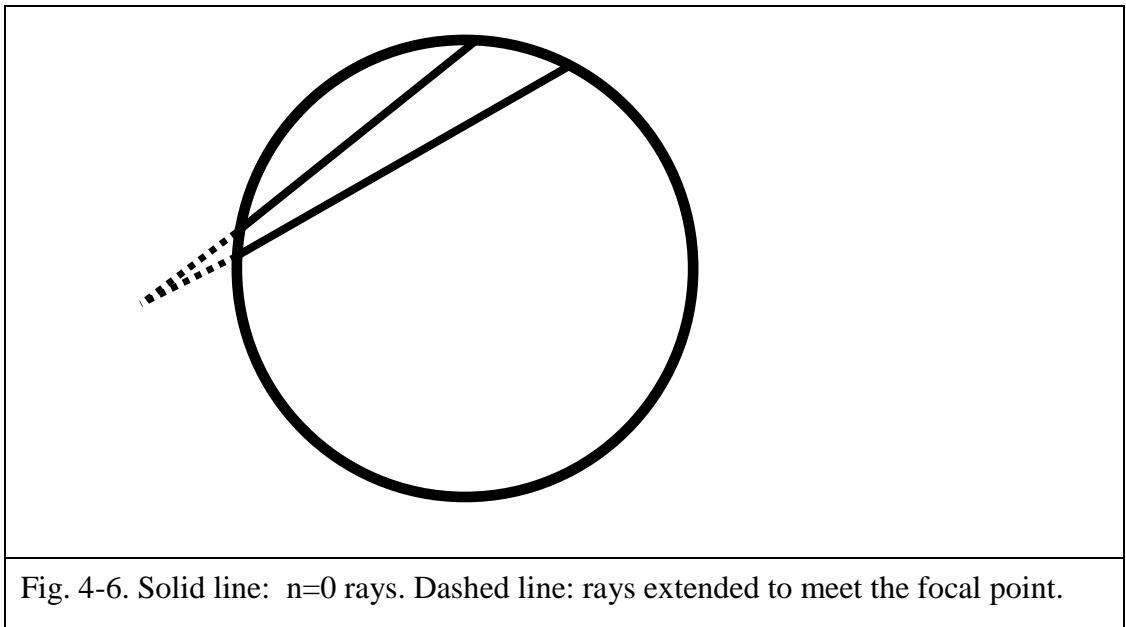
$$F_0(\alpha^+) = \left[ \begin{array}{l} \frac{-a[m_0(\alpha^+) \cos(\alpha^+) - m_0(\alpha) \cos(\alpha) + \sin(\alpha^+) - \sin(\alpha)]}{m_0(\alpha^+) - m_0(\alpha)}, \\ -a \left[ \frac{-m_0(\alpha^+) \sin(\alpha) + m_0(\alpha) \sin(\alpha^+) - m_0(\alpha^+) m_0(\alpha) (\cos(\alpha) - \cos(\alpha^+))}{m_0(\alpha^+) - m_0(\alpha)} \right] \end{array} \right]. \quad (4-7)$$

The focal point of the fluid cylinder may be inside or outside of the fluid cylinder, depending on  $h$  and the incidence angle  $\alpha$ . When  $h > 1$ , the  $n=0$  rays will diverge as shown in Fig. 4-4a and the chord of  $n=0$  rays extended to meet the focal point on the left side of the fluid cylinder is shown in Fig. 4-6. When  $h < 1$ , the  $n=0$  rays will converge as shown in Fig. 4-4b. For higher angle of incidence, the chord of  $n=0$  rays intersect inside and for lower angle of incidence, the chord of  $n=0$  rays extended and meet the focal point on the right side of the fluid cylinder. It is important to note that the rays incident at the angles  $\alpha$  and  $\alpha^- = \alpha - d\alpha$  intersect at a point  $F_0(\alpha^-)$  that is not the same as  $F_0(\alpha^+)$ .

The spreading factor of the rays,  $S_0(x, y)$ , at a point  $M_0$  that lies between  $B_0(\alpha)$  and  $B_1(\alpha)$  is determined by using the principle of energy conservation. There is no variation in pressure along the axis of the cylinder and it is assumed that the variation of intensity along a ray is inversely proportional to the distance from a focal point.  $S_0(x, y)$  is determined using the focal points  $F_0(\alpha^+)$  and  $F_0(\alpha^-)$ , and expressed, in general, as an average value:

$$S_0(x, y, \alpha) = \left\{ \left[ \overline{B_0(\alpha)F_0(\alpha^+) / M_0F_0(\alpha^+)} \right]^{0.5} + \left[ \overline{B_0(\alpha)F_0(\alpha^-) / M_0F_0(\alpha^-)} \right]^{0.5} \right\} / 2. \quad (4-8a)$$

where the overbar denotes the distance between two points. However, there are two



exceptions. First, if the magnitude of either of the two terms used to determine the average spreading factor is greater than the other by more than 5%, then  $S_0(x, y)$  is defined as the lesser of the two terms. This is because  $S_0(x, y)$  is infinity at a caustic and very large close to it. Second, if  $\alpha$  is equal to the critical angle, the spreading factor is expressed as

$$S_0(x, y, \alpha) = \left[ \frac{B_0(\alpha)F_0(\alpha^-)}{M_0F_0(\alpha^-)} \right]^{0.5}. \quad (4-8b)$$

The two rays, after reflection at  $B_1(\alpha)$  and  $B_1(\alpha^+)$ , respectively, are labeled as  $n = 1$  rays and meet the cylinder again at  $B_2(\alpha)$  and  $B_2(\alpha^+)$ , respectively. The chords  $B_1(\alpha)B_2(\alpha)$  and  $B_1(\alpha^+)B_2(\alpha^+)$  intersect at a point  $F_1(\alpha^+)$  that lies inside or outside the cylinder. In general, the  $n = q$  rays meet at

$$F_q(\alpha^+) = \left[ \frac{-a \left[ m_q(\alpha^+)c_q(\alpha^+) - m_q(\alpha)c_q(\alpha) + s_q(\alpha^+) - s_q(\alpha) \right]}{m_q(\alpha^+) - m_q(\alpha)}, \right. \\ \left. \frac{-a \left\{ -m_q(\alpha^+)s_q(\alpha) + m_q(\alpha)s_q(\alpha^+) - m_q(\alpha^+)m_q(\alpha) [c_q(\alpha) - c_q(\alpha^+)] \right\}}{m_q(\alpha^+) - m_q(\alpha)} \right] \quad (4-9)$$

in  $(x, y)$  coordinates, where  $c_q(\alpha) = \cos[\alpha + q(\pi - 2\beta)]$ ,  $c_q(\alpha^+) = \cos[\alpha^+ + q(\pi - 2\beta^+)]$ ,  $s_q(\alpha) = \sin[\alpha + q(\pi - 2\beta)]$ ,  $s_q(\alpha^+) = \sin[\alpha^+ + q(\pi - 2\beta^+)]$  and  $c_o \sin(\beta^+) = c_i \sin(\alpha^+)$  respectively.

For the  $n = 1$  rays, the focal points lie inside the cylinder when  $h = 1.1$  and the loci of these points is a closed curve that is shown in Fig. 4-7. It is obtained by using Eq. (4-9) when  $q=1$ .

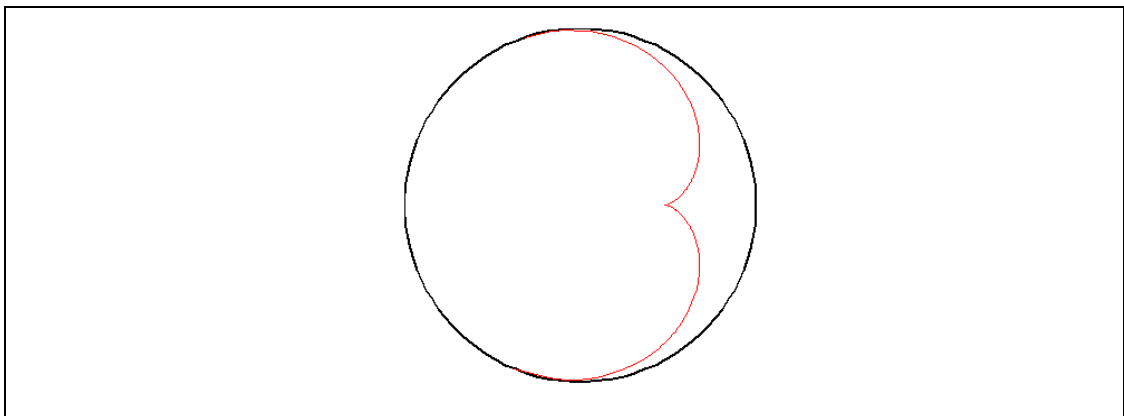


Fig. 4-7. The loci of focal points of  $n=1$  rays.

The spreading factor at a point  $M_1$  that lies between  $B_1(\alpha)$  and  $B_2(\alpha)$  is  $S_1(x, y)$ . In general spreading factor at a point  $M_q$  that lies between  $B_q(\alpha)$  and  $B_{q+1}(\alpha)$  is

$$S_q(x, y, \alpha) = \left\{ \left[ \overline{B_q(\alpha)F_q(\alpha^+) / M_q F_q(\alpha^+)} \right]^{0.5} + \left[ \overline{B_q(\alpha)F_q(\alpha^-) / M_q F_q(\alpha^-)} \right]^{0.5} \right\} / 2 \quad (4-10)$$

Alternative expressions to Eq. (4-10) are used for  $S_q(x, y)$ , as done for  $S_0(x, y)$ , when either of the two terms used to determine the average spreading factor is greater than the other by more than 5%, or if  $\alpha$  is equal to the critical angle.

#### 4.2.5 Pressure along a Ray

For the  $n = 0$  ray, the pressure at the point  $(x, y)$ , including spreading effects, is expressed as

$$P_0(x, y, \alpha) = \overline{P}_{t0}(x, y, \alpha) S_0(x, y, \alpha) \exp[j\mu_0(x, y)] \quad (4-11)$$

where  $\overline{P}_{t0}(x, y, \alpha)$  is defined in Eq. (4-1),  $\mu_0$  is 0 when  $M_0$  is between  $B_0(\alpha)$  and  $F_0(\alpha^+)$  and  $\pi/2$  when  $M_0$  is between  $F_0(\alpha^+)$  and  $B_1(\alpha)$  (Bowman *et al.*, 1969).

Similarly, the pressure at  $M_1$ , including spreading effects, is

$$P_1(x, y, \alpha) = \overline{P}_{r1}(x, y, \alpha) S_0(x_1, y_1, \alpha) \exp[j\mu_0(x_1, y_1)] S_1(x, y, \alpha) \exp[j\mu_1(x, y)] \quad (4-12)$$

where  $\mu_1$  is 0 when  $M_1$  is between  $B_1(\alpha)$  and  $F_1(\alpha^+)$  and  $\pi/2$  when  $M_1$  is between  $F_1(\alpha^+)$  and  $B_2(\alpha)$ .

In general, the pressure at a point  $M_q$  that lies between  $B_q(\alpha)$  and  $B_{q+1}(\alpha)$ , including spreading effects is expressed as

$$P_q(x, y, \alpha) = \overline{P}_{rq}(x, y, \alpha) S_q(x, y, \alpha) \exp[j\mu_q(x, y)] \prod_{n=1}^q S_{n-1}(x_n, y_n, \alpha) \exp[j\mu_{n-1}(x_n, y_n)] \quad (4-13)$$

where  $\mu_q$  is 0 when  $M_q$  is between  $B_q(\alpha)$  and  $F_q(\alpha^+)$  and  $\pi/2$  when  $M_q$  is between  $F_q(\alpha^+)$  and  $B_{q+1}(\alpha)$ , and  $\mu_n$  is 0 when  $F_n(\alpha^+)$  is between  $B_n(\alpha)$  and  $B_{n-1}(\alpha)$  and  $\pi/2$  when  $F_n(\alpha^+)$  is not between  $B_n(\alpha)$  and  $B_{n-1}(\alpha)$ .

#### 4.2.6 Interior Pressure Field

In order to determine the total pressure at a point inside the cylinder, it is necessary to first find all the eigenrays – rays that pass through the point of interest.

The  $n = 0$  ray meets the interface between the exterior and interior fluids at the



points  $(a, \pi - \alpha)$  and  $(a, 2\beta - \alpha)$  in polar coordinates. The ray passes through the point  $(r, \theta)$  if the point lies on the straight line that joins  $B_0(\alpha)$  and  $B_1(\alpha)$ . Therefore, the angle  $\alpha$  at which the  $n=0$  ray should be incident on the cylinder in order for it to pass through  $(r, \theta)$  is determined by solving

$$r[\sin\{\theta + \alpha - \pi\} - \sin\{\theta - 2\beta + \alpha\}] + a \sin\{2\beta\} = 0 \quad (4-14)$$

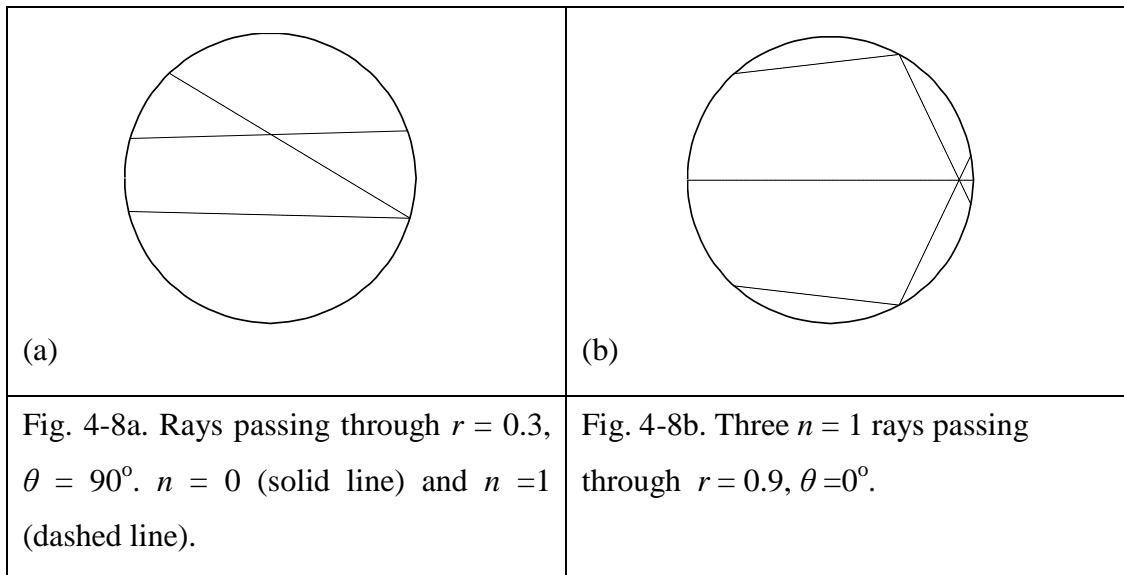
after using Snell's law to eliminate  $\beta$  and by using numerical methods. It is noted that there is only one solution to the above equation when  $c_i > c_o$ . In general,  $L_0$  rays pass through the point and the angle of incidence of these rays when they are in the exterior fluid is  $\alpha_l, l = 1, 2, 3, \dots, L_0$ .

Similarly, the  $n = q$  rays that passes through the field point are identified by solving

$$r[\sin\{\theta - 2q\beta + \alpha + (q-1)\pi\} - \sin\{\theta - 2(q+1)\beta + \alpha + q\pi\}] + a \sin(2\beta) = 0 \quad (4-15)$$

find  $\alpha_l, l = 1, 2, 3, \dots, L_q$ . The number of solutions,  $L_q$ , to the above equation depends on the location of the field point, the value of  $q$ , and the relationship between  $c_i$  and  $c_o$ .

For example, when  $c_i/c_o = 1.1$ , only one  $n = 1$  ray (dashed line) passes through the field point  $(0.3, 90^\circ, 0)$  deg is shown in Fig. 4-8a while three  $n = 1$  rays pass through the point  $(0.9, 0^\circ, 0)$  and the solutions to Eq. (4-15) when  $q=1$  at the point  $r=0.9$  and  $\theta=0^\circ$ , are  $\alpha_1 = 47.6532^\circ$ ,  $\alpha_2 = 0^\circ$ , and  $\alpha_3 = 47.6532^\circ$  deg is shown in Fig. 4-8b.



After finding all the rays that pass through the point of interest, the complex pressure due to each of them is added to determine the total pressure,  $P(x, y)$ , at the point.

$$P(x, y) = \sum_{n=0}^N \sum_{l=1}^{L_q} P_n(x, y, \alpha_l) \quad (4-16)$$

where  $P_n(x, y, \alpha_l)$  is the pressure due to the  $l$ th ray and is obtained by using Eq. (4-13). The value of  $N$  is chosen to be large enough to ensure convergence of the series to a desired accuracy. When the acoustic contrast is small, it is sufficient to use a small value of  $N$  because the reflection coefficient is small.

#### 4.2.7 Field Theory

Consider a plane wave of unit amplitude is incident on the fluid cylinder and it can be expressed in cylindrical coordinates  $(r, \theta, z)$  in series form as

$$P_i = \sum_{n=0}^{\infty} \varepsilon_n (-j)^n J_n(k_o r) \cos n\theta \quad (4-17a)$$

where  $J_n(\cdot)$  is the  $n$ th order Bessel function of the first kind and Neumann coefficient

$$\varepsilon_n = \begin{cases} 1 & n=0 \\ 2 & n>0 \end{cases} \quad (4-17b)$$

The radial component of displacement associated with incident wave is given by

$$u_i = \frac{-1}{\rho_o \omega^2} \frac{\partial P_i}{\partial r} \quad (4-18a)$$

Where  $\partial$  denotes the partial derivative.

$$u_i = \frac{-k_o}{\rho_o \omega^2} \sum_{n=0}^{\infty} \varepsilon_n (-j)^n J_n'(k_o r) \cos n\theta \quad (4-18b)$$

where  $'$  denotes the derivative.

When the incident wave meets the fluid cylinder it scatters and the scattered pressure is expressed in series form as

$$P_s = \sum_{n=0}^{\infty} A_n H_n^2(k_o r) \cos n\theta \quad (4-19)$$

where  $H_n^2(\cdot)$  is the  $n$ th order Hankel function of the second kind, and  $A_n$  is the unknown coefficient of scattered pressure.

The radial component of displacement associated with the scattered wave is given by

$$u_s = \frac{-k_o}{\rho_o \omega^2} \sum_{n=0}^{\infty} A_n H_n^{(2)'}(k_o r) \cos n\theta \quad (4-20)$$

The interior pressure  $P$  at a point  $(r, \theta, 0)$  of a fluid cylinder is expressed in series form as (Skudrzyk, 1971)

$$P(r, \theta) = \sum_{n=0}^{\infty} B_n J_n(k_i r) \cos(n\theta) \quad (4-21)$$

where  $B_n$  is the unknown coefficient of interior pressure.

The radial component of displacement associated with the transmitted interior wave is given by

$$u_t = \frac{-k_i}{\rho_i \omega^2} \sum_{n=0}^{\infty} B_n J_n'(k_i r) \cos n\theta \quad (4-22)$$

At the interface  $r = a$ , radial components of pressure and displacement in the outer fluid is equal to radial components of pressure and displacement in the outer fluid. Applying the continuity conditions at the interface, the coefficient  $B_n$  can be evaluated as

$$B_n = \frac{2(-j)^{n+1} \epsilon_n}{\pi \rho_o a \left( \frac{k_o}{\rho_o} H_n^{(2)'}(k_o a) J_n(k_i a) - \frac{k_i}{\rho_i} H_n^{(2)}(k_o a) J_n'(k_i a) \right)} \quad (4-23).$$

#### 4.2.8 Directional Response

Consider, next,  $2H$  equispaced point hydrophones as shown in Fig. 4-1.  $2H$  sectors, each with  $2J$  adjacent hydrophones, are formed by grouping these hydrophones. The outputs from the hydrophones in a sector are delayed to simulate a linear array and summed, and the outputs from a few adjacent sectors that give high outputs are used to

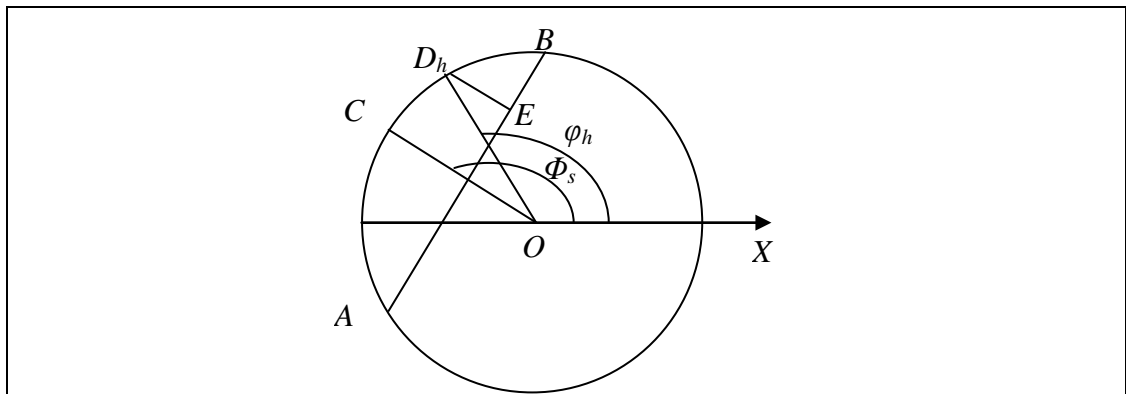


Fig. 4-9. Schematic sector of a circular array. The hydrophones are in the arc  $ACB$ . Each hydrophone is delayed by an appropriate amount to simulate a linear array from the chord  $AB$ .

determine the direction of arrival of the wave. In practical applications, the region  $r < b$  is occupied by a structure on which the array is mounted and the output from the sector that is directly illuminated by the wave is much more than that from the sector that is diametrically opposite it.

In the minor arc  $AB$ , shown in Fig. 4-9, there are  $2J$  adjacent hydrophones. They form one sector and are used to simulate a linear array on the chord  $AB$ . The angle between the normal to the linear array and the  $x$  axis is  $\Phi_s$ . The  $h$ th hydrophone is at the point  $D_h = (x_h, y_h)$  and the line  $OD_h$  makes an angle  $\phi_h = \pi(2h-1)/2H$ ,  $h = 1, 2, 3, \dots, 2H$ , with the  $x$  axis.

A sector is used to simulate a linear array by applying a phase delay that corresponds to the distance  $ED_h$ , in Fig. 4-9, to the hydrophone at  $D_h$ . For convenience, an additional delay that corresponds to the distance  $OF$  is applied to all the  $2J$  hydrophones in that sector. Therefore, the total delay applied to the  $h$ th hydrophone corresponds to  $d_h = b \cos(\phi_h - \Phi_s)$ . The delayed and summed voltage output from the  $s$ th sector is expressed as

$$V_s = M \sum_{h=s}^{2J+s-1} P(x_h, y_h) \exp(-jk_i d_h) \quad (4-24)$$

where  $M$  is the receiving acoustic sensitivity of each hydrophone expressed in V/Pa and  $P(x_h, y_h)$  is obtained by using Eq. (4-16).

Directional response is defined here as the output from the  $s$ th sector when the wave is traveling along the  $x$  axis. For a particular array, it is dependent only on the angle between the normal to the  $s$ th sector and the direction in which the wave is traveling.

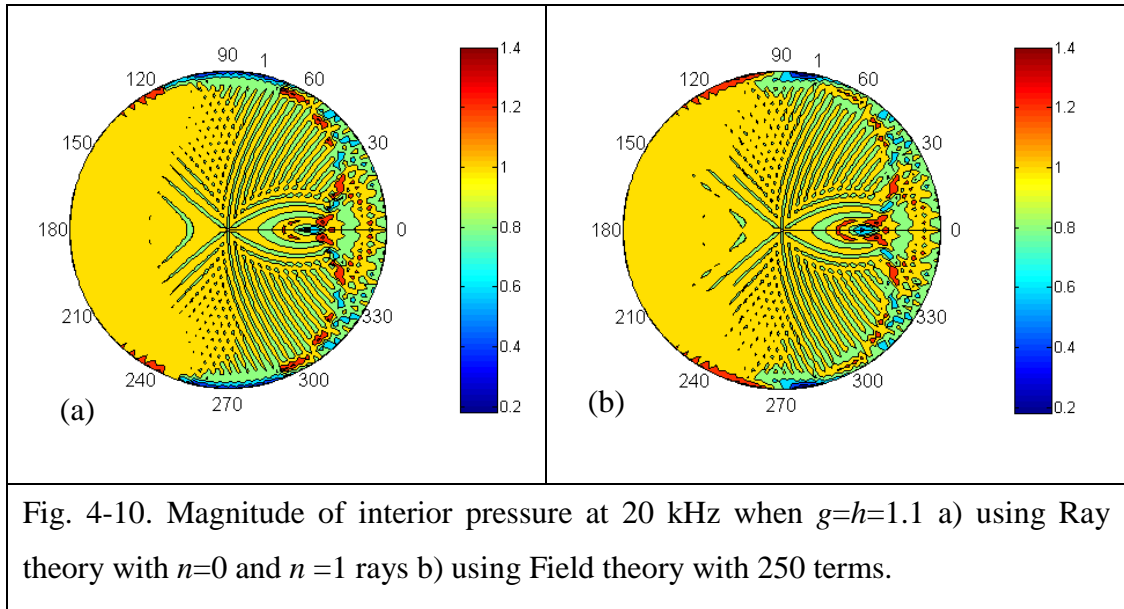
When the interior and exterior fluids are the same ( $g = h = 1$ ) and the incident wave is traveling along the  $x$  axis, the output from the  $(H-J+1)$ th sector is maximum because it is symmetric about the  $x$  axis. In general, when  $g = h = 1$ , the sector with the maximum output is the one with a normal most closely aligned with the direction in which the wave is traveling. Here, with the wave traveling along the  $x$  axis, the outputs from the sector whose centre lies on the negative  $x$  axis and the outputs from neighboring sectors are large. Numerical results are presented to quantitatively illustrate the effect of the embedded cylinder on the outputs from the linear arrays.

### 4.3 NUMERICAL RESULTS AND DISCUSSIONS

Numerical results are presented for several cases to illustrate the agreement between the results obtained using the present method and field theory and to illustrate the effect of the properties of the embedded cylinder. Unless otherwise specified,  $c_o = 1500$  m/s, and  $\rho_o = 1000$  kg/m<sup>3</sup>. The radius of the cylinder is 1 m in all the cases. Several results are presented for frequencies of 5 kHz and 20 kHz and correspond to  $ka \approx 20.9$  and 83.8, respectively. The number of terms used to obtain the field theory results depends on the frequency and varies from 30 at 5 kHz to 250 at 20 kHz and the convergence of the results is tested in all cases. At even higher frequencies, the accuracy of the ray theory results increases but more terms are required when using field theory. Unless otherwise specified, all field theory results are shown using a solid line, ray theory results are shown using dots, and only the  $n = 0$  and 1 rays are used. The effect of using an increasing number of terms in ray theory is illustrated in some figures. Ray theory results are shown using various symbols.

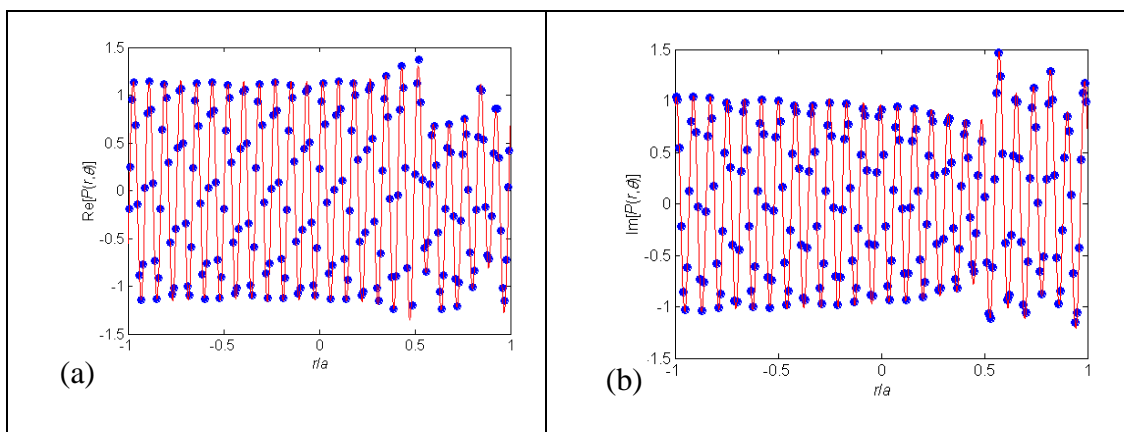
In Figs. 4-10a and 4-10b, contour plots are presented of the magnitudes of the interior pressure field computed using ray theory and field theory, respectively to illustrate the overall good agreement. The frequency is 20 kHz.  $c_i = 1650$  m/s and  $\rho_i = 1100$  kg/m<sup>3</sup>; that is,  $g = 1.1$  and  $h = 1.1$ . Evanescent rays are generated when the angle of incidence is greater than the critical angle,  $\theta_c = \sin^{-1}(c_o / c_i)$ .  $\theta_c$  is 65.38 deg when  $g=h= 1.1$ . The incident wave is traveling along the positive  $x$  axis. Therefore, as expected, the figures are symmetric about the diameter containing  $\theta=0$ . It is seen from the Figs. that the agreement between the two methods is good at most points and that intricate patterns match well. However, on  $r = a$ , and  $\theta$  near 90 and 180 deg, it is seen from the field theory results that the pressure changes rapidly and the agreement is not as good as it is at other places. If  $g = h = 1$ , then the magnitude will be one everywhere in the cylinder. It is seen from the contour plots in Fig. 4-10 that the pressure patterns inside and outside the caustic curve in Fig. 4-7 is different. The difference is expected to be greater when the acoustic contrast between the inner and outer fluids is greater because more of the  $n = 0$  ray will be reflected when the  $n = 0$  rays are incident on the concave surface.

The real and imaginary parts of the pressures for  $g = h = 1.1$ , at 20 kHz, on a few diameters, are also presented to illustrate the agreement between the results obtained



using the two methods. The real and imaginary parts of the pressures are shown in Figs. 4-11a and 4-11b, respectively, on the diameter formed by the by the  $\theta=0$  and 180 deg radii. Similarly, the pressures are shown in Figs. 4-12a and 4-12b, on the diameter formed by the by the  $\theta=30$  and 210 deg radii; and in Figs. 4-13a and 4-13b on the diameter formed by the by the  $\theta=90$  and 270 deg radii. In the figures, the position on the diameter is shown to vary from  $r/a = -1$  to  $+1$ ; where points on the  $\theta=0, 30,$  and  $90$  deg deg radii are assumed to have non-positive values. The wavelength inside the cylinder, at 20 kHz, is 82.5 mm and there are nearly 25 wavelengths in one diameter.

It is seen from Figs. 4-11a and 4-11b, where the pressure on the  $\theta=0$  and 180 deg radii is shown, that nearly 25 deep spatial oscillations occur with the real and imaginary



pressure varying from a little less than -1 to a little more than +1. This happens because the wavelength inside the cylinder, at 20 kHz, is 82.5 mm and there are approximately 25 wavelengths in one diameter. If  $g = h = 1$ , then the oscillations will be uniform and exactly between -1 and +1. In these figures, a significant change in the pattern is seen near  $r/a = 0.48$  – the point at which the focal point of the  $n = 1$  ray lies on the  $\theta=0$  line. As  $r/a$  approaches 0.48 from below, the peaks in the absolute real pressure, in Fig. 4-10a, increase and then, after crossing  $r/a = 0.48$ , decrease suddenly. The peaks in the absolute imaginary pressure, in Fig. 4-11b, decrease and then increase suddenly. It is seen from Fig. 4-10 that the magnitude of the pressure on this diameter varies from about 0.2 to 1.3. Even though there is good agreement between the results obtained using the two methods at all points, the difference in the real pressure is a little greater near  $r/a = 0.48$ .

In Fig. 4-12 the interior pressure field computed using ray theory and field theory on the diameter formed by  $\theta = 30$  and  $210$  deg radii are presented. The agreement is good. The caustic point for the  $n = 1$  ray lies on  $r/a \approx 0.78$  when  $\theta = 30$  deg and the difference between the ray and field theory results is a little more in its neighborhood.

In Figs. 4-13a and 4-13b, the pressure is presented on the diameter formed by  $\theta = 90$  and  $270$  deg radii. The spatial oscillations corresponding to 20 kHz are seen as perturbations on a curve that slowly varies between +1 and -1. If  $g = h = 1$ , the real part of pressure will be +1 and the imaginary part will be zero because this diameter lies on  $x = 0$  and the incident pressure is  $\exp(-jkx)$ . Therefore, a hydrophone kept on this diameter in the embedded cylinder will sense a pressure that is considerably different

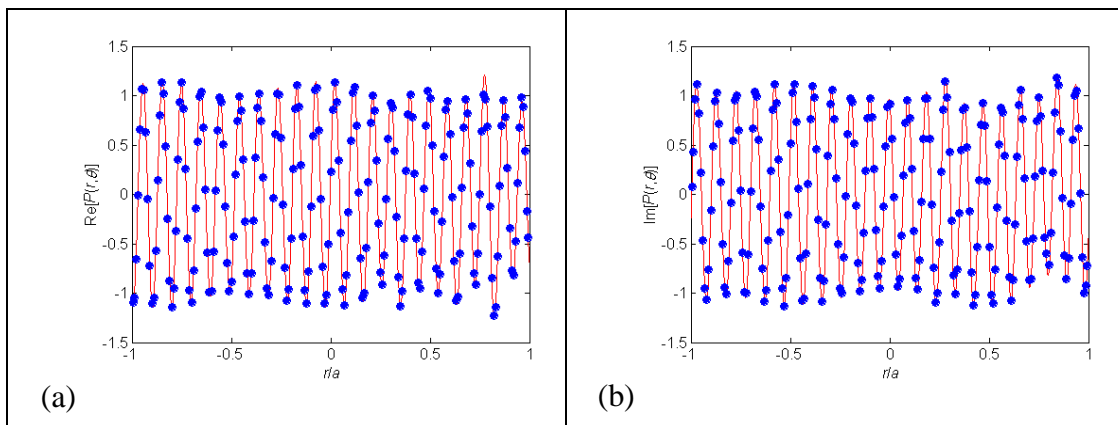


Fig. 4-12. a) Real part and b) imaginary part of interior pressure field on diameter formed by  $\theta = 30^\circ$  and  $210^\circ$  radii at 20 kHz when  $g=h=1.1$ . Solid line: Field theory with 250 terms. Diamonds: Ray theory with  $n = 0$  and 1 rays.

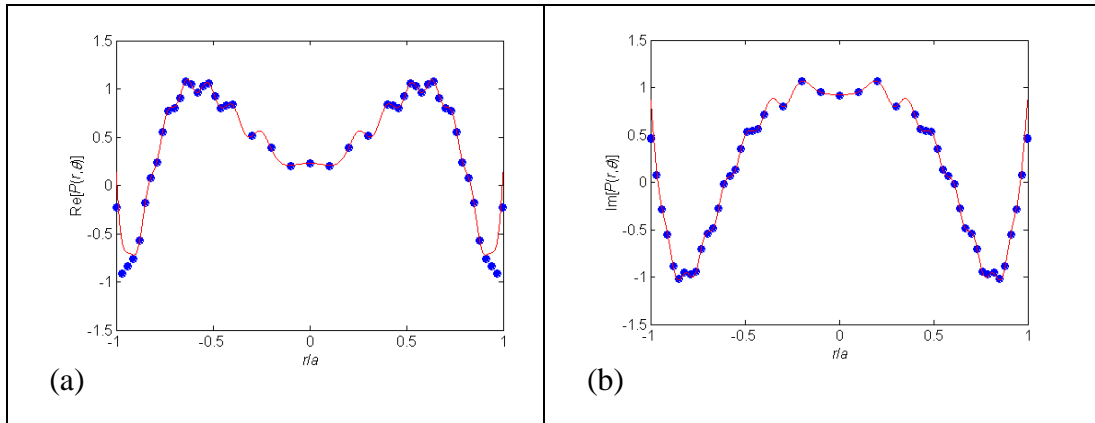


Fig. 4-13. a) Real part and b) imaginary part of interior pressure field on diameter formed by  $\theta = 90^\circ$  and  $270^\circ$  radii at 20 kHz when  $g=h=1.1$ . Solid line: Field theory with 250 terms. Diamonds: Ray theory with  $n = 0$  and 1 rays.

from the free-field pressure that would have existed if the embedded cylinder had not been present. The caustic point for the  $n = 1$  ray lies on  $r/a \approx 0.986$  when  $\theta = 90$  deg and the difference between the ray and field theory results is greater in its neighborhood.

In Figs. 4-14a and 4-14b, contour plots are presented of the magnitudes of the interior pressure field computed using ray theory and field theory, respectively to illustrate the overall good agreement for a frequency of 5 kHz at which  $ka \approx 20$ . The real and imaginary parts of the pressures are shown in Figs. 4-15a and 4-15b, respectively, on the diameter formed by the by the  $\theta= 0$  and 180 deg radii. Similarly, the pressures are shown in Figs. 4-16a and 4-16b, on the diameter formed by the by the  $\theta= 30$  and 210 deg radii; and in Figs. 4-17a and 4-17b on the diameter formed by the by the  $\theta= 90$  and 270 deg radii. Even though the value of  $ka$  is now one fourth of the earlier value, the

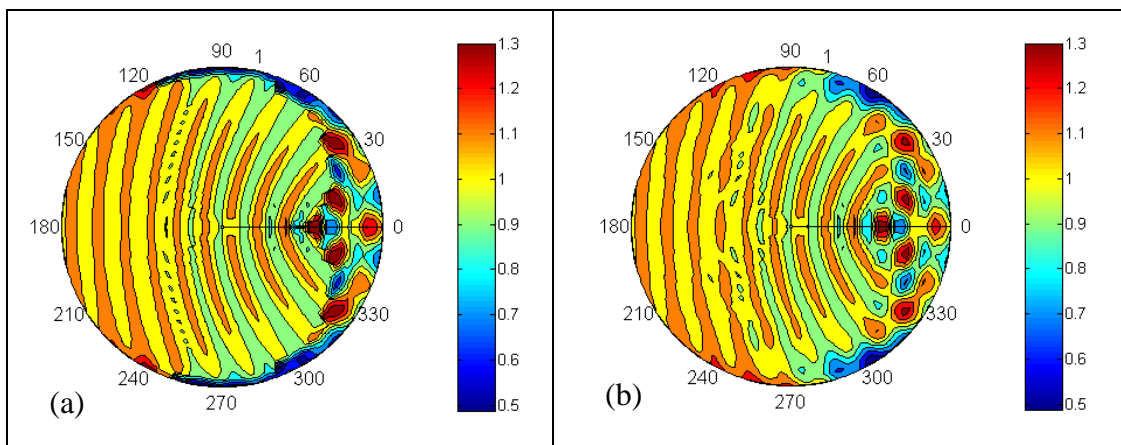


Fig. 4-14. Magnitude of interior pressure at 5 kHz when  $g=h=1.1$  a) using Ray theory with  $n=0$  and  $n = 1$  rays b) using Field theory with 250 terms.



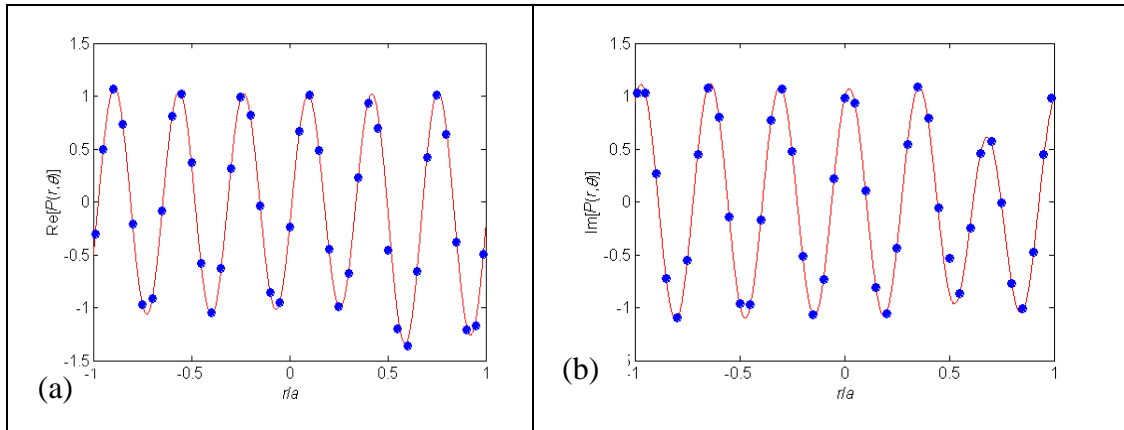


Fig. 4-15. a) Real part and b) imaginary part of interior pressure field on diameter formed by  $\theta = 0^\circ$  and  $180^\circ$  radii at 5 kHz when  $g=h=1.1$ . Red solid line: Field theory with 250 terms. Blue dots: Ray theory with  $n = 0$  and 1 rays.

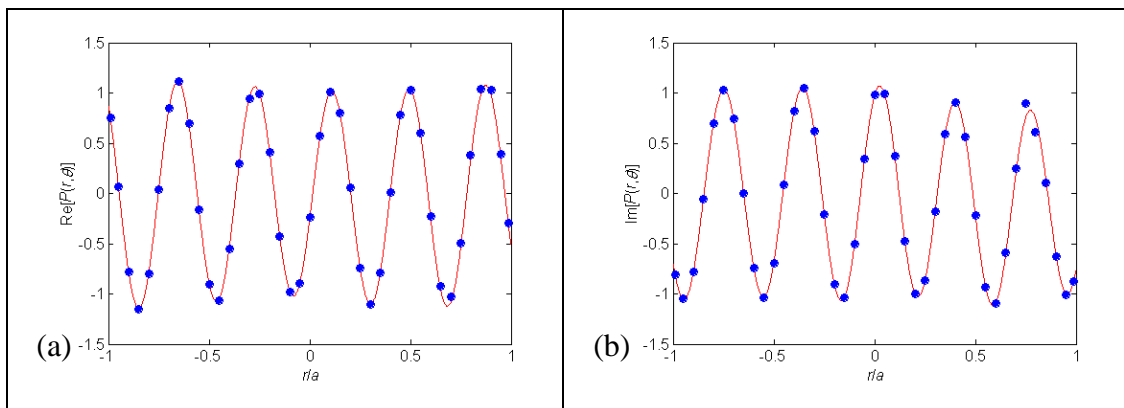


Fig. 4-16. a) Real part and b) imaginary part of interior pressure field on diameter formed by  $\theta = 30^\circ$  and  $210^\circ$  radii at 5 kHz when  $g=h=1.1$ . Red solid line: Field theory with 250 terms. Blue dots: Ray theory with  $n = 0$  and 1 rays.

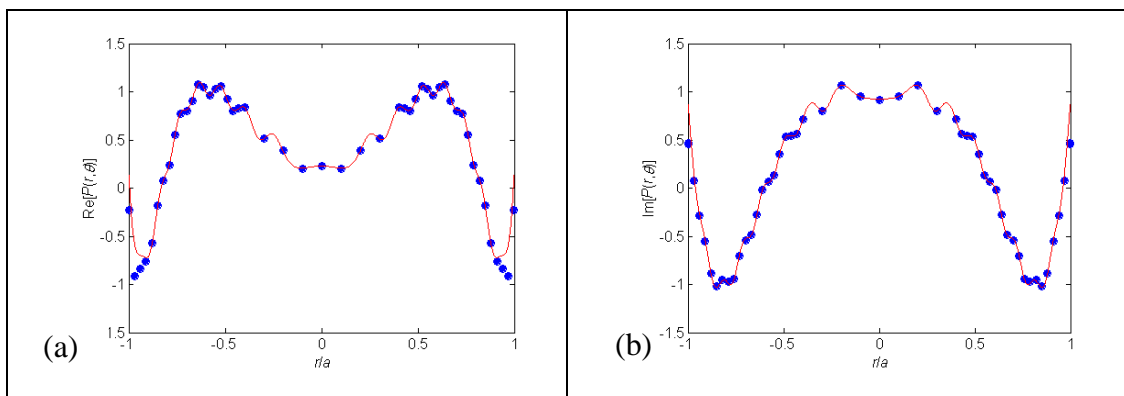
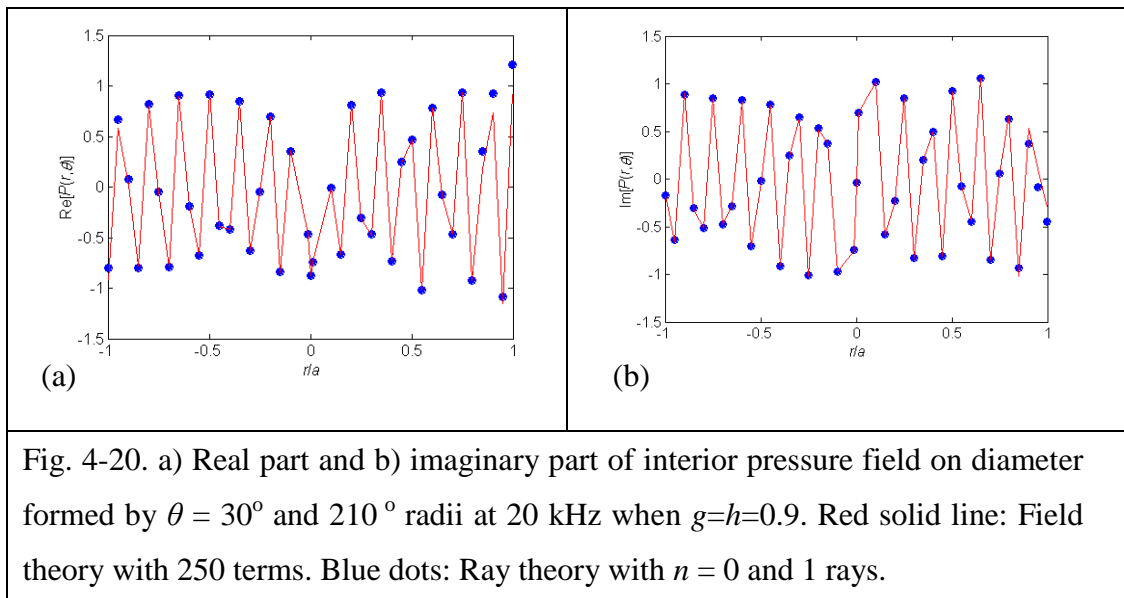
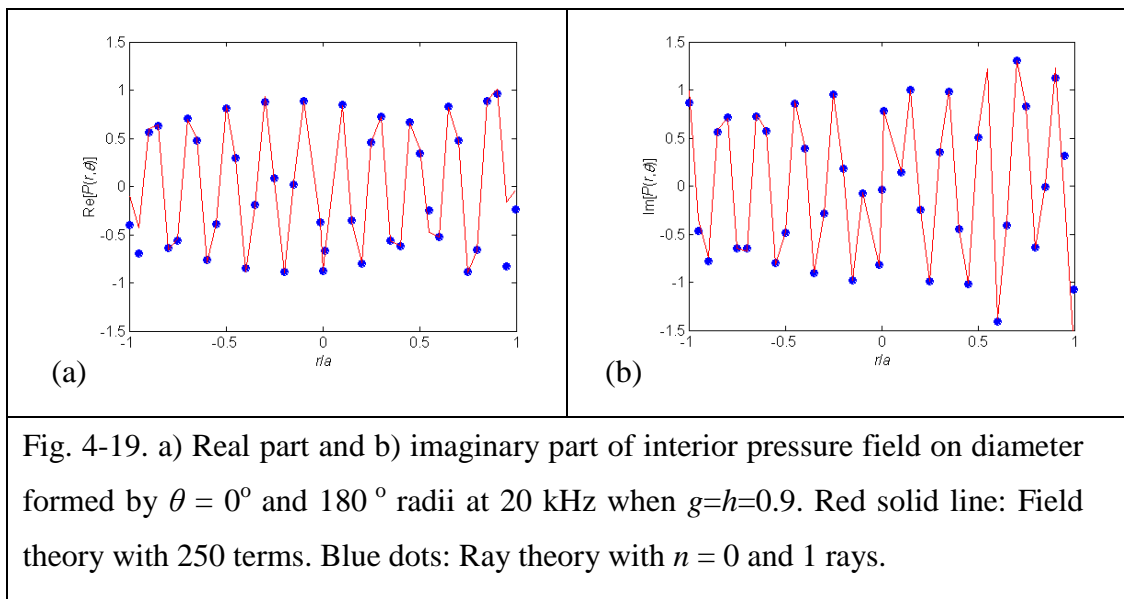
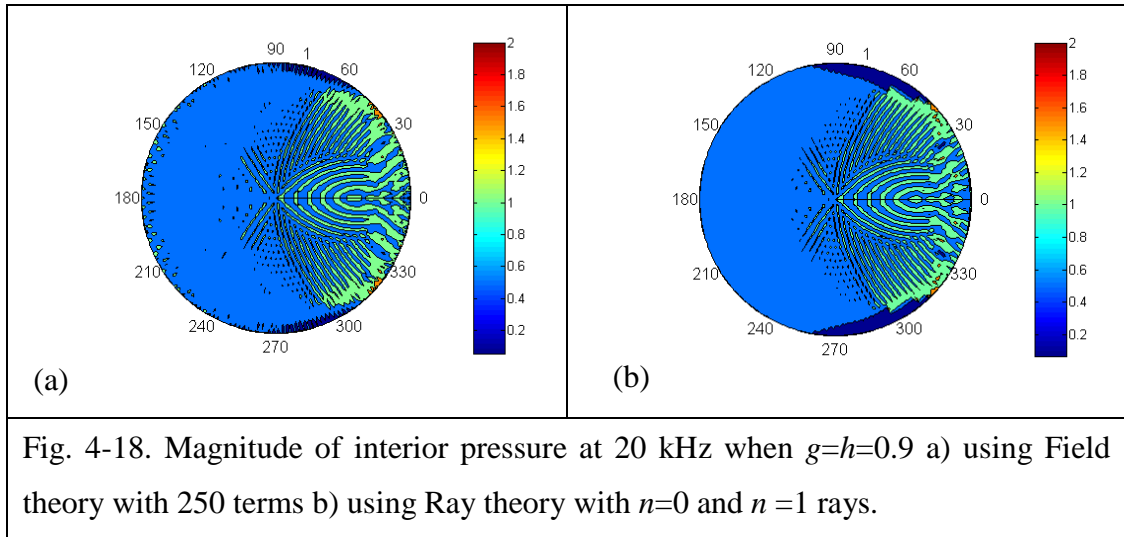


Fig. 4-17. a) Real part and b) imaginary part of interior pressure field on diameter formed by  $\theta = 90^\circ$  and  $270^\circ$  radii at 5 kHz when  $g=h=1.1$ . Red solid line: Field theory with 250 terms. Blue dots: Ray theory with  $n = 0$  and 1 rays.



observations regarding the results at  $ka \approx 80$  are valid for this case also. The caustic points depend only on  $h$  and are independent of frequency. It is seen that observations regarding the agreement near the caustic points at 20 kHz are valid for 5 kHz also.

In Figs. 4-18a and 4-18b, contour plots are presented of the magnitudes of the interior pressure field computed using ray theory and field theory, respectively to illustrate the overall good agreement when  $c_i = 1350$  m/s and  $\rho_i = 900$  kg/m<sup>3</sup>; that is  $g = 0.9$  and  $h = 0.9$ . It is seen from the figure that the magnitude of interior pressure is lower in the region where there is no  $n=0$  ray. The real and imaginary parts of the pressures are shown in Figs. 4-19a and 4-19b, respectively, on the diameter formed by the by the  $\theta = 0$  and 180 deg radii. The caustic point for the  $n = 1$  ray lies on  $r/a \approx 0.529, 0.9276$  and  $0.934$  when  $\theta = 0$  deg and the difference between the ray and field theory results is a little more in its neighborhood. Similarly, the pressures are shown in Figs. 4-20a and 4-20b, on the diameter formed by the by the  $\theta = 30$  and 210 deg radii and the caustic point for the  $n = 1$  ray lies on  $r/a \approx 0.7534, \text{ and } 0.787$  when  $\theta = 30$  deg. Similarly, the pressures are shown in Figs. 4-21a and 4-21b on the diameter formed by the by the  $\theta = 90$  and 270 deg radii.

In Figs. 4-22a and 4-22b, contour plots are presented of the magnitudes of the interior pressure field computed using ray theory and field theory, respectively to illustrate the overall good agreement for a frequency of 5 kHz at which  $ka \approx 20$ . The real and imaginary parts of the pressures are shown in Figs. 4-23a and 4-23b, respectively, on the diameter formed by the by the  $\theta = 0$  and 180 deg radii. Similarly, the pressures are shown in Figs. 4-24a and 4-24b, on the diameter formed by the by the  $\theta = 30$  and 210 deg radii; and in Figs. 4-25a and 4-25b on the diameter formed by the by the  $\theta = 90$  and 270 deg radii. Even though the value of  $ka$  is now one fourth of the earlier value, the observations regarding the results at  $ka \approx 80$  are valid for this case also.

Next, results are presented for higher values of  $g$  and  $h$  at which the reflection coefficient for rays traveling inside the embedded cylinder are higher. For  $g = 2$  and  $h = 1.5$ , the  $n = 2, 3, \dots$  rays can be expected to have a greater effect on the error than for the earlier case of low  $g$  and  $h$ . For a frequency of 20 kHz, real parts of the pressures on three diameters are shown in Figs. 4-26a, 4-27a, and 4-28a; and the imaginary parts are shown in Figs. 4-26b, 4-27b, and 4-28b. It is seen that including more rays yields better agreement between the two methods.

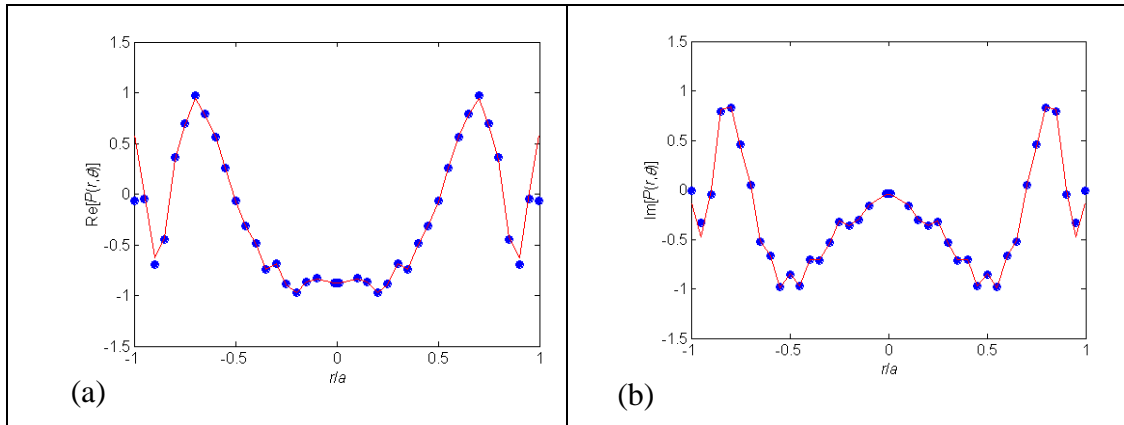


Fig. 4-21. a) Real part and b) imaginary part of interior pressure field on diameter formed by  $\theta = 90^\circ$  and  $270^\circ$  radii at 20 kHz when  $g=h=0.9$ . Red solid line: Field theory with 250 terms. Blue dots: Ray theory with  $n = 0$  and  $1$  rays.

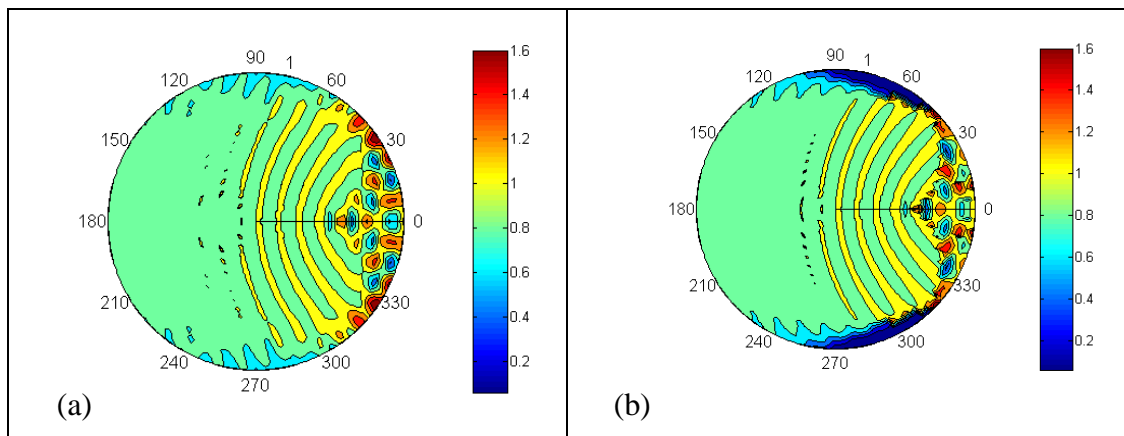


Fig. 4-22. Magnitude of interior pressure at 5 kHz when  $g=h=0.9$  a) using Field theory with 250 terms b) using Ray theory with  $n=0$  and  $n = 1$  rays.

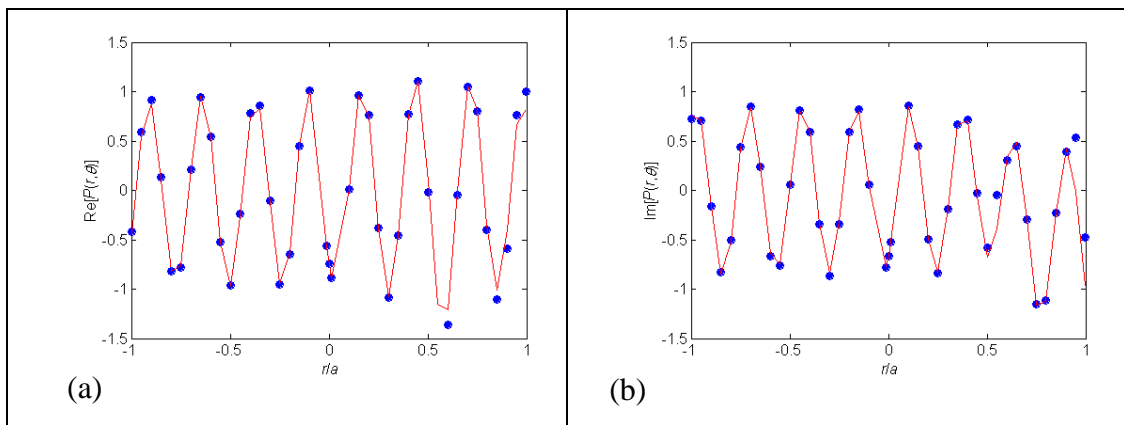


Fig. 4-23. a) Real part and b) imaginary part of interior pressure field on diameter formed by  $\theta = 0^\circ$  and  $180^\circ$  radii at 5 kHz when  $g=h=0.9$ . Red solid line: Field theory with 250 terms. Blue dots: Ray theory with  $n = 0$  and  $1$  rays.

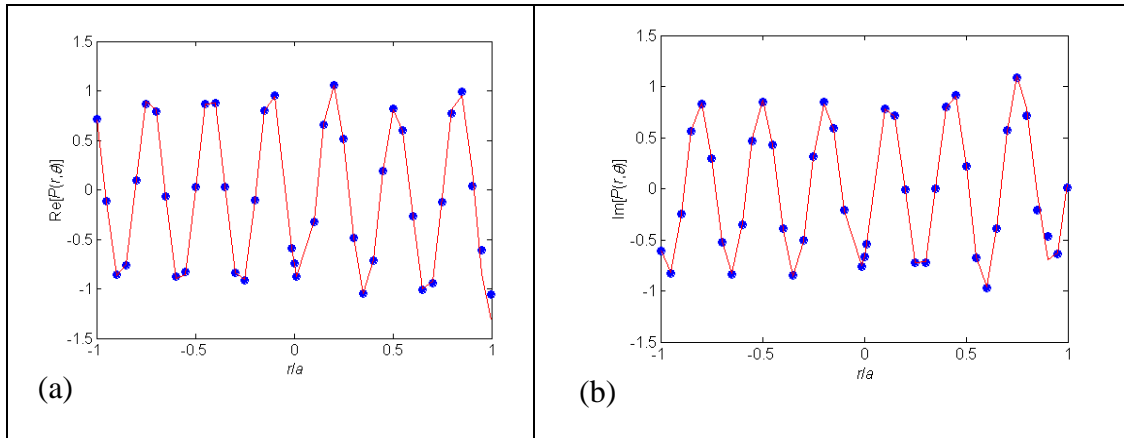


Fig. 4-24. a) Real part and b) imaginary part of interior pressure field on diameter formed by  $\theta = 30^\circ$  and  $210^\circ$  radii at 5 kHz when  $g=h=0.9$ . Red solid line: Field theory with 250 terms. Blue dots: Ray theory with  $n = 0$  and 1 rays.

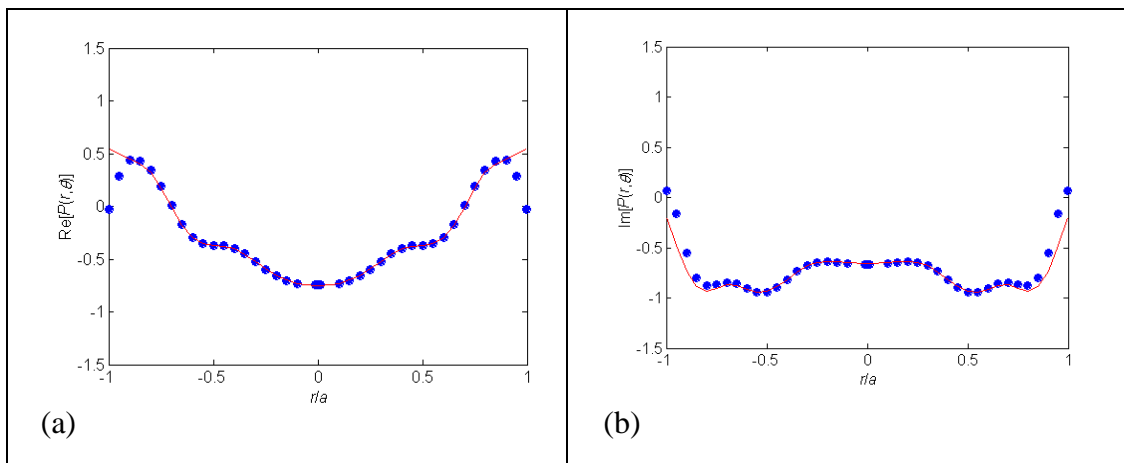


Fig. 4-25. a) Real part and b) imaginary part of interior pressure field on diameter formed by  $\theta = 90^\circ$  and  $270^\circ$  radii at 5 kHz when  $g=h=0.9$ . Red solid line: Field theory with 250 terms. Blue dots: Ray theory with  $n = 0$  and 1 rays.

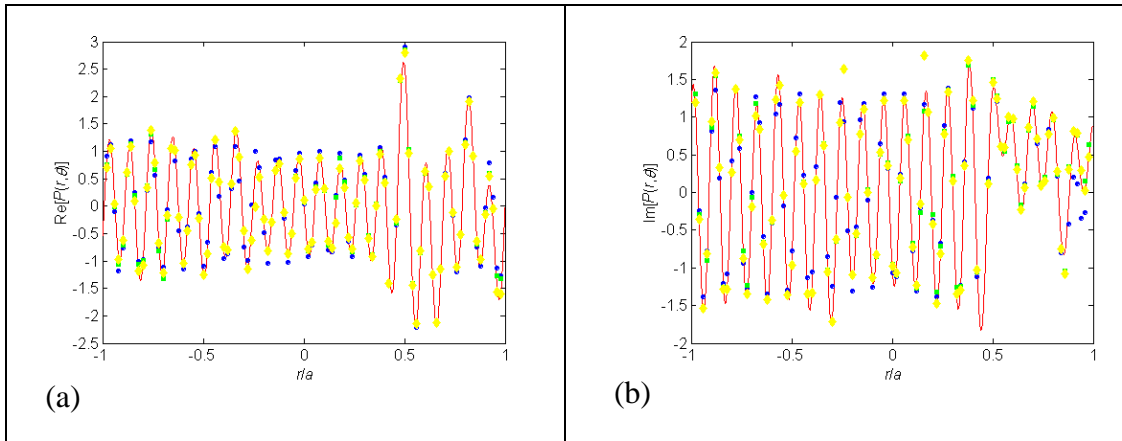


Fig. 4-26. a) Real part and b) imaginary part of interior pressure field on diameter formed by  $\theta = 0^\circ$  and  $180^\circ$  radii at 20 kHz when  $g=1.4$  and  $h=1.4$ . Red solid line: Field theory with 250 terms. Blue dots: Ray theory with  $n = 0$  and 1 rays. Green squares: Ray theory with  $n = 0, 1$  and 2 rays. Yellow diamonds: Ray theory with  $n = 0, 1, 2$  and 3 rays.

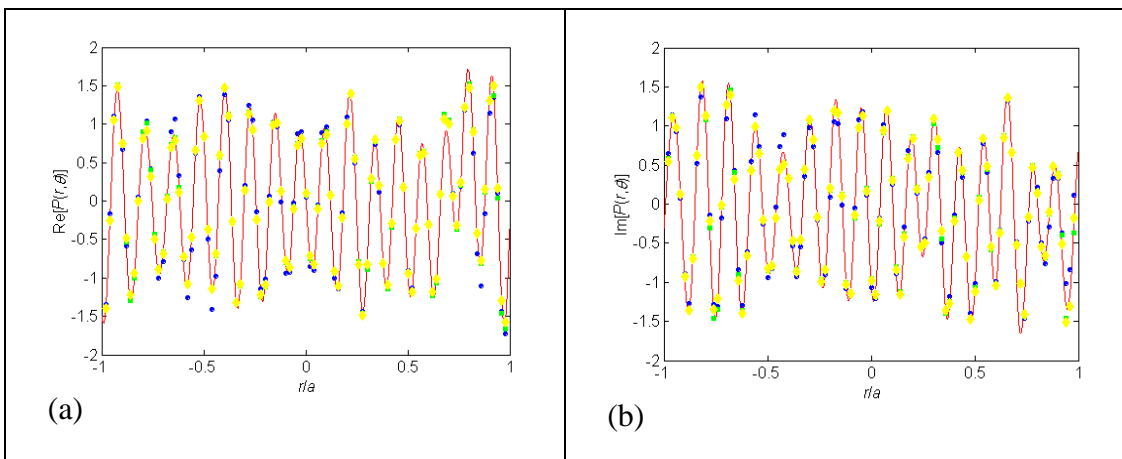


Fig. 4-27. a) Real part and b) imaginary part of interior pressure field on diameter formed by  $\theta = 30^\circ$  and  $210^\circ$  radii at 20 kHz when  $g=1.4$  and  $h=1.4$ . Red solid line: Field theory with 250 terms. Blue dots: Ray theory with  $n = 0$  and 1 rays. Green squares: Ray theory with  $n = 0, 1$  and 2 rays. Yellow diamonds: Ray theory with  $n = 0, 1, 2$  and 3 rays.

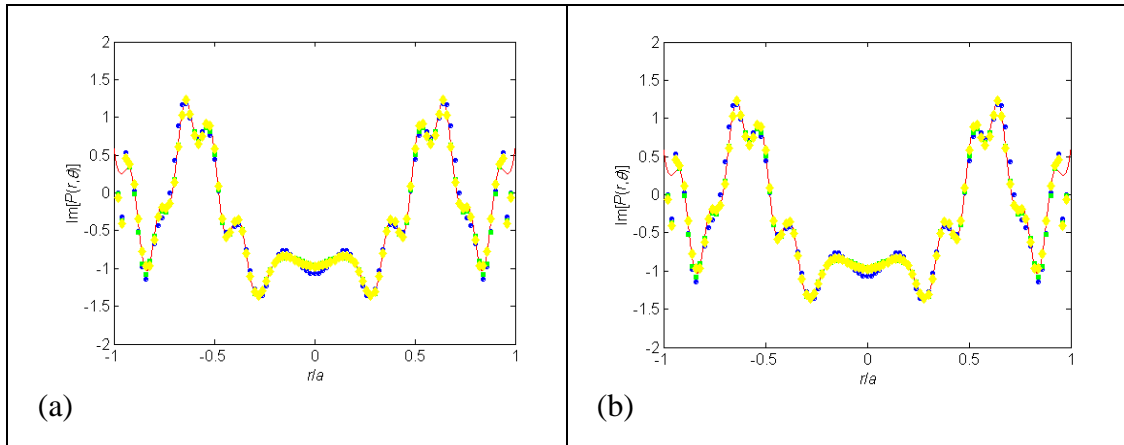


Fig. 4-28. a) Real part and b) imaginary part of interior pressure field on diameter formed by  $\theta = 90^\circ$  and  $270^\circ$  radii at 20 kHz when  $g=1.4$  and  $h=1.4$ . Red solid line: Field theory with 250 terms. Blue dots: Ray theory with  $n = 0$  and 1 rays. Green squares: Ray theory with  $n = 0, 1$  and 2 rays. Yellow diamonds: Ray theory with  $n = 0, 1, 2$  and 3 rays.

The effect of increasing the number of rays is more pronounced at 5 kHz. This is seen in Figs. 4-29, 4-30, and 4-31 where the real and imaginary parts of the pressures are shown on three diameters.

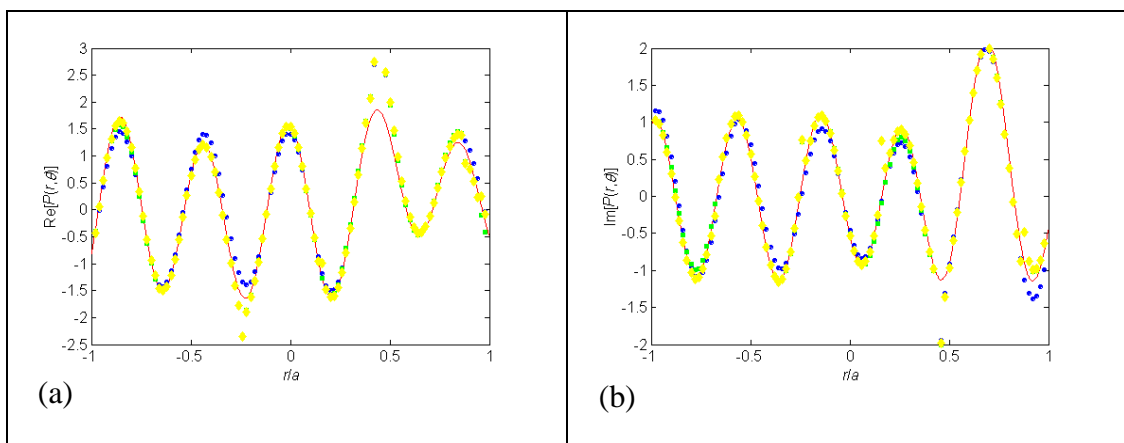


Fig. 4-29. a) Real part and b) imaginary part of interior pressure field on diameter formed by  $\theta = 0^\circ$  and  $180^\circ$  radii at 5 kHz when  $g=1.4$  and  $h=1.4$ . Solid line: Field theory with 250 terms. Diamonds: Ray theory with  $n= 0$  and 1 rays. Squares: Ray theory with  $n= 0, 1$  and 2 rays. Dots: Ray theory with  $n= 0, 1, 2$  and 3 rays.

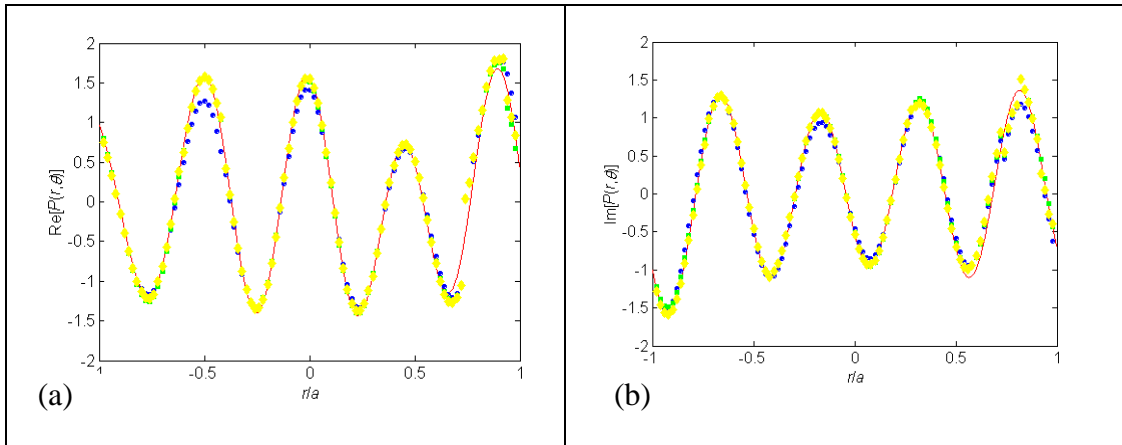


Fig. 4-30. a) Real part and b) imaginary part of interior pressure field on diameter formed by  $\theta = 30^\circ$  and  $210^\circ$  radii at 5 kHz when  $g=1.4$  and  $h=1.4$ . Red solid line: Field theory with 250 terms. Blue dots: Ray theory with  $n = 0$  and 1 rays. Green squares: Ray theory with  $n = 0, 1$  and 2 rays. Yellow diamonds: Ray theory with  $n = 0, 1, 2$  and 3 rays.

The pressures, as a function of frequency, at three points on the plane of symmetry, are shown in Figs. 4-32 – 4-34 for  $g = h = 1.1$ . The points are  $r=a/2$  and  $\theta = 180$  deg;  $r=0$  and  $\theta = 0$  deg; and  $r=3a/4$  and  $\theta = 0$  deg. In the Figs.,  $ka$  varies from 20 to 100 and only the  $n = 0$  and 1 rays are used. There is good agreement in all cases between results obtained using the ray and field theories.

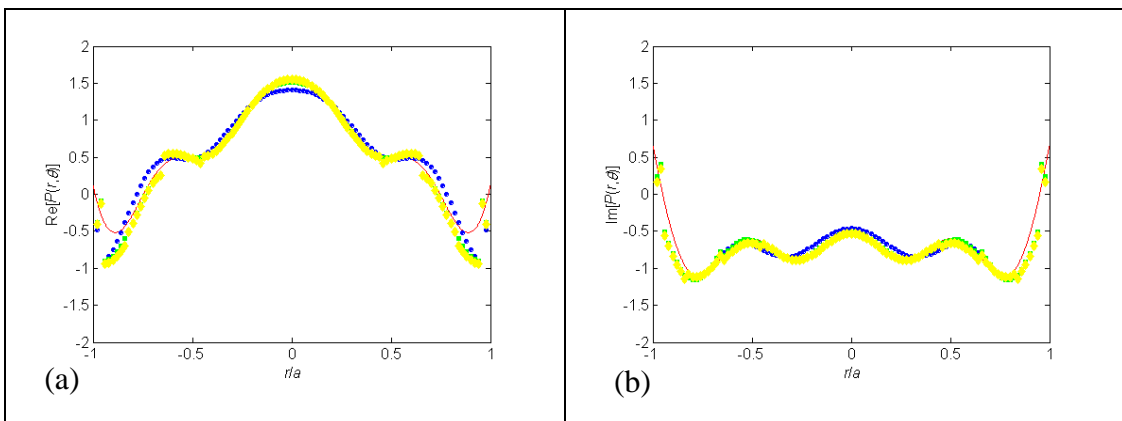


Fig. 4-31. a) Real part and b) imaginary part of interior pressure field on diameter formed by  $\theta = 90^\circ$  and  $270^\circ$  radii at 5 kHz when  $g=h=1.4$ . Red solid line: Field theory with 250 terms. Blue dots: Ray theory with  $n = 0$  and 1 rays. Green squares: Ray theory with  $n = 0, 1$  and 2 rays. Yellow diamonds: Ray theory with  $n = 0, 1, 2$  and 3 rays.



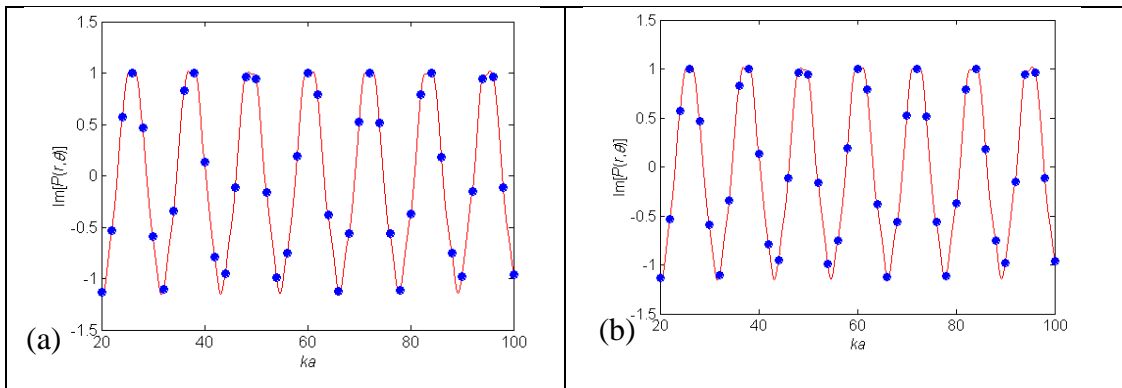


Fig. 4-32. a) Real part and b) imaginary part of internal pressure field at the point  $r=a/2$  and  $\theta = 180^\circ$  from  $ka = 20$  to 100 when  $g=h=1.1$ . Red solid line: Field theory with 250 terms. Blue dots: Ray theory with  $n = 0$  and 1 rays.

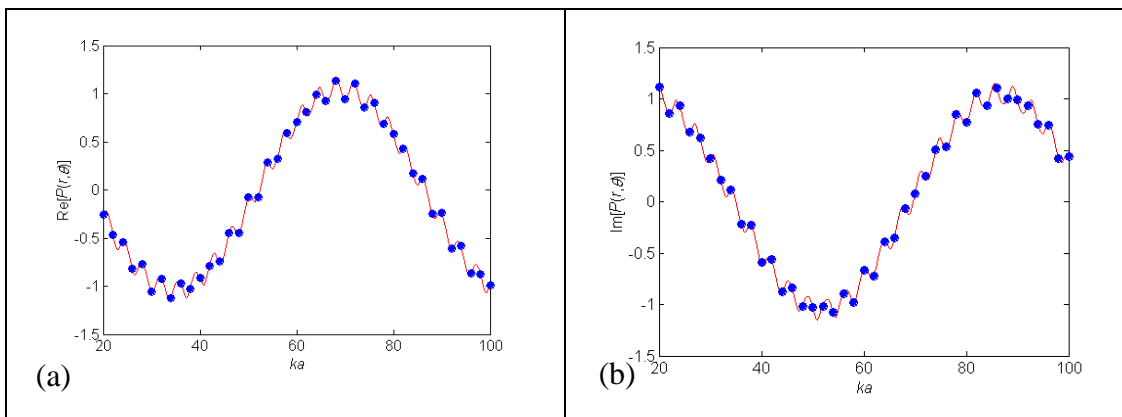


Fig. 4-33. a) Real part and b) imaginary part of internal pressure field at the point  $r=0$  and  $\theta = 0^\circ$  from  $ka = 20$  to 100 when  $g=h=1.1$ . Red solid line: Field theory with 250 terms. Blue dots: Ray theory with  $n = 0$  and 1 rays.

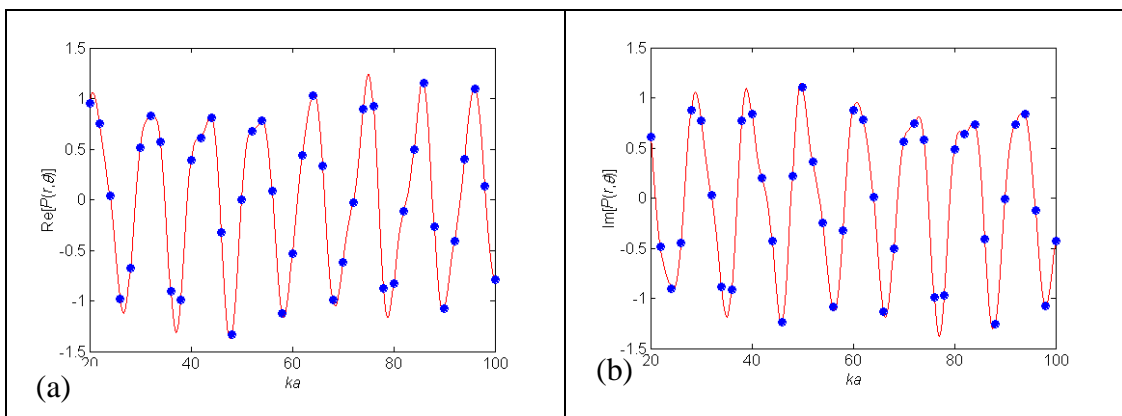


Fig. 4-34. a) Real part and b) imaginary part of internal pressure field at the point  $r=3a/4$  and  $\theta = 0^\circ$  from  $ka = 20$  to 100 when  $g=h=1.1$ . Red solid line: Field theory with 250 terms. Blue dots: Ray theory with  $n = 0$  and 1 rays.

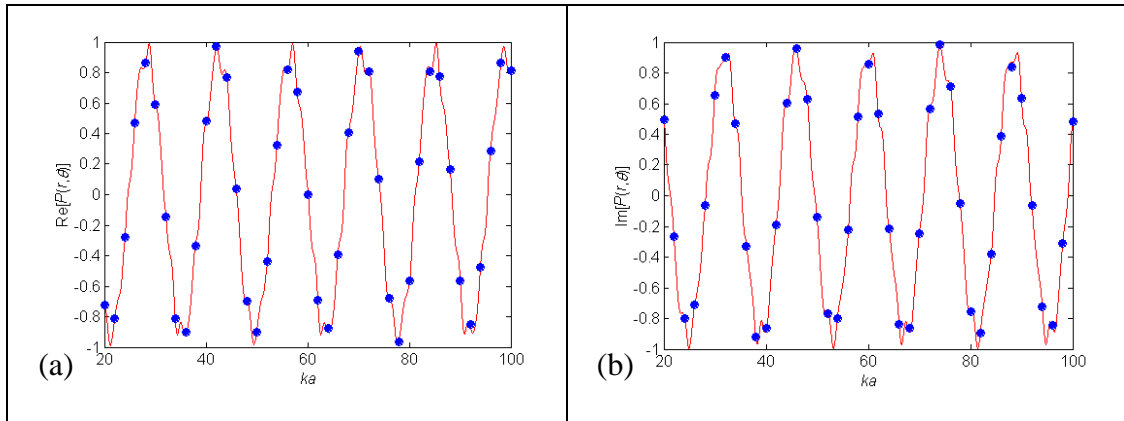


Fig. 4-35. a) Real part and b) imaginary part of internal pressure field at the point  $r=a/2$  and  $\theta = 180^\circ$  from  $ka = 20$  to 100 when  $g=h=0.9$ . Red solid line: Field theory with 250 terms. Blue dots: Ray theory with  $n = 0$  and 1 rays.

The pressures, as a function of frequency, at three points on the plane of symmetry, are shown in Figs. 4-35 – 4-37 for  $g = h = 0.9$ . The points are  $r=a/2$  and  $\theta = 180$  deg;  $r=0$  and  $\theta = 0$  deg; and  $r=3a/4$  and  $\theta = 0$  deg. In the Figures,  $ka$  varies from 20 to 100 and only the  $n = 0$  and 1 rays are used. There is good agreement in all cases between results obtained using the ray and field theories.

When the acoustic contrast increases, a higher value of  $N$  in Eq. (4-16) is required for convergence. The effect of increasing  $N$  on the interior pressure computed using ray theory is shown in Table I and the results are compared with those obtained using field theory. In field theory, 300 terms are used and the results have converged. The pressures are shown at  $r = 0.5$  m and  $\theta = 90, 120, 150,$  and  $180$  deg. at 20 kHz for  $g = h = 1.4$ . It is

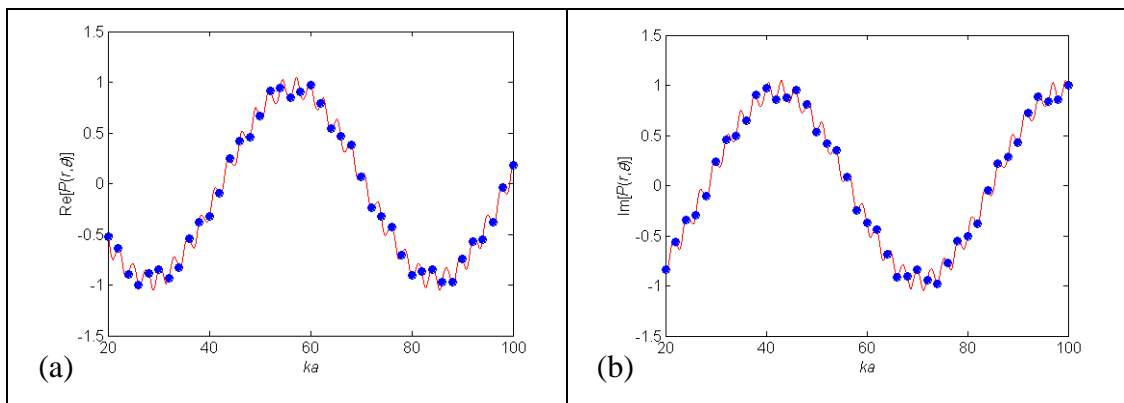


Fig. 4-36. a) Real part and b) imaginary part of internal pressure field at the point  $r=0$  and  $\theta = 0^\circ$  from  $ka = 20$  to 100 when  $g=h=0.9$ . Red solid line: Field theory with 250 terms. Blue dots: Ray theory with  $n = 0$  and 1 rays.

seen from the Table 4-I that the ray theory results converge to those obtained using field theory when  $N$  is increased.

Table 4-I. Magnitude of interior pressure at 20 kHz when  $g=h=1.4$  at  $r=0.5$  m.

Angle (degree)	Magnitude of Pressure				
	Field theory	Ray Theory			
		$N = 0$	$N = 1$	$N = 2$	$N = 3$
90	1.40	1.09	1.36	1.40	1.42
120	1.39	1.15	1.40	1.42	1.41
150	1.18	1.20	1.27	1.19	1.20
180	1.59	1.21	1.34	1.60	1.60

The outputs from a circular array with  $2H=32$  hydrophones and  $2J=12$  hydrophones in each sector are shown in Figs. 4-38 and 4-39. The outputs,  $V_s$ , are computed using ray theory and Eq. (4-24) with  $M = 1$ , and are shown for  $s = 3$  to 17 because the normal to the linear array simulated using the 11th sector makes an angle of 180 deg with the  $x$  axis. The angles that the normals to the simulated linear arrays make with the  $x$  axis of the coordinate system are shown on the abscissas of Figs. 4-38 and 4-39.

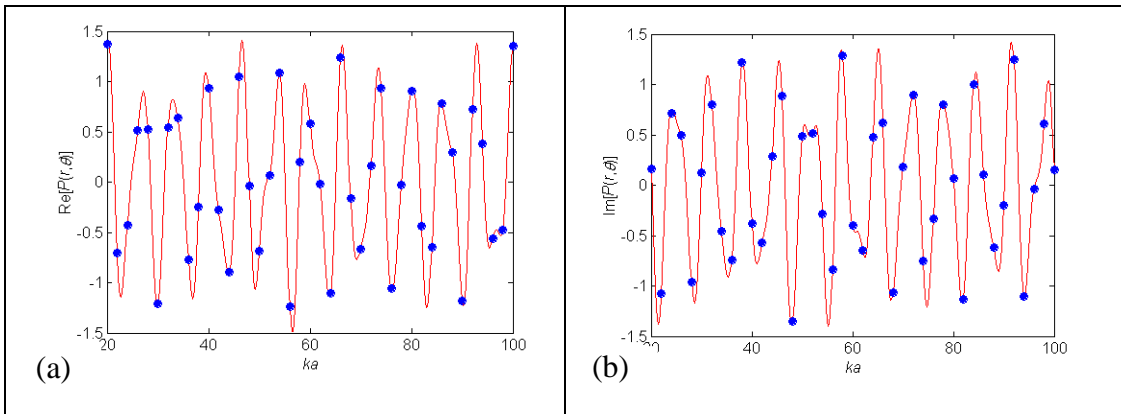


Fig. 4-37. a) Real part and b) imaginary part of internal pressure field at the point  $r=3a/4$  and  $\theta = 0^\circ$  from  $ka = 20$  to 100 when  $g=h=0.9$ . Red solid line: Field theory with 250 terms. Blue dots: Ray theory with  $n = 0$  and 1 rays.

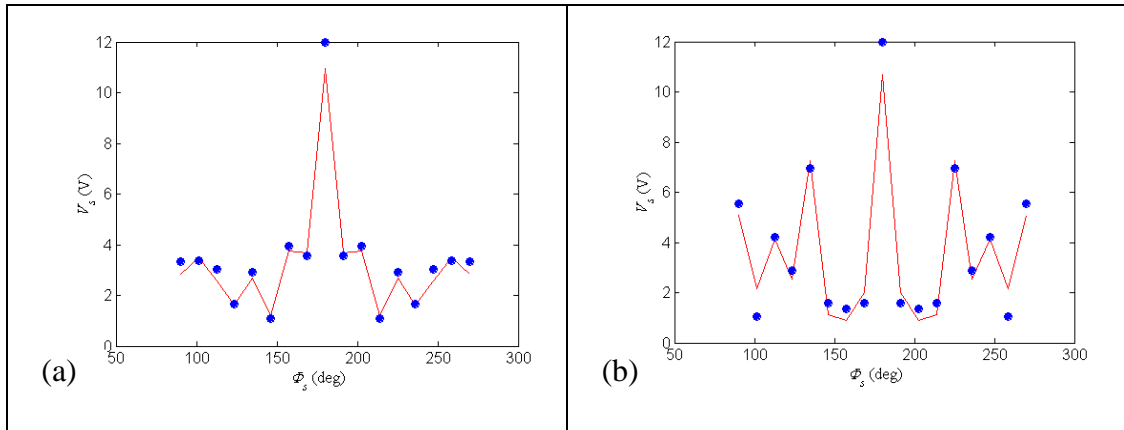


Fig. 4-38. Directional response of 12 out of 32 hydrophones in the circular array for frequency of a) 5 kHz and b) 20 kHz when  $g = h = 0.9$ . Red solid line: Presence of embedded cylinder. Blue dots: Absence of embedded cylinder.

Results are shown in Fig. 4-38 and 4-39 for  $g = h = 1.1$  and for  $g = h = 0.9$ , respectively. Results are shown for 5 and 20 kHz. A red solid line and blue dots are used to show results for the cases where an embedded cylinder is present and absent (homogenous infinite fluid), respectively. When the fluid is homogenous, the output from the 11<sup>th</sup> sector is 12 because the pressure due to the plane wave of unit amplitude is in-phase at each of the 12 hydrophones that are in the simulated linear array. When the embedded cylinder is present, and  $g = h = 1.1$ , the output from the 11<sup>th</sup> sector is more than 12 at 5 kHz and nearly equal to 12 at 20 kHz even though the rays diverge when they first enter the cylinder. For  $g = h = 0.9$ , the rays converge when they first enter the cylinder

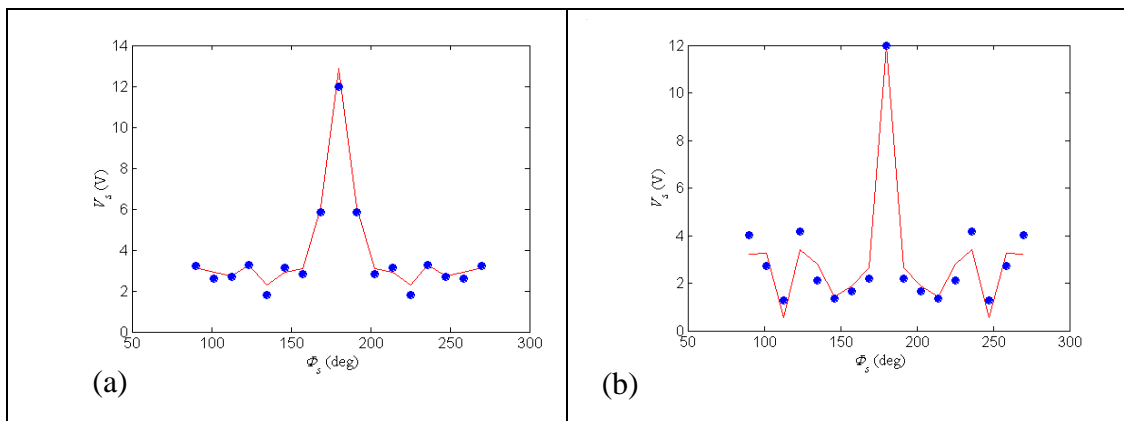


Fig. 4-39. Directional response of 12 out of 32 hydrophones in the circular array for (a) frequency of a) 5 kHz and b) 20 kHz when  $g = h = 1.1$ . Red solid line: Presence of embedded cylinder. Blue dots: Absence of embedded cylinder.

but the output from the 11<sup>th</sup> sector is less than 12. The outputs from the other sectors when the array is in the embedded cylinder are more in some cases and less in others than the outputs in infinite homogenous fluid. This will give rise to some differences in the computed direction of arrival. At 20 kHz, it is seen from Fig. 4-38b that the outputs from the 7<sup>th</sup> and 15<sup>th</sup> sectors are large but not equal to that of the 11<sup>th</sup> sector. Grating lobes do not occur even though the spacing between the hydrophones in the simulated linear array is more than the wavelength at this frequency because the spacing is non-uniform.

#### 4.4 CONCLUSIONS

A ray theory method is presented to determine the interior pressure field in a fluid cylinder embedded in an infinite fluid and excited by a plane wave. Geometrical and physical acoustics approximations are used. A caustic is formed at the point at which two converging rays intersect, and the pressure at that point, even though it is finite, cannot be determined by using these two rays. Therefore, another ray that is adjacent, but on the other side, is used to determine the pressure. When the point is not a caustic, the average pressure obtained by using rays adjacent on both sides is used.

Numerical results, obtained using ray theory, are presented for various embedded cylinders. Good agreement is obtained with results computed using a modal series solution approach. Some embedded cylinders have density and sound-speed higher than that in the surrounding infinite fluid and others have lower density and sound-speed. Representative contour plots of the interior pressure as well as the pressures on diameters of the cylinder and circles within the cylinder are presented. When the density and sound-speed contrasts are low, only two families of rays are used: those that have not been reflected even once when traveling inside the cylinder ( $n = 0$ ) and those that have been reflected once ( $n = 1$ ). When the density and sound-speed contrast is increased, using the  $n = 2$  and 3 rays also, yields convergence of the pressure. The pressure is also presented for  $ka = 20$  to 100 at a point on the plane of symmetry.

The directional responses of linear arrays simulated using one circular array in the embedded cylinder are presented. It is seen from the numerical results that in some cases the output from the array is a little more than that due to a plane wave even when the rays diverge immediately after entering the cylinder. In other cases, it is a little less than that due to a plane wave even when the rays converge immediately after entering the cylinder.

The method presented here can be used to determine the interior pressure field in objects with more complex shapes such as sonar domes. The effect of interior structures with reflection coefficients that are frequency dependent can also be included. The response of arrays within the embedded object can then be determined and be used, if necessary, to prepare look-up tables to correct for errors in determining the direction of arrival of waves from distant sources.

### CONCLUSIONS

#### 5.1 SUMMARY

In this thesis, analytical methods are presented to determine acoustic radiation from cylindrical arrays and the effect of scattering from cylindrical bodies on the response of arrays of hydrophones. The significant conclusions that can be drawn from the present work are as follows:

1. Analytical methods are presented to determine the directional and omnidirectional radiation from cylindrical transducer arrays. Expressions are derived for pressure fields when the entire array is vibrating in-phase, a sector of the array is vibrating in-phase, and a sector of the array is phase-shaded to simulate radiation from a rectangular piston. Far-field pressure is computed in all cases and on-axis pressure radiated by a cylindrical sector in an infinite cylindrical baffle is compared with that radiated by a rectangular piston in an infinite rigid planar baffle.

2. Analytical methods are presented to determine the effect of scattering from stiffeners that are used in domes on the error in finding the direction of arrival of plane waves from distant sources. The stiffener is modeled as an infinite elastic cylinder and the sum of the incident and scattered pressures is computed at hydrophone locations in a linear array. Two classical data-dependent signal processing methods are then used to determine the direction of the arrival. The error in finding the direction of arrival is illustrated for several special cases. It is shown that the error varies approximately as radius of the cylinder to the power of  $7/4$ .

3. Analytical methods are presented to determine the effect of scattering from a fluid cylinder embedded in an infinite fluid on the output from a circular array within the embedded fluid cylinder. The interior pressure field is computed using ray theory and is shown to be in good agreement with that computed with the field theory. It is sufficient, when the acoustic contrast between the interior and exterior fluids is not strong, to use just a few rays to determine the interior pressure field. Directional responses, to plane waves, of sectors of the circular array of uniformly distributed hydrophones in the embedded cylinder are then computed and compared the results with the output from an array in an infinite homogenous fluid.

## **5.2 RELEVANCE AND APPLICATIONS**

The significant contributions that can be drawn from the present work are as follows:

1. Acoustic radiation from cylindrical arrays is used when it is necessary to ensonify the entire surrounding volume. Exciting the entire array creates an omnidirectional pressure field in the azimuthal plane. However, when only part of the array is excited, after phase-shading, high pressure field is created in the direction of interest. Therefore, in some cases, instead of simultaneously radiating in all directions, a beam is formed in the direction of interest, and a little later, the beam is steered to an adjacent sector. The entire volume is thus ensonified sector-by-sector using higher fields. This is often done in practical sonar applications and the analysis is therefore of immense value.

2. Analytical methods are presented to determine scattering from an elastic cylinder and its effect on the performance of a nearby linear array of hydrophones. Arrays are always housed within sonar domes. The domes are often strengthened using stiffeners as this permits the use of thinner metal plates that are more transparent. The distance that should be maintained between the dome and the array depends on several factors that include the effect of scattering on the ability to detect the source of the sound waves and determine the direction of their arrival. Therefore, the analysis has immense practical value.

3. Sonar domes that house arrays of transducers are usually doubly curved because of hydrodynamic and structural considerations. They are also filled with fresh water whose acoustic characteristics are not the same as that of sea water. Further, the size of the dome is such that the normalized frequency is high. Because of the above, the pressure field inside the sonar dome cannot be easily computed using analytical or finite element methods. The high frequency ray method presented here is eminently suitable for sonar dome analysis including the effects of transmission through thin plates.

## **5.3 FUTURE WORK**

Finally, some suggestions are made for further work.

1. An analytical method is presented to study radiation from a cylindrical array of rectangular pistons with specified uniform displacement. This can be extended to study radiation from circular pistons as axisymmetric transducers are often used. Further, the electroacoustic transducers themselves can be modeled to study interaction between the transducers.



2. An analytical method is presented to study the effect of one stiffener near a linear array on the error in estimating the direction of arrival. The method can be used to study the effect of the dome and multiple stiffeners.

3. A method based on ray theory is used to determine the interior pressure field in an embedded fluid cylinder. The method can be extended to determine the pressure field inside a three-dimensional sonar dome. The effect of interior structures with reflection coefficients that are frequency dependent can also be included. The interior pressure can then be used to determine the error in estimating the direction of arrival due to the shape of the dome and the materials used to manufacture the dome.

## REFERENCES

1. Akay, A., Sener, S. and Gaunaurd, G. C., (1993), Acoustic scattering from fluid-filled, concentric, submerged, cylindrical, elastic shells, *Journal of the Acoustical Society of America*, 94(6), pp 3277-3294.
2. Alemer, J. D., Delsanto, P. P., Rosario, E., Nagl, A. and Uberall, H., (1986), Spectral Analysis of the scattering of acoustic waves from a fluid cylinder, II: Denser fluid inside, *Acustica*, 61, pp 7-13.,
3. Anderson, V. C., (1950), Sound scattering from a fluid sphere, *Journal of the Acoustical Society of America*, 22, pp 426-431.
4. Benthien, G. W., (1990), Numerical Modeling of Array Interactions, *Proceedings of the International Workshop, Power Transducers for Sonics and Ultrasonics*, Hamonic, B. F., Wilson, O. B., Decarpigny, J. N. (Eds.), pp109-124.
5. Beyer, R.T., (1999) *Sounds of our Times*, Springer- Verlag Inc., New York.
6. Boag, A., Leviatan, Y., and Boag, A., (1988), Analysis of acoustic scattering from fluid cylinders using a multi filament source model *Journal of the Acoustical Society of America*, 83 (1), pp 1-8.
7. Bowman, J. J., Senior, T. B. A., and Uslenghi, P. L. E., (1969), *Electromagnetic and acoustic scattering by simple shapes*, North-Holland Publishing company – Amsterdam, pp 22-23, 26-27, & 29.
8. Brill, D. and Uberall, H., (1970), Transmitted waves in the diffraction of sound from liquid cylinders, *Journal of the Acoustical Society of America* 47(5), pp 1467-1469.
9. Bruno, O. P., Geuzaine, C. A., Monro, J. A., and Reitich, F., (2004) Prescribed error tolerances within fixed computational times for scattering problems of arbitrarily high frequency: the convex case, *Philosophical Transactions of the Royal Society of London A*, Vol. 362, pp 629 – 645.
10. Bucaro, J. A., Houston, B. H., Simpson, H., Dragonette, L.R., Kraus, L., and Yoder, T., (2009), Exploiting forward scattering for detecting submerged proud/half-buried unexploded ordnance, *Journal of the Acoustical Society of America*, 126(6), EL171-176.
11. Bucaro, J. A., Kraus, L., Houston, B.H., Simpson, H., and Sarkissian, A., (2011), Forward scatter target strength extraction in a marine environment, *Journal of the Acoustical Society of America*, 129(6), 3453-3456.

12. Bucciarelli, L. L. and Dworsky, N., (1980), *Sophie Germain: An Essay in the History of the theory of Elasticity*, Reidel Publishing Co., Dordrecht, Holland.
13. Burdic, W. S., (1984), *Underwater acoustic system analysis*, Prentice-Hall, Inc., Englewood Cliffs, Boston, USA .
14. Carter, G. C., (1981), Time delay in estimation for passive sonar signal processing, *IEEE Transactions on Acoustics, Speech and Signal Processing*, Vol. ASSP-29, pp 463-470.
15. Chandra, K., and Thompson, C., (1992), Improved perturbation method for scattering from a fluid cylinder, *Journal of the Acoustical Society of America*, 92(2), pp 1047-1055.
16. Chen, C.Y., (1996), *Early Chinese Work in Natural Science: A Reexamination of the Physics of Motion, Acoustics, Astronomy, and Scientific Thoughts*, Hongkong University Press, Chp. 2.
17. Clay C. S., and Medwin, H., (1977), *Acoustical Oceanography: Principles and Applications*, John Wiley & Sons, New York, pp 66-67.
18. Crighton, D. G., (1992), *Modern Methods in Analytical Acoustics*, Springer – Verlag, London.
19. Devey, J., (Ed.) (1902), *Novum Organum by Lord Bacon*, P.F. Collier, New York.
20. Ding, L., (1997), Direct laboratory measurement of forward scattering of individual fish, *Journal of the Acoustical Society of America*, 101(6) pp 3398-3404.
21. Ebenezer, D. D., (1998), Effect of cylindrical baffles on directivity pattern and bandwidth of underwater communication transducer arrays, *Proceedings of Undersea Defence Technology*, Pacific, Sydney, Australia, pp 174-178.
22. Ebenezer, D. D., and Stepanishen, P. R., (1991) A wave-vector-time domain technique to determine the transient acoustic radiation loading on cylindrical vibrators in an inviscid fluid with axial flow, *Journal of the Acoustical Society of America*, 89 (1), 39–51.
23. Eli Maor, (2007), *The Pythagorean Theorem: A 4,000-Year History*, Princeton University Press, pp 18, 19.
24. Fahy, F., (1985), *Sound and Structural Vibration: Radiation, Transmission and Response*, Academic, London.
25. Faran Jr., J. J., (1951), Sound scattering by solid cylinders and spheres, *Journal of the Acoustical Society of America*, 23, pp 405-418.

26. Foote, K. G., (2007), Internal field in an immersed absorbing fluid sphere excited by a plane acoustic wave, *Journal of the Acoustical Society of America*, 122 (5), pp 3033.
27. George, P. C., and Paulraj, A., (1985), Optimising the active sonar system design, *Defence Science Journal*, 35, pp 295-311.
28. Godin, O. A., and Palmer, D. R., (2008), *History of Russian Underwater Acoustics*, World Scientific Publishing Company, Singapore.
29. Graff, K. F., (1975), *Wave Motion in Elastic Solids*, Clarendon press, Oxford.
30. Greenspom, J. E., and Sherman, C. H., (1964), Mutual radiation impedance and nearfield pressure for pistons on a cylinder, *Journal of the Acoustical Society of America*, 36(1), pp 149-153.
31. Han, D., Fossati, C., Bourennane, S., and Saidi, Z., (2009), Bearing and Range Estimation Algorithm for Buried Object in underwater acoustics, *Research Letters in Signal Processing*, Vol. 2009, Article ID 257564, 4 pages, doi: 10.1155/2009/257564.
32. Horiki, Y., and Newman, E. H., (2006), A self-calibration technique for a DOA array with near-zone scatterers, *IEEE Transactions on Antennas and Propagation*, 54(4).
33. Junger, M. C., (1982), Scattering by slender bodies of revolution, *Journal of the Acoustical Society of America*, 72(6), pp 1954-1956.
34. Junger, M. C., and Feit, D., (1972), *Sound, Structures and Their Interaction*, MIT Press, Cambridge, MA, pp 92-95, 304-305.
35. Laird D. T., and Cohen, H., (1952), Directionality patterns for acoustic radiation from a source on a rigid cylinder, *Journal of the Acoustical Society of America*, 24(1), pp 46-49.
36. Lam, Y. W., (1992), Fluid-structure coupling in underwater sonar arrays with piston type transducers, *Applied Acoustics*, 36, pp 31-49.
37. Kaufman, A. A., Levshin, A.L., and Larner, K.L., (2002), *Acoustic and elastic wave fields in Geophysics II*, Elsevier, Amsterdam, pp 10-11.
38. Kinsler, L. E., Frey, A. R., Coppens, A. B., and Sanders, J. V., (1982), *Fundamentals of Acoustics*, John Wiley & Sons, pp 135-140.
39. Knight, W. C., Pridham, R. G., and Kay, S. M., (1981), Digital signal processing for sonar, *Proceedings Of IEEE*, 69(11), pp1451-1508.

40. Kravtsov, Y.A., and Orlov, Y. I., (1993), *Caustics, catastrophes and wave fields*, Springer -Verlag Berlin Heidelberg, Germany, pp 1 and 8.
41. Loeser, H. T., (1981), Sonar and the ship, *Naval Engineers Journal*, pp 89-93.
42. Love, A. E. H., (1927), *A Treatise on the Mathematical Theory of Elasticity*, Dover Publications, New York.
43. Marston P. L., (1992), Geometrical and catastrophe optics methods in scattering, *Physical Acoustics*, Vol. XXI, High Frequency and Pulse scattering Edited by A.D. Pierce and R. N. Thurston Academic, New York, pp 31-37 and 161-182.
44. Marston, P. L., (1997), Quantitative ray methods for scattering, *Encyclopaedia of Acoustics*, Edited by M. J. Crocker. Wiley, New York, pp 483- 492.
45. Marston P. L., and Langley D. S., (1983), Glory and rainbow-enhanced acoustic backscattering from fluid spheres: Models for diffracted axial focusing, *Journal of the Acoustical Society of America*, 73(5), pp 1464-1475.
46. Mathew, J., and Ebenezer, D. D., (2009), High Frequency Rays in an Infinite Fluid Cylinder Excited by a Plane Acoustic Wave, *Journal of Acoustic Society of India*, 36, pp 163-167.
47. Mathew, J., Nishamol, P. A., and Ebenezer, D. D., (2010), Effect of an elastic cylinder near an array on the pressure field due to a plane acoustic wave, *Proceedings of National Symposium on Acoustics*, Rishikesh, India, pp 31-37.
48. Medwin H., and Clay, C.S., (1998), *Fundamentals of Acoustical Oceanography*, Academic Press, Boston, pp 244-245.
49. Meleshko, V. V., (2003), Selected topics in the history of two dimensional biharmonic problem, *Applied Mechanics Review*, 56(1).
50. Mitri, F. G., Fella Z. E. A., and Chapleon, J. Y., (2004), Acoustic backscattering form function of absorbing cylinder targets, *Journal of the Acoustical Society of America*, 115, pp 1411-1413.
51. Montagu ,B., Ed., (1834), *The works of Francis Bacon*, Vol. 15, William Pickering, London, pp 225.
52. Morris, R., (1984), Some practical consideration in the design of sandwich transducers and their array, *IEE Proceedings*, 131, Part F, N0.3, pp 280-285 .
53. Morse P. M., and Ingard, K. U., (1968), *Theoretical Acoustics*, McGraw-Hill, New York, pp 401-403.
54. Nielsen, R. O., (1991), *Sonar signal processing* Artech House, MA, USA.

55. Pierce, A. D., (1989), *Acoustics – An Introduction to its Physical Principles and Applications*, Mc Graw Hill Inc., New York, pp 3.
56. Raman, C. V., (1922), *The acoustical knowledge of the ancient Hindus*, Asutosh Mookerjee Silver Jubilee, Volume 2 pp 179-185.
57. Raichel, D. R., (2000), *The Science and applications of Acoustics*, Springer-Verlag Inc., New York.
58. Rolleigh, R. L., Pruitt, J. G., and Stokes, R. H., (1977), Vertical side-lobe suppression in cylindrical arrays, *Journal of the Acoustical Society of America*, 61(2), pp 397-402.
59. Rumerman, M. L., (1991), Increased accuracy in the application of the Sommerfeld-Watson transformation to acoustic scattering from cylindrical shells, *Journal of the Acoustical Society of America*, 90(5), pp 2739-2750.
60. Sabra, K. G., Conti, S., Roux, P., Akal, T., Kuperman, W. A., Stevenson, J. M., Tesei, A. and Guerrini, P., (2010), Experimental demonstration of a high-frequency forward scattering acoustic barrier in a dynamic coastal environment, *Journal of the Acoustical Society of America*, 127 (6), pp 3430 – 3439.
61. Schneider, H., Berg, R., Gilroy, L., Karasalo, I., MacGillivray, I., TerMorschhuizen M., and Volker, A., (2003), Acoustic scattering by a submarine: Results from a benchmark target strength simulation workshop, *Proceedings of 10th International Congress on Sound and Vibration*, Sweden, pp 2475-2482.
62. Schock, S. G., Tellier, A., Wulf, J., Sara, J., and Ericksen, M., (2001), Buried object scanning sonar, *IEEE Journal of Oceanic Engineering*, 26(4) pp 677-689.
63. Sherman, C. H., (1968), Special relationships between the farfield and the radiation impedances of cylinders, *Journal of the Acoustical Society of America*, 43, pp 1452-1454.
64. Sherman, C. H., and Butler, J. L., (2007), *Transducers and Arrays for Underwater Sound*, Springer, New York, USA.
65. Skudrzyk, E., (1971), *The Foundations of Acoustics*, Springer-Verlag, New York, pp 446-448.
66. Soedel, W., (1993), *Vibrations of Shells and Plates*, Marcel Dekker, New York, USA.
67. Sokolnikoff, I. S., (1956), *Mathematical theory of elasticity*, McGraw-Hill, New York, pp 184.

68. Stansfield, D., (1990), *Underwater electroacoustic transducers*, Bath University Press, Chp. 2.
69. Stanton, T. K., Chu, D., Weibe, P. H., and Clay, C. S., (1993b), Average echoes from randomly oriented random length finite cylinders: Zooplankton models, *Journal of the Acoustical Society of America*, 94(6), pp 3463-3472.
70. Stanton, T. K., Clay, C. S., and Chu, D., (1993a), Ray representation of sound scattering by weakly scattering deformed fluid spheres: Simple physics and application to zooplankton, *Journal of the Acoustical Society of America*, 94(6), pp 3454-3462.
71. Stepanishen, P. R., (1978), Radiated power and radiation loading of cylindrical surfaces with non-uniform velocity distributions, *Journal of the Acoustical Society of America*, 63, pp 328–336.
72. Stepanishen, P. R., (1982), Modal coupling in the vibrations of fluid loaded cylindrical shells, *Journal of the Acoustical Society of America*, 71, pp 813–823.
73. Stepanishen, P. R., and Ebenezer, D. D., (1991), An eigenvector method to determine the transient response of cylindrical shells in a fluid with uniform axial flow, *Journal of the Acoustical Society of America*, 89, pp 565 – 573.
74. Tarlekar, G. H., (1991) *The Natyasastra*, 2<sup>nd</sup> Edition, Motilal Banarsidass.
75. Teutsch, H., and Kellermann, W., (2006), Acoustic source detection and localization based on wavefield decomposition using circular microphone arrays, *Journal of the Acoustical Society of America*, 120(5), pp 2724-2736.
76. Vasu, S. C., (1891), *The Astadhyayi of Panini*, Reprinted 2003, Motilal Banarsidass.
77. Waite, A. D., (2002), *Sonar for Practising Engineers*, John Wiley & Sons, England pp 40-41, 129, 138.
78. Warren, L. R., (1988), Hull-mounted sonar ship design evolution and transition to low-frequency applications, *IEEE Journal of Oceanic Engineering*, 13 (4), pp 296-298.
79. Whewell, W., (1858), *History of the Inductive Sciences from the Earliest to the Present Time*, 3<sup>rd</sup> Ed., Vol. II Book VIII History of Acoustics, D. Appleton, New York. pp 25, 35-36.
80. Xia, J., Wang, C., and Zheng, C., (2006), Research on the Xian Qin Huangzhong pipe: An attempt to calculate the inside diameter of Huangzhong pipe with modern acoustic formula, *Studies in the History of Natural Sciences*, No. 3.

81. Ye, Z., Hoskinson, E., Dewey, R.K., Ding, L., and Farmer, D.M., (1997), A method for acoustic scattering by slender bodies. I. Theory and verification, *Journal of the Acoustical Society of America*, 102(4), pp 1964-1976.
82. Yokoyama, T., Asami, T., Mori, K., Nakamura T., and Hasegawa, A., (2004) “Consideration of radiation impedance calculation methods for cylindrical array sound source,” *Japanese Journal of Applied Physics*, Vol. 43(5B), pp 3154 – 3162.



## PUBLICATIONS BASED ON WORK

### Journal Papers

1. P. A. Nishamol, **Jasmine Mathew**, and D. D. Ebenezer, “Acoustic radiation from cylindrical transducer arrays,” *Journal of Sound and Vibration*, Vol. 323, pp 989-1002 (2009).
2. **Jasmine Mathew**, and D.D. Ebenezer, “Directional response of a circular array in an embedded fluid cylinder using ray theory,” *Journal of Sound and Vibration* (Communicated).
3. **Jasmine Mathew**, and D. D. Ebenezer, “High frequency rays in an infinite fluid cylinder excited by a plane acoustic wave,” *Journal of Acoustical Society of India*, Vol. 36, pp 163-16, (2009).
4. **Jasmine Mathew**, D. D. Ebenezer and P. A. Nishamol, “Error in finding the direction of arrival, using a linear array, due to scattering from an elastic cylinder,” *Journal of the Acoustical Society of America*. (Communicated).

### Conference papers

1. **Jasmine Mathew**, P. A. Nishamol and D. D. Ebenezer, “Effect of an elastic cylinder near an array on the pressure field due to a plane acoustic wave,” *Proceedings of National Symposium on Acoustics*, Rishikesh, 2010.

## DOCTORAL COMMITTEE

Convenor and  
Supervising Guide  
Dr. D. D. Ebenezer  
Scientist G  
Naval Physical and Oceanographic Laboratory  
Kochi

Members  
Dr. A. Unnikrishnan  
Scientist H  
Naval Physical and Oceanographic Laboratory  
Kochi

Dr. K. P. B. Moosad  
Scientist F  
Naval Physical and Oceanographic Laboratory  
Kochi

Dr. M. P. Ajaikumar  
Scientist F  
Naval Physical and Oceanographic Laboratory  
Kochi

Dr. R. S. Chakravarti  
Former Head  
Department of Mathematics  
CUSAT, Kochi

## CURRICULUM VITAE

**1. Name** : Jasmine Mathew

**2. Date of Birth** : 11.03.1982

### **3. Educational Qualifications**

#### **2001 Bachelor of Science (B. Sc.)**

Institution : Nirmala College, Muvattupuzha,  
Mahatma Gandhi University, Kottayam

Specialization : Mathematics

#### **2004 Master of Science (M. Sc.)**

Institution : Cochin University of Science and Technology

Specialization : Mathematics

#### **2005 JRF NET (CSIR)**

Specialization : Mathematical Science

#### **Doctor of Philosophy (Ph. D.)**

Institution : Cochin University of Science and Technology

Specialization : Applied Mathematics

Registration date: 27.05.2008

### **4. Experience**

**2005 – 2007** Junior Research Fellow in NPOL, Kochi

**2007 – 2009** Senior Research Fellow in NPOL, Kochi